The Dissertation Committee for Charles Andrew Michelson certifies that this is the approved version of the following dissertation:

Picture of a decision: neural correlates of perceptual decisions by population activity in primary visual cortex of primates

Committee:

_____
Eyal Seidemann, Supervisor

_____
Wilson Geisler

_____
Alex Huk

_____
Lawrence Cormack

_____
David Heeger

Picture of a decision: neural correlates of perceptual decisions by population activity in primary visual cortex of primates

by

Charles Andrew Michelson, B.S., M.S.

Dissertation

Presented to the Faculty of the Graduate School of

The University of Texas at Austin

in Partial Fulfillment

of the Requirements

for the Degree of

Doctor of Philosophy

The University of Texas at Austin

December, 2012

Acknowledgements

I would like to thank my advisor, Eyal Seidemann, for his dedication to these projects. I would also like to thank the members of my committee for their ongoing insights and suggestions. The computational models presented here would not have come to light without the help of Jonathan Pillow.

Past and present members of the lab enriched my projects on a daily basis with technical assistance and engaging discussions, and have become friends. I especially want to thank Chris Palmer, Yuzhi Chen, Tihomir Cakic, and Bill Bosking.

My parents, Charlie and Julie Michelson, and my family have supported and encouraged me in innumerable ways. I want to thank Todd, Frank, and George for their friendship and moral support over the years. And finally, I am so grateful to have the love and support of Julie Le, who is always there for me.

Picture of a decision: neural correlates of perceptual decisions by population activity in primary visual cortex of primates

Charles Andrew Michelson, Ph.D.

The University of Texas at Austin, 2012

Supervisor: Eyal Seidemann

The goal of this dissertation is to advance our understanding of perceptual decisions. A perceptual decision is a decision that is based on sensory evidence. For example, a monkey must choose whether to eat a food item based on sensory information such as its color, texture or odor. Previous research has identified regions of the brain involved in the encoding of sensory information as well as areas involved in transforming encoded representations of stimuli into signals useful for forming decisions about those stimuli. Researchers carried out much of this work by painstakingly observing the firing of single neurons or small groups of neurons while a subject performs a task, and used this information to propose and evaluate models of the decision process. However, previous studies have also shown that sensory stimuli are encoded in a distributed fashion across populations of neurons rather than in individual or small groups of neurons. Thus it is likely that populations of neurons, rather than individual neurons, are responsible for the formation of a decision. Here I directly address the question of how decisions are formed through the collective activity of populations of cortical neurons. I used voltage-sensitive dye imaging, a technique that allowed me to simultaneously monitor millions of

neurons in sensory cortex, while primates performed a simple yet challenging binary decision task. I also used psychophysical techniques and computational modeling to address fundamental questions about the nature of perceptual decisions. Here I provide new evidence that choice-related neural activity is distributed across a broad population of neurons, and that most of the decision-related neural activity occurs as early as primary sensory cortex. I propose a physiological and computational mechanism for the subject's decision process in our task, and demonstrate that this process is likely sub-optimal due to intrinsic uncertainty about sensory stimuli. Overall, I conclude that in our task, perceptual decisions are likely to be limited primarily by the quality of evidence that resides in populations of neurons in sensory cortex, secondarily by sub-optimal decoding of these sensory signals, and to a much lesser extent by additional downstream neural variability.

Table of Contents

List of Figures

List of Tables

List of Abbreviations

cdf	Cumulative density function
CI	Confidence interval
CNS	Central nervous system
CP	Choice probability
CR	Correct Rejection
CTMR	Choice-triggered map ratio
DF	Decision fraction
DOG	Difference of Gaussians
DV	Decision variable
ERP	Event-related potential
FA	False Alarm
FEF	Frontal eye fields
fMRI	Functional magnetic resonance imaging
H	Hit
IT	Inferotemporal cortex
LEP	Lower envelope principle
LFP	Local field potential
LGN	Lateral geniculate nucleus
LIP	Lateral intraparietal area
M	Miss
M1	Primary motor cortex
MF	Measurement fraction
ML	Maximum likelihood
MPC	Medial prefrontal cortex
MST	Medial superior temporal area
MT	Middle temporal area
MU	Multi-unit
NS	Neural sensitivity
PC	Pacinian corpuscle fibers
pdf	Probability density function
PET	Positron emission tomography
QA	Quickly adapting fibers
RGC	Retinal ganglion cell
ROC	Receiver operating characteristic
S1	Primary somatosensory cortex
S2	Secondary somatosensory cortex
SCCI	Stimulus-choice correspondence index
SDT	Signal detection theory
SMA	Supplementary motor area
SNR	Signal-to-noise ratio

SR	Saccade ratio
SU	Single unit
TE	Visual area TE
TEO	Visual area TEO
V1	Primary visual cortex
V2	Secondary visual cortex
V3	Visual area V3
V3a	Visual area V3a
V4	Visual area V4
VSDI	Voltage-sensitive dye imaging

Chapter 1: General Introduction

Most animals are continuously faced with a challenging problem: how to use information from the environment to guide behavior. A monkey in the wild, for example, must decide where to forage for food, which foods to eat, and which mate to choose. Each of these complex decisions requires the animal to gather information from the environment, evaluate how this information bears on its goals, and take action.

A long-term goal of systems neuroscience is to understand the relationship between perception, decision-making, and behavior. How are physical stimuli represented (encoded) in the brain? Which brain areas are responsible for representing which kinds of information? Once the physical attributes of a stimulus have been encoded in a sensory area of the brain, how are they interpreted by other brain regions? And how will this information guide behavior?

In this dissertation I address two broad questions which further our understanding of these processes. First, when an organism is engaged in a task that requires the use of sensory information, where in the brain are the signals that relate to decisions and how are these signals distributed across neurons? Much work has been done to elucidate how sensory information is encoded in early sensory areas of the brain, and modern techniques in neuroscience have allowed researchers to ask whether this information could be the basis on which animals gather evidence in favor of, or against, taking a particular action. Here I ask whether such decision-related information can be found as

early as the primary visual cortex (V1), the first cortical area in which visual information is encoded in the primate brain.

Second, I ask how the information encoded in this early sensory area is read out, or decoded, by subsequent areas of the brain in order to guide behavior. A small visual stimulus such as the Gabor target used in this dissertation can activate millions of neurons in V1. How then does the monkey combine these signals to form a decision about this stimulus? Two well-known properties of sensory cortical encoding offer clues as to how subsequent brain areas might use these encoded signals. First, individual nerve cells in the primate cortex tend to respond preferentially to specific low-level features of a visual stimulus, such as the color or size of an object. It is reasonable to suggest that the brain might selectively monitor those cells that respond to stimulus features that are relevant to the organism's task at hand. For example, when determining which fruits will be the most delicious, the brain might monitor cells sensitive to the fruit's color, which often indicates ripeness. These cells' responses should be better suited to this task than cells that encode, for example, motion across the visual field. Secondly, some cells that encode the feature of interest do so with higher fidelity than others, and are therefore more useful in making an estimate of this physical attribute. Thus we might expect the brain to preferentially monitor those cells that carry more reliable information. Are only the most informative neurons used? Or does the monkey combine information from many or all of those neurons, including those that are less reliable? Here I address this question by looking at entire populations of neurons in the primary visual cortex while a

monkey performs a simple task, and use the monkey's decisions to assess how these distributed signals are combined to form a simple decision.

This dissertation is composed of four chapters. Chapter 1 is a general introduction to the study of perceptual decision-making, emphasizing the theoretical questions and experimental paradigms that have led up to the studies presented here, and is geared towards the general reader interested in perceptual decisions. Chapters 2 and 3 are formatted like stand-alone research papers, and describe the experiments and computational modeling that represents the bulk of my doctoral work. Chapter 4 describes my general conclusions, and revisits the key questions introduced in Chapter 1 in light of our experimental and computational results.

In this dissertation I variously use "I" and "we" to indicate work that was done by myself or as a part of a collaborative group. While I carried out the VSDI experiments and performed the analyses described here, all of this work was guided by a collaboration including my advisor, Eyal Seidemann, and colleagues. Three colleagues' assistance warrants additional acknowledgment because their contributions over multiple years directly impacted the results presented here. I credit Jonathan Pillow for his formalization and derivation of the maximum likelihood estimator used in the modeling of Chapter 2. Yuzhi Chen provided frequent Matlab and programming assistance, including the application of the optimal decoder to the VSDI and simulated data presented in Chapters 2 and 3. Finally, Tihomir Cakic tirelessly provided technical support in carrying out the VSDI experiments.

1.1 A framework

A useful framework for addressing questions about perceptual decision-making identifies three distinct stages in the formation of a simple binary perceptual decision (Fig. 1.1). First, information about physical stimulus enters the nervous system via the sensory periphery and is encoded in an early sensory area. For example, the image of an object is transduced by the retina and represented by a pattern of neural activity in the primary visual cortex. Second, this information is decoded. Visual information represented by a large number of cells in the primary visual cortex is combined in a way that is useful to the animal and relevant to the task, and this combined (decoded) information may be represented in a downstream motor area, such as the frontal eye fields or pre-motor cortex; alternatively, decision-related signals could occur in another downstream area and serve to gate a motor response. Third, the combined information is evaluated against a decision criterion to form the basis of a motor response. For example, in a task that requires the animal to make an eye movement based on sensory information, the decoded information may drive activity in eye movement related

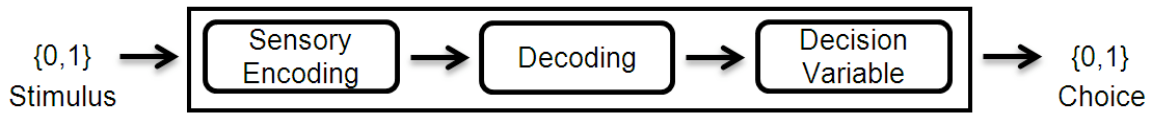

Figure 1.1. General framework for the formation of a binary perceptual decision. Sensory stimuli are encoded in sensory cortex ('Sensory Encoding'); the sensory representation is decoded by a later brain area to obtain signals useful for performing a task ('Decoding'); a single value ('Decision Variable') is compared against a criterion to determine the binary choice on each trial.

structures, such as the frontal eye fields, superior colliculus, dorsolateral prefrontal cortex, or cerebellar vermis. These three conceptual stages (encoding, decoding, and decision) are internal to the animal's nervous system, and form the critical chain that connects stimulus to behavior.

1.2 Visual system

Here I study the neural correlates of these stages within the context of the primate visual system. The primate visual system is an excellent model system in the study of perceptual decisions. First, vision is central to primates: there are at least 30 distinct visual areas in the human brain. Second, the primate visual system has been well studied. Because the fundamental response properties of visual cortical neurons have been extensively characterized, existing work in the visual system provides a firm basis for studying higher order relationships, such as relationships among brain areas and the relationship between populations of neurons and behavior. Finally, the visual system in the monkey shares features in common with that of humans, making the results potentially applicable to our species as well. Many human visual areas have homologous structures in the monkey. Within such visual areas, many cell types, response properties, and functional connectivity are common to both species.

Nevertheless, this work may be highly relevant to other sensory systems as well. Much progress has been made in identifying and characterizing brain areas that serve auditory and somatosensory functions (in traditions beginning with, e.g., Kiang et al., 1965; Mountcastle, 1957; Siebert, 1965; Talbot et al., 1968), and some of the questions

addressed here have been asked within the context of these other systems. However, the work presented here represents one of the first studies to address these questions in a behaving organism with measurements across entire populations of visual cortical neurons with excellent spatial and temporal resolution, and indeed represents one of the first such studies in any sensory system. The results presented here could provide new insight into how neuronal signals are used to form simple decisions, and suggest similar experiments that can be performed in other systems. Future researchers may wish to ask whether the findings presented here represent principles that underlie sensory systems generally.

1.3 Signal Detection Theory

Signal detection theory (SDT) is a framework in which to study decision-making. It is widely used in the research mentioned in this introduction, and is also employed in the studies presented in this dissertation. It assumes that decisions about sensory stimuli are based on evidence contained in a neural signal corrupted by noise (Green and Swets, 1966). To illustrate, suppose that a subject must detect the presence of a visual stimulus such as a flash of light (e.g., Barlow et al., 1971; Hecht et al., 1942). On some trials, a flash will be presented and on other trials it will not. The subject's task is to respond with "Yes" or "No" to indicate whether he detected the flash. Assume also that there are neurons within the brain that encode the intensity of light, responding with a large number of action potentials during intense flashes and fewer action potentials (or none) during weak flashes (e.g., Barlow et al., 1971). In the absence of variability, the subject's

task is easy: respond "Yes" when the neuron fires an action potential, and response "No" when it does not. But because of the intrinsic variability of many neurons (e.g., Arieli et al., 1996; De Valois et al., 1967; Tolhurst et al., 1983), the relationship between flash intensity and the physiological response is only true on average – *usually* trials with a flash will produce a stronger response (more action potentials) than trials without a flash. Sometimes however, due to the stochastic firing of neurons, a strong flash of light will produce a weaker response than expected, and vice versa. The activity of a sensory neuron in this task is best represented as a pair of stochastic distributions. If the flash stimulus is weak, the mean of the distribution belonging to flash trials will be only slightly greater than the mean of the distribution belonging to no-flash trials. If the noise is sufficiently large relative to the difference between the means of the two distributions, then the two distributions will overlap, making it impossible for the observer using these signals to perform the task with 100% accuracy. Instead, the observer must make an informed guess. Typically within this framework, the observer applies a criterion somewhere between the means of the two distributions. If the physiological response to a single trial exceeds the criterion, the subject reports "Yes", otherwise he reports "No". The subject's choice behavior and accuracy depends on the difference between the means of the distributions and their variability, as well as the placement of the criterion. Intuitively, a subject can perform most accurately when the means of the distributions are widely separated relative to their variability.

Studies based on signal detection theory in the context of binary decisions, such as the example described above, have at their core four categories of behavioral

responses. Because there are two possible stimulus conditions (e.g., flash or no-flash) and two possible behavioral responses ("Yes" or "No"), there are four possible outcomes on each trial. On trials in which a flash was presented, if the observer reports "Yes" the trial is said to be a 'Hit', whereas if the observer reports "No" it is said to be a 'Miss'. On trials that did not contain a flash, if the observer reports "Yes" it is classified as a 'False Alarm' (FA), whereas if he reports "No" it is said to be a 'Correct Rejection' (CR).

In this dissertation, I study the relationship between a monkey's behavioral responses in a visual detection task and the simultaneously measured physiological responses in V1. The visual stimulus I used in these experiments is a Gabor patch (a sine wave grating within a 2-dimensional Gaussian envelope) because this stimulus is well suited to drive responses in V1 cells. I am interested in the co-variation not only between neural responses and the presence or absence of a *stimulus*, but also between neural responses and *behavior*, irrespective of this stimulus-response relationship. Thus to ensure that any observed co-variation between neuronal activity and choice are not due simply to differences in the stimulus, it is critical that these measurements be made on repeated trials of identical stimuli, and that the monkey makes a mixture of "Yes" and "No" responses for each stimulus condition. This experimental constraint means that the subject must make errors, and therefore the task must be difficult. To control task difficulty in the experiments presented here, I manipulated the contrast of the Gabor stimuli presented to the subject. Visual contrast is defined here as the difference between the maximum luminance of a visual stimulus minus its minimum luminance, divided by their sum. A Gabor stimulus whose sine wave grating has large amplitude will contain

regions of very high and very low luminance, observable as light and dark regions, making it easily detectable against a grey computer screen. A low contrast Gabor, on the other hand, contains a low amplitude sine wave and thus has only a subtle difference between its highest and lowest luminance, making it difficult for an observer to detect against a grey computer screen. Thus in these studies, to drive V1 cells effectively while simultaneously keeping the task difficult, I used Gabor targets at low contrast.

1.4 Experimental strategy

To understand the neural basis of perceptual decision-making, the ultimate goals are to discover (1) which brain areas and neurons are responsible for the steps outlined above: encoding, decoding, and decision; and (2) how the process unfolds. To implicate a given brain area or group of neurons as critical components in this processing chain, certain criteria must be met (Parker and Newsome, 1998). The researcher aims to: (1) identify neuronal signals which co-vary with attributes of sensory stimuli, (2) demonstrate that the signals are sufficient to perform a task that requires decisions about these stimuli, (3) demonstrate that the task-relevant signals co-vary with the subject's choices in the task, and finally (4) demonstrate that the signals contained in these neurons are necessary to perform the task. Here I review progress in establishing these criteria in a handful of brain areas across a few model species.

1.5 Finding stimulus-related signals in the brain

To implicate a set of neurons in the processing of sensory stimuli and formation of a decision, researchers must establish that those neurons are related to the stimulus, and hence relevant to a task requiring the subject to make decisions about that stimulus. Sensory neurons must change their firing patterns in response to various stimuli that are presented to the organism (Parker and Newsome, 1998). An enormous body of work has identified stimulus-related response properties in many brain areas. In the visual system, the groundbreaking work of Hubel and Wiesel identified neurons in cat (e.g., Hubel and Wiesel, 1962) and monkey (e.g., Hubel and Wiesel, 1968) primary visual cortex that responded selectively to visual features such as retinal position, line orientation, ocular dominance, color, and direction of motion. They defined classes of cells in V1 that differed in their receptive field properties, labeling them as "simple", "complex", or "hyper-complex" (Hubel and Wiesel, 1968), and described the functional organization of these cells into groups that share a preferred stimulus orientation, eye of origin, and responsiveness to motion. Subsequently, the response properties of cells in many areas of the visual system have been discovered and described, linking areas such as MT to motion perception (e.g., Dubner and Zeki, 1971; Maunsell and Van Essen, 1983), MST to optic flow and heading direction (e.g., Bradley et al., 1996; Saito et al., 1986; Tanaka et al., 1989), FEF and LIP to eye movement planning and decision variables (e.g., Bruce and Goldberg, 1985; Bruce et al., 1985; Gnadt and Andersen, 1988; Huk and Shadlen, 2005; Platt and Glimcher, 1997; Roitman and Shadlen, 2002), and IT to the recognition of complex objects such as hands (Gross et al., 1972) and faces (Desimone et al., 1984;

Tsao et al., 2006). Subsequent studies described higher order relationships among these areas such as the functional specialization of dorsal and ventral processing streams to serve object recognition and spatial localization functions, respectively (Mishkin and Ungerleider, 1982). Similarly groundbreaking studies have identified the basic response properties of early sensory cells in the auditory (e.g., Kiang et al., 1965; Siebert, 1965) and somatosensory (e.g., Mountcastle, 1957; Talbot et al., 1968) systems.

These pioneering studies showed that the firing patterns of sensory nerve cells respond to specific stimuli, and to specific attributes of a given stimulus, making them excellent candidates for the neurons that underlie perceptual decisions about those stimuli.

1.6 Are the signals sufficient to perform the task?

In a landmark study, Newsome et al. (1989) carried out experiments to compare the behavioral performance of a subject engaged in a binary decision task with that of a hypothetical observer who performs the same task, but whose decisions are based on the activity of individual sensory neurons collected from the same subject. The researchers measured neural activity in area MT of a Rhesus macaque monkey while the subject performed a visual motion direction discrimination task (Newsome et al., 1989). The subject viewed a motion stimulus consisting of a field of moving dots, some of which moved at random, and some of which moved coherently in one direction. The researchers controlled the difficulty of the task by varying the percentage of dots that moved coherently. When a large fraction of the dots moved in one direction, the monkey

was able to report the direction of motion with almost 100% accuracy. However as the researchers reduced the percentage of dots moving coherently, the monkey's performance dropped correspondingly, until the monkey performed at chance (50% accuracy) when the randomly moving dots had no coherent motion in one direction or another. The researchers used these results to construct a *psychometric* curve describing the accuracy of the monkey as a function of coherence. The curve began at chance on zero coherence trials, increased sigmoidally over intermediate coherences, and saturated at 100% for easy (high coherence) trials.

The researchers then used the simultaneously collected neuronal responses to construct a *neurometric* curve, which describes the ability of a single neuron to determine the direction of motion. Neurons in MT are known to change their response properties as a function of both the direction and speed of a moving stimulus, and each neuron responds best to a particular combination of these attributes. In addition, MT neurons tuned to these stimulus attributes increase their firing rates with higher motion coherence. While these neurons increase their firing rates *on average*, there is nonetheless variability in the spike rate measured at a particular coherence level, and spike counts collected across trials form stochastic distributions. The researchers collected these distributions by recording the firing rates of each neuron as it responded to motion in its preferred direction, and also in the opposite direction, at the various motion coherence levels. When motion coherence was high, the two distributions of spike counts (those collected on 'preferred' direction trials and those collected on 'non-preferred' (or 'null') direction trials) were widely separated, making it easy for a researcher with access to these

distributions to distinguish which direction of motion was presented. When motion coherence was low, however, the distributions tended to overlap considerably, making it difficult to discriminate direction of motion. The researchers employed a method based on signal detection theory (reviewed above) that allowed them to compute the performance of a hypothetical observer with access to these distributions in determining the direction of motion, and summarized the accuracy of the observer as a function of motion coherence in what they called the *neurometric* function. Here too, the accuracy of this hypothetical observer increased with increasing motion coherence.

By quantitatively comparing the psychometric and neurometric functions, the researchers found that the shape and position of these curves were similar. Indeed, when they compared the threshold value for each curve (coherence level at which the psychometric or neurometric function crosses 82% correct) they found that on average, the thresholds from the hypothetical observer were the same, or even lower than, those of the monkey. This finding showed, surprisingly, that on average the activity of a single neuron was sufficient to account for the sensitivity of the subject, and in some cases carried more information than was needed to account for the subject's accuracy (Newsome et al., 1989).

Results from subsequent studies have been mixed. On one hand, many additional studies have found that behavioral sensitivity can be accounted for by the responses of single cells or small groups of cells when measured in appropriate tasks, in brain areas including V1 (Chen et al., 2006; Geisler and Albrecht, 1997; Nienborg and Cumming, 2006; Palmer et al., 2007; Parker and Hawken, 1985; Skottun et al., 1987; Tolhurst et al.,

1983), V2 (Nienborg and Cumming, 2006), MT (Britten et al., 1996; Britten et al., 1992; Croner and Albright, 1999; Uka and DeAngelis, 2003), MST (Celebrini and Newsome, 1994), LIP (Law and Gold, 2008), S1 (de Lafuente and Romo, 2005; Hernandez et al., 2002), S2 (Romo et al., 2003), somatosensory afferents (Mountcastle et al., 1972; Talbot et al., 1968), and LGN (De Valois et al., 1967). On the other hand, some studies employing similar experimental paradigms demonstrated, instead, that behavior performance could not be explained by the sensitivities of single neurons or small groups of neurons (e.g., Cohen and Newsome, 2009; Liu and Newsome, 2005; Osborne et al., 2004; Prince et al., 2000; Purushothaman and Bradley, 2005).

Two important criticisms of the Newsome et al. (1989) study concern task timing and neuron selection. In this study the researchers used a fixed, 2-s time interval over which to collect and average neuronal activity. This interval is now generally regarded as an unrealistically long duration, since monkey inter-saccadic fixation intervals typically last only a few hundred milliseconds. Critics point out that by integrating too long, the researchers overestimated the information available to the monkey during the task, and hence biased the result in favor of the neuron. This concern was substantiated when the study was repeated in a reaction-time version of the same task (Cohen and Newsome, 2009), in which the researchers found that the neuronal sensitivity did not exceed the behavioral sensitivity.

A second criticism of this and similar studies can be made on the basis of neuron selection. Researchers often match stimulus features to those preferred by the cell under study. For example, researchers studying MT advance an electrode into the area and

monitor fluctuations in neural activity that correlates with attributes of motion stimuli. Once a cell is found and isolated, researchers often adjust the speed and direction of motion of the stimulus display to match the neuron's preferred attributes. Thus in studies comparing the sensitivity of a neuron with that of the subject, the neurons start with an advantage because they are effectively selected to show sensitivity to the stimuli being tested. While this practice does not invalidate a conclusion that neurons capable of matching or exceeding behavioral sensitivity exist, the criticism nevertheless highlights a natural question about how the brain uses information from sensory neurons: if the brain were to use the signals from the most sensitive neuron, it too must find that neuron. How? The topic of neuron selection is discussed in more detail below in the section on the lower envelope principle.

In some of the studies mentioned above, while the activity of a single neuron was not sufficient to account for the subject's behavior, the combined activity of two or more neurons could account for the psychophysical sensitivity. For example, Romo et al., (2003) measured activity of single neurons in primary somatosensory cortex (S1) while a monkey performed a vibrotactile discrimination task, and found that while individual neurons were not sufficiently sensitive to account for the behavior, subtracting the responses from two neurons with a common noise source provided enough information to match the subject's accuracy (Romo et al., 2003). The topic of combining information across multiple neurons to improve the quality of the stimulus-related information is central to this dissertation, and is introduced in more detail below in the section on readout and pooling and is pursued empirically in Chapter 3.

A third criticism of many of these earlier studies is that the comparison between neuronal and behavioral performance was made using data sets that were not collected simultaneously, or on the same trials, or in many cases even in the same animal or species. For example, Hecht and colleagues (1942) quantified the absolute number of photons needed for human observers to detect a flash of light, and Barlow and colleagues (1971) measured neuronal detection thresholds in cat retinal ganglion cells (RGCs) and compared it to the human data of Hecht from 30 years previous.

In light of this third criticism, and despite concerns related to task timing, the Newsome et al. (1989) study represents a new and powerful experimental paradigm: the simultaneous measurement of perceptually relevant neurons while an awake subject performs a simple task. In this paradigm, researchers could measure both neural activity *and* behavior, and they devised ways to evaluate the performance of the signals against the performance of the animal in directly comparable ways. The simultaneous measurement approach also enabled researchers to address the next key question in implicating a neuron in the decision processing chain: whether the firing of that neuron predicts choice.

1.7 Are the signals correlated with the subject's individual choices?

To determine whether the activity of a neuron contributes to a perceptual decision, it is helpful to determine first whether these signals co-vary with the subject's choices. To answer this question, it is critical to design an experimental paradigm, such as in the Newsome et al. (1989) study, in which neural activity and behavior are

measured simultaneously. Because of the technical difficulties imposed by these experiments, there have been comparatively few studies that measured neural activity and behavior at the same time. Many such simultaneous comparisons are carried out in awake, behaving monkeys since monkeys can be trained to perform a wide variety of tasks.

Britten and colleagues measured the activity of cells in MT while a monkey performed the same motion direction discrimination task described above (Britten et al., 1996). This time, they turned their attention to the relationship between the variable neuronal responses and the monkey's varying behavioral choices. They reasoned that if the monkey uses cells in MT to perform the task, the activity of those cells should correlate with the monkey's choices. Importantly, since the physiology and the behavior were collected simultaneously, the researchers could investigate this relationship on a trial-to-trial basis. For example, if a monkey uses the responses of an MT neuron that prefers motion in the upward direction to detect upward motion, when this cell fires more strongly the monkey should be more likely to judge the direction of motion as upwards. Stronger motion coherences in the upward direction indeed lead to stronger responses in a direction-selective cell preferring upward motion, as reviewed above. However, stronger motion coherence trials are also easier for the monkey to discriminate, making it more likely that the subject would choose the upward direction on these easier trials. Thus it is possible that any observed relationship between firing rate and choice could be due trivially to changes in motion coherence. For this reason, the researchers restricted their analysis to only those trials in which the net motion coherence was zero. This

ensured that any neuronal-choice co-variation is not due to the particular stimulus presented on a given trial. Nevertheless, the firing rate of an MT cell is inherently variable and across many presentations of zero coherence trials the firing rate of that neuron is best described with a stochastic distribution.

To quantify the relationship between neuronal firing and choice, they developed a metric, which they termed choice probability (CP), and which quantifies the ability of a neuron's responses to predict choices on a trial-to-trial basis. Choice probability was defined as the area under the receiver operating characteristic (ROC) curve applied to two distributions of neural responses belonging to the two possible choices a subject made during the same stimulus condition. The area under the curve ranges from 0.5 (when the two distributions are completely overlapping) to unity (when the distributions are non-overlapping). Choice probability represents the accuracy with which an experimenter who observes this neuron can classify trials as belonging to the correct response distribution.

Importantly, the choice probability measure defined by the ROC analysis has a number of advantages over other measures of discriminability (Parker and Newsome, 1998). First, it summarizes the ability of an observer to discriminate between distributions with a single number. In comparison, measures that rely the mean difference between two distributions also require a measure of their variability, the usefulness of which depends in turn on the shape of the distributions. Second, the ROC value can be compared directly with measures of psychophysical sensitivity, such as the subject's percent correct. Third, the ROC is a non-parametric measure, not relying on the

shape of the underlying distributions. In contrast, a discriminability measure such as d', defined as the difference in the means of the two distributions divided by their pooled standard deviation, depends on the assumption that the two distributions are normally distributed, whereas spike rates are usually modeled as a Poisson process. In this case, the distributions can deviate significantly from normality, particularly when the spike rates are low. In Chapter 2, I consider additional properties of the choice probability measure, and introduce a new metric for quantifying the relationship between neural activity and choice that has some advantages over choice probability.

The critical finding of the Britten et al. (1996) study was that the choice probability values were significantly greater than the chance value of 0.5. Their average choice probability value for MT neurons in the direction discrimination task was 0.555. This means that an observer of the spike rates of MT neurons tuned to the direction of motion presented could correctly guess the monkey's choices 55.5% of the time (Britten et al., 1996).

Significant choice probabilities have since been discovered in a variety of brain areas, including MT (Cohen and Newsome, 2009; Croner and Albright, 1999; Dodd et al., 2001; Law and Gold, 2008; Liu and Newsome, 2005; Purushothaman and Bradley, 2005; Uka and DeAngelis, 2004), MST (Celebrini and Newsome, 1994), LIP (Roitman and Shadlen, 2002; Shadlen and Newsome, 2001), S2 (Romo et al., 2002), MPC (de Lafuente and Romo, 2005), V2 (Nienborg and Cumming, 2006; Nienborg and Cumming, 2007), as well as TE and TEO in the ventral visual pathway (Uka et al., 2005). An exciting sequence of studies measuring choice probability along an ascending pathway

involved in somatosensory perception found increasing choice probability values as the researchers ascended the pathway from sensory to motor areas, including S1, S2, VPC, MPC, and M1 (de Lafuente and Romo, 2006; Romo et al., 2004).

In a study highly relevant to the current work, Palmer et al. (2007) conducted an experiment in which monkeys were engaged in a visual detection task with a Gabor patch target (nearly identical to the task employed in this dissertation) (Palmer et al., 2007). The researchers recorded single- and multi-unit activity as well as local field potential signals from V1 while the monkey performed the task. For each low-contrast target condition, the monkeys made a mixture of correct and incorrect responses (Hits and Misses), allowing the researchers to apply the choice probability analysis of Britten et al. (1996) to this V1 dataset. They found a mean CP value near 0.60, suggesting that on average, a neuron from their database could predict the monkey's decision with 60% accuracy for these target-present trials. The choice probabilities were roughly similar for SU, MU, and LFP measures. Interestingly, however, when they applied the same analysis to the target-absent trials (comparing spike rates on False Alarms with those on Correct Rejections), they found no significant CP. Nevertheless, whereas previous studies had failed to find significant choice-related activity in V1 (e.g., de Lafuente and Romo, 2005; Nienborg and Cumming, 2006) this study is the first to show significant single-cell CP in V1.

1.8 Are the signals necessary to perform the task?

Having identified signals that (1) are relevant to a particular task, (2) carry sufficient information to perform the task, and (3) show trial-to-trial co-variation with the subject's choices, the final piece of the puzzle in implicating a single neuron in the stimulus-to-choice processing chain is to determine whether these signals are *necessary* to perform the task. There are two main types of experiments used to establish this causal relationship.

First, in experiments in which neural activity and behavior are measured simultaneously, it is possible to ask whether physically altering the neural activity will correspondingly alter behavior. In another landmark study, Salzman (1992) et al. reasoned that if MT neurons are used in the decision process, electrical stimulation of MT cells that are likely to be used by a monkey to perform the direction discrimination task should bias the monkey's responses in favor of the preferred direction of the stimulated neurons (Salzman et al., 1992). They began by describing the monkey's behavior with a psychometric curve, which in this case described the proportion of trials in which the monkey chose the neuron's preferred direction of motion. When motion coherence was high the monkey nearly always chose the neuron's preferred direction, whereas when it was ambiguous (zero coherence trials) they monkey made a mixture of choices to the preferred and non-preferred direction, and when it was negative (motion was presented in the opposite of the neuron's preferred direction) the monkey almost never chose the cell's preferred direction. As before, this psychometric function rose sigmoidally from zero to

unity as motion coherence ranged from large negative values, through zero coherence, and finally to large positive values (Salzman et al., 1992).

On a fraction of trials, the researchers stimulated MT cells by injecting a small amount of current through tungsten microelectrodes positioned at the center of a cluster of cells representing the direction of motion being discriminated. They found that electrical stimulation shifted the psychometric curve leftward, meaning that stimulation was associated with a higher proportion of choices to the neurons' preferred direction. Furthermore, they showed that the degree to which this behavioral function shifted leftward depended monotonically on the amount of current injected into the stimulation site. This result provides strong evidence that monkeys indeed use the responses of MT neurons to perform the direction discrimination task.

Other microstimulation studies have similarly demonstrated a causal relationship between choice behavior and neural activity in relevant brain areas, including V1 (Tehovnik et al., 2004), MT (DeAngelis et al., 1998; Ditterich et al., 2003; Groh et al., 1997; Liu and Newsome, 2005; Murasugi et al., 1993; Salzman et al., 1990; Salzman et al., 1992; Salzman and Newsome, 1994; Seidemann et al., 1998), MST (Britten and van Wezel, 1998; Celebrini and Newsome, 1995), FEF (Fujii et al., 1998; Seidemann et al., 2002), S1 (Romo et al., 2000; Romo et al., 1998), MPC (de Lafuente and Romo, 2005), SMA (Mitz and Wise, 1987), cerebellum (Noda and Fujikado, 1987a; Noda and Fujikado, 1987b), and the striatum (Alexander and DeLong, 1985a; Alexander and DeLong, 1985b), linking these areas to specific actions or judgments (for a review, see Cohen and Newsome, 2004).

Second, researchers can ask whether removing or inactivating the relevant neurons would produce performance deficits. Researchers investigating the contribution of area MT to performance on the motion direction discrimination task reasoned that selective lesions to area MT should selectively reduce the monkey's ability to perform the task (Newsome and Pare, 1988). In this study the researchers injected into area MT small amounts of ibotenic acid, a neurotoxin that kills neuronal cell bodies while leaving the underlying white matter unaffected (Newsome and Pare, 1988). After being injected with the neurotoxin, monkeys performing the direction discrimination task showed substantially reduced performance, with behavioral thresholds increasing by 400-800%. To ensure that this result was selective to MT and the motion direction discrimination task, the researchers performed two types of controls. First, they tested the performance of the same monkeys before and after the lesions in the contralateral hemifield, and found that behavioral thresholds were unaffected. Second, they measured performance on an unrelated orientation discrimination task, in which monkeys were required to discriminate between two orientations of a stationary sine wave grating at threshold contrasts. Presumably, performance in the contrast-sensitivity task is mediated by neurons in areas outside MT and performance on this task should therefore be unaffected by the lesions. Indeed the researchers found that thresholds on this task were indistinguishable before and after the MT lesions, in both hemifields. These results provide further strong evidence that cells in MT are necessary to perform the motion direction discrimination task (Newsome and Pare, 1988).

Interestingly, the monkeys' performance recovered several days following the ibotenic lesions. This result indicates that over a short time, the brain was able to adapt to the injury, either by using signals from cells in MT that were not affected by the neurotoxin, or by using signals from other brain areas, or both. The researchers addressed these possibilities by injecting additional amounts of ibotenic acid into the site with the goal of creating a full unilateral lesion of MT. Following these additional lesions, performance again dropped to levels similar to those following the first round of injections, but performance *again* recovered somewhat (though not fully) over a period of three weeks following the second round of lesions (Newsome and Pare, 1988). This fact underscores the parallel nature of neural processing and reminds us to consider that multiple brain areas could contribute to the performance of a particular psychophysical task, even when one area is known to be involved. Nevertheless, this lesion study demonstrates unequivocally that cells in area MT are involved in the performance of the motion direction discrimination task.

Other lesion studies have similarly demonstrated a causal relationship between perceptual judgments or motor actions and various brain areas including MT (Newsome and Pare, 1988; Newsome et al., 1985; Yamasaki and Wurtz, 1991), and MST (Dursteler and Wurtz, 1988; Yamasaki and Wurtz, 1991).

When neither microstimulation nor lesion data are available, it is still possible to address the question of causality (though often not as definitively) by investigating the time course of signals that correlate with behavior. For example, if the observed choice-related signals occur only after the subject indicates his choice, it is clearly not possible

that the signals caused the behavior. More likely, these signals are the result of a feedback mechanism in which a copy of the decision related information that drives the motor response is sent back to the encoding area (e.g., Nienborg and Cumming, 2010; Nienborg and Cumming, 2009), perhaps as a signature of attention (e.g., Nienborg and Cumming, 2009; Ress et al., 2000), or to adjust bias or expectations for future trials (e.g., Gold and Shadlen, 2003). On the other hand, if the choice-related signals occur before the subject indicates his choice, it is less clear whether these signals *led* to the decision. In these cases, researchers have appealed to the shape of the choice-related signals over time, and parsimony, to argue that the signals in their studies are causally related, or not causally related, to the decision.

Multiple studies have appealed to a short latency between the onset of the stimulus-evoked response and the choice-related signal to assert that the choice-related signals occur as part of a feed-forward process (Britten et al., 1996; Celebrini and Newsome, 1994; Dodd et al., 2001; Liu and Newsome, 2005; Nienborg and Cumming, 2006; Palmer et al., 2007; Uka and DeAngelis, 2004), though some studies have rejected this bottom-up interpretation in favor of a top-down explanation, again based on the shape of the choice-related signals over time (e.g., Nienborg and Cumming, 2009; Uka and DeAngelis, 2003).

Recent evidence for a top-down mechanism in a perceptual decision task comes from Nienborg and Cumming (2009). The researchers investigated the relationship between V2 neurons and a monkey's behavior in a course depth disparity discrimination task. The monkey viewed a circular random dot stereogram that contained a disparity

signal that changed randomly on each video frame, and was required to choose at the end of each trial whether the stimulus appeared to be "near" or "far". This task design allowed the researchers to use reverse correlation to estimate the monkey's psychophysical kernel – a picture of the mean disparity signal on trials in which the monkey chose "near" compared with those in which he chose "far". They computed the amplitude of the kernel as it evolved in time across the trial, and also computed the monkey's choice probability as it unfolded over the same time interval. They found that the amplitude of the psychophysical kernel rose sharply at the beginning of the trial and decreased steadily as the trial progressed; in contrast, the time course of the choice-related signal started low, then rose to a plateau. However, the rise in the choice-related signal occurred well after the peak of the kernel amplitude signal. This finding shows that the V2 neurons' correlation with choice emerged only *after* the monkey made its decision and is therefore inconsistent with a feed-forward explanation of the relationship between neural activity and choice. The authors concluded that the observed choice-related signal in V2 was the result of a top-down mechanism similar to attention (Nienborg and Cumming, 2009).

1.9 Populations

Taken together, the studies reviewed above constitute a great achievement in elucidating the neural basis of perceptual decisions. Researchers have not only identified cells in the brain that are potentially useful in forming a decision about sensory stimuli, but have also found cells whose activity co-varies with behavioral choice, and in some

cases, have shown that these cells are necessary to perform the task and indeed causally influence the subject's decision. Such neurons are unequivocally implicated in the processing chain that connects stimulus to behavior.

But there are critical questions that remain unanswered, and which must be answered if we are to have a complete picture of how a perceptual decision is formed from sensory evidence. These questions are central to this dissertation.

First, if such neurons are indeed used by the subject in the formation of a decision, why is the observed relationship between neural activity and behavior so weak? Specifically, why are the choice probability values reported in the above experiments so low? Choice probabilities such as 0.555 reported in the MT experiments and 0.60 in the V1 experiments suggest that cells in these brain areas, which ostensibly provide the information upon which a subject can base an informed decision, can account for only approximately 56% or 60% of the choice-related information. While the significant choice probabilities suggest that these neurons are related to behavior, why are the behavioral predictions nevertheless so weak? What else is driving the decision?

Second, although the accuracy of a subject can often be explained by the activity of a single neuron, it seems unlikely that an organism would use just a single cell to perform any task. A natural question is: if a single neuron carries so much information, why doesn't the animal combine information from many such cells to improve the quality of the sensory evidence, and thereby gain additional information to perform even better? Furthermore, if some cells have been shown to carry *more* information than is necessary

to account for the monkey's behavior, why does the monkey not use this information? What is the source of the inefficiency?

It is critical to address both of these classes of questions by turning our attention to the activity of *populations* of neurons, rather than just single neurons, involved in a perceptual task. Neurons, of course, do not exist in isolation; they are part of a vast network in which the average neuron may receive inputs from a heterogeneous population of one thousand or more other cells, giving rise to a complex structure of inter-neuronal correlations (e.g., Zohary et al., 1994) that may vary as a function of cortical distance (e.g., Chen et al., 2006), similarity in response properties (e.g., Kenet et al., 2003; Ts'o et al., 1986; Tsodyks et al., 1999) and brain area (Leopold and Logothetis, 2003), and whose structure may be modulated by behavioral context (e.g., Gold and Shadlen, 2003). Furthermore, sensory physiologists have known for many years that neural responses to sensory stimuli are distributed across large populations of neurons in sensory cortex, and thus in principle, useful task-relevant information may be distributed across this population as well.

To achieve a complete picture of the formation of a perceptual decision, we must therefore have a cohesive model that explains the role of populations of neurons in the formation of the decision. The population model should account for multiple, well-established observations together: (1) that sensitivities of some individual or small groups of neurons are comparable to behavioral sensitivities, (2) weak choice probabilities of individual neurons, and (3) the presence of weak inter-neuronal correlations.

Two classes of models have been proposed. The first type of model is based on the *lower envelope principle*, which states that the behavior of the subject is determined by the activity of the most sensitive neurons of the population. The second type of model proposes that neuronal signals across the population are *pooled* by a central mechanism, which then uses the combined signals to form the decision. Here I review the evidence for each model.

The Lower Envelope Principle

The lower envelope principle (LEP) hypothesizes that in order to form a decision, subjects rely on the activity of the most sensitive neuron, or the neuron that carries the most task-relevant information. A striking illustration of the lower envelope principle comes from the data of Mountcastle and colleagues (Mountcastle et al., 1972; Talbot et al., 1968). The researchers employed a tactile flutter detection task, in which primate subjects were required to detect the presence of an oscillating mechanical stimulus applied to the hand. There are two classes of nerve fibers which innervate the hand and carry information related to a periodic stimulus: quickly adapting (QA) fibers, which respond best to low frequency oscillations and thus act as low-pass filters, and Pacinian corpuscle (PC) fibers, which respond best to higher frequencies. The researchers measured the responses of these cells in the monkey across a broad range of frequencies, and computed neuronal detection thresholds by determining how well a hypothetical observer with access to the neuronal response distributions could detect the stimulus. They found that at each stimulus frequency, the detection thresholds of the nerve fibers

varied from cell to cell, in both QA fibers and PC fibers. They also found that in the low frequency ranges, the *lowest* detection thresholds were found in the QA fibers whereas in the higher frequency ranges the lowest thresholds were found in the PC fibers, as expected. The researchers then defined the theoretically best detection performance across all frequency ranges as the curve that followed the lowest detection thresholds of *either* the QA *or* the PC fibers, which was determined by the QA fibers in the low frequencies and the PC fibers in the high frequencies.

The researchers compared these neural sensitivities to psychophysical detection thresholds in both monkey and human observers across the same frequency range and obtained an intriguing result: detection thresholds in both species, when plotted as a function of stimulus frequency, followed the lower envelope of the neuronal detection thresholds obtained from the QA or PC fibers. In other words, the psychophysical thresholds were predicted by the most sensitive neurons at each frequency, regardless of whether the best neuronal performance was achieved by QA or PC fibers. This striking result provides support for the idea that behavioral sensitivity is determined by the sensitivity of the most informative neurons.

The lower envelope principle could explain the results of the many studies reviewed above in which neuronal sensitivity of single neurons was comparable to the behavioral sensitivity of the subject. Furthermore, there have been a variety of additional studies that are compatible with this principle, including studies measuring behavioral and neuronal performance in tasks suited for neurons in MT (Purushothaman and

Bradley, 2005), LGN (De Valois et al., 1967), cat auditory cortex (Eggermont, 1999), somatosensory cortex (Talbot et al., 1968), and V1 (Tolhurst et al., 1983).

However, there are important concerns with the biological plausibility of implementing such a mechanism in the brain. Foremost among them: if a single neuron is responsible for the behavioral performance of a subject, how does the decision mechanism select this neuron from the thousands of candidates? For the brain to achieve this feat, it would need to monitor a large pool of neurons, determine which neuron provides the highest fidelity information about the stimulus, and then ignore all other neurons in the pool. Furthermore, in this rubric where behavior is determined by a single neuron, Parker and Newsome remind us that logically, it can't be the same neuron on every trial (Parker and Newsome, 1998). For example, in a variant of the flutter detection task described above, suppose that the stimulus consists not just of a pure frequency of stimulation, but of a combination of frequencies. In this case, because there is variation in the neuronal responses from trial to trial, it is likely that detection on a given trial could be best accomplished by monitoring one of the QA fibers, or one of the PC fibers (Parker and Newsome, 1998), but that the most informative fiber may reside in the QA population on one trial and in the PC population on the next.

Furthermore, this problem of selection may be magnified in the central nervous system. As Parker and Newsome (1998) point out, many of the studies providing support for the LEP come from investigations in the peripheral nervous system. Anatomically, peripheral pathways diverge as they enter the central nervous system, implying that the same signals, which in the periphery may be confined to a small number of neurons,

become distributed over a much larger population as they make their way into ever-higher regions of the CNS. This means that the challenge of finding the right neuron is likely magnified as afferent signals reach more central areas.

Pooling

The pooling hypothesis suggests that perceptual decisions are determined not by the activity of the most sensitive neuron, but rather by the combined activity of a population of neurons. Shadlen et al. performed one of the earliest comprehensive modeling exercises demonstrating the success of the pooling concept (Shadlen et al., 1996). They focused on data gathered over the years from monkey MT in the classic motion direction discrimination paradigm (Britten et al., 1996; Celebrini and Newsome, 1994; Newsome et al., 1989; Zohary et al., 1994). In this study, the authors sought to use the pooling hypothesis to reconcile three observations of these MT studies: that single MT neurons are on average sufficiently sensitive to account for the monkey's accuracy; that MT neurons are weakly correlated with choice; and that MT neurons are weakly correlated with one another.

A critical observation is at the heart of their strategy and reasoning: correlations among neurons limit the effectiveness of pooling. This fact has been long recognized, though this work is among the earlier studies to incorporate it into a cohesive theory. To illustrate, consider first a population of statistically independent MT neurons. Each neuron carries information about the direction of motion, responding more strongly to high coherence motion than to low coherence motion. As reviewed above, the ability of

this neuron to discriminate direction of motion is limited by the stochastic nature of its responses. However, by averaging this neuron's responses with those of a second, statistically independent neuron, the average variability is reduced because the neurons share no common noise. By incorporating ever more neurons into the calculation, the variability continues to be averaged out in the familiar way, providing a reduction in noise proportional to the square root of the total number of neurons included in the average.

In contrast, if the neurons included in the averaging pool share a common noise source, then a simple average of their responses will reduce noise less effectively. In the limit where all neurons share 100% of their variability with one another, averaging would provide no additional information whatsoever. In reality, neurons in MT are neither independent nor 100% correlated; they may share approximately 0.12 of their variability on average (Zohary et al., 1994). This finding implies that as neurons are added to the pool, the discrimination performance of the pool will improve, but only to a limit.

The presence of correlated noise is expected to increase choice probability. Consider a case where the animal's choice is based solely on the population in MT. If the neurons share 100% of their variability with one another, then the activity of a single neuron is identical to that of the pool, and because no other factor drives the subject's decision in this example, variation in choice is entirely accounted for by this neuron. In the presence of weaker correlations, however, the variation in this single neuron explains only a fraction of the total variability of the population upon which the subject's choices are based; under these circumstances we expect the relationship between this neuron's

variability and the subject's choice behavior to weaken. If the neurons in the pool shared no common noise, the single neuron would account for an immeasurably small fraction of the subject's choice behavior (Shadlen et al., 1996).

The researchers also considered the effect of downstream noise, or independent noise that influences the subject's decision but that is added after the pool has been averaged. The presence of downstream noise should decrease the subject's accuracy even while the sensitivity of single neurons remains the same; it should also decrease choice probability. This type of independent noise degrades the fidelity with which the pooled response represents the stimulus feature, and thus reduces the amount of task-related information available to the subject at this critical decision stage. The addition of downstream noise also obscures the relationship between the variability of single MT neurons and that of the subject's choices because under these circumstances the subject's decisions are based in part on random variation that is not captured in the experimenters' measurement.

The researchers explored these relationships in a series of computational models. They varied the number of neurons contributing to each pool, and sought to find a pool size that could account simultaneously for the measured neuronal sensitivity, behavioral sensitivity, inter-neuronal correlations, and choice probability. Their model architecture consisted of two pools of neurons, one pool preferring the direction of motion presented, and the other preferring the opposite direction. On each trial, the responses in each pool are averaged together, and the averages from the two pools are compared. If the 'preferred' pool's average response is greater, then their simulated monkey chose

"preferred"; otherwise the subject chose "null." In this model the researchers fixed the average correlations among neurons to 0.12, following the experimental observations of Zohary et al. (1994). The key free parameters in their model were the number of neurons N in each pool, the sensitivity of each neuron, a scaling factor to model the inclusion of sub-optimal neurons, and pooling noise (variability added to the decision variable *after* averaging each pool).

In the simplest model, only the best available neurons were considered (neurons collected in the experiments whose tuning preferences were matched to the stimuli). No pooling noise was added at this stage. The researchers ran simulated experiments by presenting a simulated motion signal to the neurons and observing their responses. When only one neuron contributed to each pool, the sensitivity matched that of the observed sensitivities, consistent with their experimental observation (Newsome et al., 1989). Increasing the number of neurons improved discrimination thresholds, but only to values too low to account for the real experimental results. Examining the effect on choice probability, they found that in this framework a single neuron should provide a CP near 0.80, a value too high to match the real data. Adding neurons to the pool did reduce choice probability, but due to even the modest correlation coefficient used, this reduction was limited in principle, and leveled off to a value near 0.65, still too high to account for the real data. Thus this simple version of the model could not find a single pool size that could reconcile all the experimental observations simultaneously.

To improve their model, the researchers reasoned that including non-optimal neurons in each pool should reduce the sensitivity of the pool as a whole because they

will corrupt the high fidelity signals provided by optimal neurons. This version of the model is perhaps more plausible if one assumes that the animal has difficulty selecting the best neurons in a given task, as suggested above in the section on the lower envelope principle. When including less sensitive neurons, the researchers found that while the sensitivity of a randomly selected neuron was lower than that observed experimentally (consistent with their reasoning that non-optimal neurons corrupt the high quality signals), they could easily regain the sensitivity of the model by averaging over just four or so neurons to reduce this noise. On the other hand, the addition of non-optimal neurons had no effect on choice probability, regardless of pool size, and so the modeled CP remained too high to match the data.

Finally, the researchers added central pooling noise downstream to the sensory neurons, and were able to find a value for this noise that made the predicted thresholds match those of the real subjects, and a value that matched the observed CP values; but no single value of pooling noise could match both simultaneously. However, by adding both downstream pooling noise *and* non-optimal neurons, they found values of pooling noise, and a pool size, that could simultaneously account for both the sensitivity results as well as the choice probability results.

With this success in hand, the researchers aimed to account for an additional experimental observation: that more sensitive neurons showed higher choice probabilities (Britten et al., 1996; Celebrini and Newsome, 1994). The empirically reported inter-neuronal correlation of 0.12 for area MT is an average value, but there is considerable variability in this value across neuron pairs (Zohary et al., 1994). To

explore the consequences of this fact, the researchers added heterogeneity to the structure of pairwise correlations across the population. They reasoned that neurons that are more tightly correlated with the rest of the neurons contributing to the average should co-vary more tightly with the pooled average, and therefore the decisions (Shadlen et al., 1996). Indeed, by assigning correlation coefficients between pairs of neurons proportional to their sensitivity, they were able to reproduce the result that higher CP values are associated with more sensitive neurons.

This investigation and others that support a pooling mechanism (e.g., Britten et al., 1992; Darian-Smith et al., 1973; Kiang et al., 1965; Siebert, 1965) and those that address the effects of inter-neuronal correlations on signal quality and choice behavior (e.g., Gawne et al., 1996; Gawne and Richmond, 1993; Johnson, 1980; Johnson et al., 1973; van Kan et al., 1985) are critical to this dissertation, because they lay out the framework for simultaneously accounting for key empirical measures (neuronal sensitivity, behavioral sensitivity, choice probability, and inter-neuronal correlations) by appealing to populations rather than single neurons. They uncover three general principles that are central to the modeling studies presented in this dissertation:

1. Inter-neuronal correlations reduce pooling efficacy
2. Inter-neuronal correlations increase choice probability
3. Downstream noise reduces both behavioral sensitivity and choice probability

Pooling and lower envelope principle compared

Geisler and Albrecht (1997) performed a study that considers both the lower envelope principle and the pooling hypothesis. To determine whether visual neurons contain sufficient information to perform various tasks, the researchers measured spiking activity from neurons in V1 of anesthetized cats and monkeys, while the animals were shown drifting sine wave gratings of various contrasts, spatial positions, orientations, spatial frequencies, temporal frequencies, and directions of motion. The responses of these cells were fitted with descriptive functions, allowing the researchers to determine each neuron's hypothetical performance on a detection, discrimination, or identification task. They then compared the performance of these neurons to the performance of human and monkey observers engaged in an identical task, and found that the responses of the best performing cells in V1 were able to account for the accuracy of the subjects. However, they also tested the pooling hypothesis by combining the signals across neurons in a mathematically optimal fashion, and found that the optimally pooled signals also were able to account for performance. Thus their results appeared to be compatible with both the lower envelope principle and population pooling. However, one observation was incompatible with the idea that performance could be explained by the most sensitive neurons. The researchers point out that in a contrast discrimination task, the most sensitive neuron covers only a limited range of contrasts, unlike psychophysical performance. Based on this observation, they conclude that contrast discrimination performance more likely reflects the pooled information of a variety of neurons, each with its own contrast sensitivity function (Geisler and Albrecht, 1997).

In practice, the lower envelope principle may be regarded as a special case of the pooling hypothesis because basing behavioral responses on the activity of a single neuron is the formal equivalent of a pooling procedure with a weight of unity assigned to the neuron in question and weights of zero assigned to all other neurons. Thus in practice, distinguishing between the two hypotheses may be achieved by first assuming the more general pooling framework, and then discovering the actual weights assigned to the various neurons that potentially contribute to a decision. This analysis is performed in Chapter 3.

1.10 Accounting for behavioral sensitivity with neuronal populations

A recent study (Chen et al., 2006) used voltage-sensitive dye imaging (VSDI, reviewed below) to examine the neuronal sensitivity of an entire population of neurons by imaging the activity of V1 as a monkey performed a visual detection task (a task similar to that used in the present experiments). The VSDI responses to a small Gabor stimulus were distributed across a population of cells over a few mm of cortex. As in the studies reviewed above, the researchers asked whether the sensitivity of the VSDI population signals could account for the sensitivity of the monkey. They examined a family of candidate pooling models that combined the signals across space to form the decision variable. The pooling models examined included one that chooses only the maximal response location on each trial, a model that chooses only the location with the best signal-to-noise ratio, simple average models with uniform weights over various sized regions, and models that compute a weighted average of the signals, with weights

proportional to either the signal amplitude at each location or signal-to-noise ratio at each location. Importantly, as discussed above, the presence of weak spatial correlations across the population of neurons limited the effectiveness of these pooling rules. The researchers derived the mathematically optimal readout mechanism, which takes into account the observed correlations across space. Due to the structure of the correlated noise, the optimal model consisted of a weighted average with weights defined by a difference of Gaussians, where positive weights were given to a region centered on the peak of the evoked response and negative weights were given to the surrounding region. The accuracy of this optimal model in the visual detection task outperformed that of the monkey. The authors concluded because the V1 signals contain more than enough information to account for the monkey's accuracy, there must be some form of inefficiency in how the monkey uses these signals. This inefficiency could be due to the monkey's use of a non-optimal pooling rule, or the presence of downstream decision noise, or both.

Importantly, while the Chen et al. study answered how a monkey *should* read out V1 population signals to perform a detection task, in this dissertation I ask how a monkey *does* read out the population signals. This allows us to address the source of the monkey's inefficiency. In this dissertation, I present a theoretical model that explains how the quality of the population signal is degraded by the monkey's readout algorithm, and use this model to determine the sources of inefficiency in task performance. This model is the subject of Chapter 3.

1.11 Kinds of inefficiency

The Chen et al. study demonstrates that populations of neurons in V1 carry more than enough information to account for the monkey's performance in the visual detection task (Chen et al., 2006), implying that some signals that are available to the monkey are not being used. What is the source of the inefficiency? In principle, there are at least two reasons why the monkey may not be able to make efficient use of all the information carried by the neural population.

First, to extract the most information possible from the V1 population, it is necessary to pool the signals appropriately, as the Chen et al. study shows. The researchers found that the mathematically optimal pooling procedure was to weight the signals across space by a difference of Gaussians, consisting of positive weights on the center of the evoked response and negative weights in a surround region. This procedure effectively whitens the spatially correlated noise, maximizing the information gained by pooling while minimizing common noise. It is possible, however, that uncertainty about the stimulus could limit the monkey's ability to use such an algorithm. If the monkey has internal uncertainty about the stimulus, such as its exact location in visual space, the Chen et al. optimal model cannot be effective because it assumes that the readout mechanism has perfect knowledge about where the stimulus will appear.

A recent pair of experimental and modeling studies supports the idea that a subject's performance is significantly limited by the ability of the brain to decode sensory information (Law and Gold, 2008; Law and Gold, 2009). In this work, the researchers recorded single unit activity in areas MT and LIP while monkeys learned to perform the

motion direction discrimination task. They found that as training progressed across sessions, the improvement in psychophysical performance was accompanied by an improvement in sensitivity of LIP neurons, but not in MT neurons (Law and Gold, 2008). LIP receives rich anatomical projections from MT and carries decision-relevant signals based on motion direction evidence from MT neurons (Huk and Shadlen, 2005; Mazurek et al., 2003). Thus this study demonstrates that training improves signal quality in the decision stage, but not in the encoding stage, a result consistent with the idea that training improves decoding of sensory signals. The researchers confirmed in a subsequent modeling study that the observed improvement in behavior could indeed be explained by a reinforcement learning procedure in which LIP signals reflect an increasingly efficient decoding of fixed, stimulus-related signals in MT (Law and Gold, 2009).

A second way in which high quality information in a sensory area could be degraded is by the addition of downstream, stimulus-irrelevant noise. For example LIP neurons, which accumulate evidence provided by area MT about a motion stimulus (Huk and Shadlen, 2005), are inherently variable. If such a neuron's response is evaluated against a criterion in order to determine the decision, this additional random variability will sometimes cause the neuron's response to cross the criterion and elicit a behavior even before sufficient evidence has been reached, and vice versa. A similar effect can occur when the subject has some uncertainty or variability in the value of the criterion itself. This variability, termed criterial noise, also results in the mixing of the two distributions by causing some responses from the lower distribution to exceed the criterion, and vice versa, and produces the same effects.

1.12 Stimulus versus choice

In another of the few studies measuring population activity in early visual cortex while subjects performed a pattern detection task, Ress and Heeger (2003) found an interesting relationship between neural activity and choice. The researchers measured population activity in V1, V2, V3, V3a, and V4 by fMRI while four human subjects attempted to detect slight contrast increments against a noisy background. Behavioral responses were collected and grouped into the usual signal detection theory categories of Hit, Miss, False Alarm, and Correct Rejection. The retinotopically specific activity in these areas was then analyzed separately for each of the behavioral categories. They found that the activity during Hit trials exceeded that during Miss trials, and that activity during False Alarm trials exceeded that during Correct Rejection trials, results that are expected from the signal detection theory framework (Ress and Heeger, 2003). Importantly, they also found that the activity on False Alarm trials exceeded that on Miss trials. In other words, the activity in these early visual areas corresponded more closely to the subject's choice than to the physical stimulus.

At first this result may be surprising: we might expect that early sensory areas encode stimuli, and should therefore represent stimulus-related activity, while later brain areas hold decision variables, and should represent decision-related activity. However, that False Alarm activity exceeds Miss activity is in fact the expected result from signal detection theory if the majority of the choice-related noise was captured in their measurements, as I show in Chapter 2. It is plausible that the researchers captured the majority of the choice-related activity, for two reasons. First, the activity was measured

over a large population of neurons, perhaps leaving few task-relevant sensory neurons unaccounted for. And second, consistent with the conclusions of the Law and Gold studies reviewed above, variability in downstream decisional areas is likely to be reduced in well-trained subjects. This reduction can occur either by the application of an increasingly efficient spatial pooling algorithm or by a direct reduction in noise of the decision variable or criterion, leaving little choice-related neural variability unaccounted for during sensory population measurements. In Chapter 2, I demonstrate that the relationship between False Alarm activity and Miss activity is a critical indicator of how much choice-related variability is present in an experimenter's measurement of a given brain area.

1.13 Voltage-sensitive Dye Imaging (VSDI)

Optical imaging with voltage-sensitive dyes (VSDs) is a modern technique that measures neural population responses at high spatial and temporal resolution (Grinvald et al., 1988; Grinvald and Hildesheim, 2004; Shoham et al., 1999). In this technique, blue dye molecules applied topically to the cortex bind to neuronal membranes and produce a linear change in fluorescence in response to changes in membrane potential. The dye signal is thought to represent locally summed, sub-threshold neural activity (Shoham et al., 1999). The signal is therefore similar to measurements of local field potential (LFP) and event related scalp potentials (ERPs), though it may have a stronger contribution from intracellular components (Grinvald et al., 1984). Compared with measurements of similar time resolution, VSDI pools over a larger region than single- and multi-unit

recordings, but is more spatially localized than the local field potential (Grinvald, 2005), and thus does not suffer from the source localization problems that scalp potentials do. Compared with other measurements of population activity, such as the hemodynamic measurements of PET and fMRI, the VSDI signal provides higher spatial resolution, albeit over a smaller region. Its main advantage over other imaging techniques is that it can simultaneously achieve the time resolution of single unit electrophysiology and ERPs, while providing high-spatial resolution across a distributed population of neurons.

Voltage-sensitive dye imaging has been used to measure neural activity in the squid giant axon (Grinvald and Hildesheim, 2004), whisker barrels of rat somatosensory cortex (Petersen et al., 2003; Petersen and Sakmann, 2001), the optic tectum of the frog (Grinvald et al., 1984), salamander olfactory bulb (Cinelli et al., 1995a; Cinelli and Kauer, 1995; Cinelli et al., 1995b), visual cortex of the cat (Arieli et al., 1996), and has been successfully applied to measuring population responses in the awake behaving monkey (Seidemann et al., 2002; Slovin et al., 2002). The development of an artificial dura, which replaces the optically opaque dura mater in a subject with an optically transparent silicone substitute (Arieli et al., 2002), has allowed researchers to image cortical dynamics in monkeys over long periods of time. With this advancement, researchers can measure VSDI signals from the same patch of cortex across multiple sessions spanning up to a year without significant damage to the tissue due to infection or phototoxicity (Chen et al., 2006; Chen et al., 2008; Slovin et al., 2002).

Recent VSDI experiments in awake, behaving monkeys have shown the excellent sensitivity of the dye measurements (Chen et al., 2006). Chen et al. measured neural

population responses in monkey V1 while the animal performed a threshold visual detection task (a task similar to that used in the experiments presented in this dissertation). As reviewed above, the researchers compared detection thresholds of an ideal observer with access to the dye signals to behavioral detection thresholds of the monkey. They found that detection thresholds as determined by the neural population activity were lower than the simultaneously collected behavioral thresholds, demonstrating that the sensitivity of the dye measurement exceeds the sensitivity of the entire organism (Chen et al., 2006).

VSDI is thus the ideal technique for addressing the questions outlined in this introduction. First, VSDI permits the measurement of a large population of neurons, and therefore allows us to address fundamental questions about perceptual decision-making in the context of populations rather than single neurons. Second, because VSDI can be achieved in awake, behaving monkeys, we can employ this technique in a choice-probability paradigm. Together with simple computational models, this experimental approach allows us to quantify the fraction of choice-related variability present in a sensory cortical population, and also allows us to estimate, for the first time, a spatial pooling algorithm that may provide the mechanism for a simple decision.

1.14 Summary

A considerable body of research has evaluated the role of sensory neurons in the formation of a perceptual decision by examining their responses to stimuli, their overall sensitivity in comparison with behavioral sensitivity, their co-variation with behavioral

choice, and their causal relationship to choice. Across a variety of brain areas and sensory modalities, researchers have often found that (1) the sensitivity of a single or small groups of neurons can account for the subject's performance, (2) single neurons show weak co-variation with choice, and (3) neurons within a given brain area are weakly correlated with one another.

Modeling studies have attempted to reconcile these findings into a cohesive framework by appealing to *populations* of neurons rather than neurons in isolation. The general conclusions of such exercises are that (1) inter-neuronal correlations reduce pooling efficacy, (2) inter-neuronal correlations increase choice probability, and (3) downstream noise reduces both behavioral sensitivity and choice probability.

Two recent studies measuring neural activity and behavior simultaneously in a visual detection task have demonstrated significant choice probability in monkey V1 for the first time (Palmer et al., 2007), and demonstrated that optimally pooled populations of V1 neurons can more than account for the monkey's sensitivity (Chen et al., 2006; Chen et al., 2008) in this task.

In this dissertation, I employ a visual detection task with large repetitions of trials at the monkey's behavioral threshold, while simultaneously imaging neural population activity in V1 by VSDI as the monkey performs the task. This allows the simultaneous *population* measurement of each of the critical variables reviewed in this introduction: neural sensitivity, behavioral sensitivity, inter-neuronal correlations, and choice-related signals.

Within this research paradigm, I pursue two classes of questions that further our fundamental understanding of how decisions are formed:

1. How is choice-related variability distributed across sensory cortex, and what fraction of choice-related variability is present in population activity in V1, the earliest cortical area in which visual information is encoded in the primate brain? To what degree does this sensory cortical variability limit perceptual decisions?
2. How does the monkey combine information across the sensory population to form the basis of a decision; and to what degree does this decoding process limit perceptual decisions?

Chapter 2: Perceptual decisions are limited primarily by variability in early sensory cortex

2.1 Abstract

Understanding how perceptual decisions are formed in the brain is a long-standing goal of systems neuroscience. Previous research in monkeys has found neural activity that correlates with decisions as early as primary sensory cortex, but these single-neuron recordings show only weak correlations with choice. This weak relationship implies that single sensory cortical neurons capture only a small fraction of the choice-related variability: such variability may be distributed across a large population of cells in sensory cortex, and may also occur in other areas downstream from early sensory cortex. Here we use a combination of direct measurement of neural population responses in primary visual cortex (V1) by voltage-sensitive dye imaging and a simple computational model to show that V1 encompasses most of the choice-related variability in highly trained monkeys engaged in a demanding visual pattern detection task. Our results are consistent with previously reported observations of weak single-neuron choice-related signals, and weak inter-neuronal correlations. Overall, our results suggest that simple perceptual decisions are formed by pooling information across a large population of weakly correlated sensory neurons, and that most choice-related variability is already present at the earliest stages of sensory cortical processing.

2.2 Introduction

When an organism is faced with a challenging perceptual task, is behavioral performance limited primarily by neural variability that is already present in early sensory cortical areas, or is it limited primarily by variability that occurs in brain areas downstream from early sensory cortex? One potential way to address this fundamental question is to measure neuronal activity in the relevant early sensory cortical area within the relevant epoch and assess the extent to which the measured activity is correlated with variability in perceptual decisions. If such measurements are highly predictive of behavioral choice, then most choice-related variability must reside in the sensory area, implying that downstream circuits can add only a small amount of *independent* choice-related variability.

Previous studies of the relationship between neural and behavioral variability have discovered co-variations between responses of individual neurons in sensory cortex and a subject's behavioral choices to repeated presentations of an identical near-threshold sensory stimulus (Britten et al., 1996; Celebrini and Newsome, 1994; Cook and Maunsell, 2002; de Lafuente and Romo, 2005; Dodd et al., 2001; Nienborg and Cumming, 2006; Nienborg and Cumming, 2009; Palmer et al., 2007; Purushothaman and Bradley, 2005; Uka and DeAngelis, 2004). These co-variations, however, tend to be very weak, implying that individual neurons capture only a small fraction of the neural variability related to decisions. The large amount of choice-related variability that is unaccounted for in single-neuron studies may be distributed across other (unmeasured) sensory neurons, and may also occur downstream from the sensory area. Even if the

majority of choice-related variability occurred in a distributed sensory cortical population, single neurons still may not provide strong predictions of choice because sensory neurons are only weakly correlated with one another (e.g., Zohary et al., 1994), and therefore, one neuron's responses are only weakly related to the population response. Thus single-neuron studies cannot provide strong constraints on whether perceptual decisions are predominantly limited by sensory or downstream variability.

In contrast to single-neuron electrophysiology, methods for measuring neural population responses, such as voltage-sensitive dye imaging (VSDI) (Grinvald and Hildesheim, 2004), have the potential to provide stronger constraints by capturing a larger fraction of the choice-related variability within the sensory area. Because even simple, spatially localized stimuli evoke responses over a broad region of sensory cortex (Chen et al., 2006; Grinvald et al., 1994; Palmer et al., 2011), and because these sensory cortical neurons are only weakly correlated with one another, subjects can benefit from combining these distributed signals to inform decisions. Thus, perceptual decisions may be based on the combined activity from a large population of sensory neurons. In this case, population measures may show stronger co-variations with choice, and thus account for a greater fraction of the choice-related neural variability. However, such methods tend to be susceptible to various sources of variability unrelated to choice, such as measurement noise, which can weaken the relationship between the measured neural activity and behavior.

To address the possibility that choice-related activity is distributed across many sensory neurons, we used VSDI to record from a large population of neurons in primary

visual cortex (V1) of two monkeys while they performed a difficult visual detection task. To better understand the relationship between measurements of neural variability and perceptual decisions, we developed a simple computational model and metric. This model is advantageous over previous methods, as it can be used to quantify the fraction of choice-related variability captured in a measurement of neural population response independent of choice-unrelated variability. Together, this approach allows us to determine a lower bound on the fraction of choice-related variability that occurs in the primary visual cortex during performance of a detection task.

2.3 Materials and Methods

Task and visual stimuli

All procedures were approved by the University of Texas Institutional Animal Care and Use Committee and conformed to NIH standards. Similar task and VSDI processing methods have been described previously (Chen et al., 2006; Chen et al., 2008). Briefly, monkeys were trained to perform a reaction-time visual detection task. Each trial began after the monkey established fixation on a 0.1° square fixation point displayed against a uniform gray background. The target was a small Gabor patch (sinusoidal grating modulated by a 2-D Gaussian envelope; $\sigma = 0.17°$, spatial frequency = 2.76 cycles/°, phase = 90°) that appeared at a fixed location (eccentricity = 4.28° for Monkey T, 1.58° for Monkey C). The Gabor stimuli appeared at one or two discrete target contrast levels at or near the monkey's psychophysical detection threshold (2.6%-5%), and were held constant throughout each session.

During the stimulus-detection task, in order to indicate a "target-present" choice, the monkey was required to shift gaze to the location of the target within 900 ms from target onset (but not sooner than 75 ms after target onset) and maintain gaze at that location for an additional 100 ms in order to receive the liquid reward. The target remained on for 300 ms or until the monkey initiated a saccade. On all trials in which the monkey made a saccadic eye movement towards the target location during the relevant temporal interval, shortly after the monkey initiated a saccade a small point appeared at the target location to help the monkey maintain post-saccadic fixation and to provide a visual reminder of the correct target location. In target-absent trials, the monkey was required to maintain fixation within a small window (< 2° full width) around the fixation point for an additional 900 ms in order to obtain a reward. The monkeys made a mixture of correct and incorrect responses on both target-absent and target-present trials, allowing us to examine neural activity during Hit, Miss, FA, and CR outcomes (for details see Table 2.1). On some trials, the monkey's behavioral responses were classified as invalid, and were not analyzed further. These trials included cases in which the monkey's gaze left the fixation window too early, or left the fixation window during the allowed interval but did not arrive in the target window, or arrived in the target window during the allowed interval but did not remain in the target window for the required time. Out of the total number of trials presented to the monkey, 93% for Monkey T and 92% for Monkey C were classified as valid trials culminating in a Hit, Miss, FA, or CR outcome. Visual stimuli were presented on a gamma-corrected 21" color display at a fixed mean

luminance of 30 cd/m^2. The display subtended 20.5° x 15.4° at a viewing distance of 108 cm, had a pixel resolution of 1024 x 768, 30-bit color depth, and a refresh rate of 100Hz.

On each day of data collection, the monkey initially performed the detection task in a short block of trials that included a range of target contrasts. One or two contrasts producing a mix of behavioral outcomes were chosen for use in the subsequent imaging experiment. In cases in which more than one target contrast was used during imaging, the normalization described below was applied separately to trials belonging to each target condition. This additional normalization was done to ensure that differences in physiology were related to the monkey's choices and not to differences in the physical stimulus.

VSDI recording and signal pre-processing

While the monkey performed the task, we recorded neural population signals in V1 using the voltage-sensitive dyes RH-1838 and RH-1691 (Shoham et al., 1999). Imaging data was obtained using the Imager 3001 system (Optical Imaging, Inc.), collected at a resolution of 512x512 pixels at a sampling rate of 100 Hz.

During analysis, the data was further binned to a resolution of 64x64 pixels, where each pixel corresponds to 0.5x0.5 mm^2 of cortex. Our basic VSDI signal pre-processing is divided into five steps: (i) normalize the responses at each site (a binned group of pixels) by the average fluorescence at that site across all trials and camera frames; (ii) average responses over a limited spatial region to obtain a single waveform for each trial; (iii) subtract from each waveform the temporal average over an 80 ms

interval centered on the stimulus onset time; (iv) average responses over a post-stimulus temporal interval to obtain a single number for each trial; (v) remove trials with aberrant VSDI responses. The normalization in step (i) serves to minimize the effects of uneven illumination and staining. The spatial averaging in (ii) is over a rectangular area of 2.5x2.5 mm^2 centered on the location with the most reliable response (maximal *d*') obtained on control trials at high (25%) target contrast. The temporal interval over which each trial's optical responses are averaged in step (iv) begins 120 ms before the median response time on Hit and False Alarms trials, and ends 20 ms before the median response time, or 20 ms before the response time in that particular trial, whichever was earlier. The median RT ranged from 319 to 407 ms across experiments in Monkey T, and from 263 to 274 ms in Monkey C. We explored other temporal intervals over which to average activity, including intervals that were longer as well as shorter than that used here, and also explored temporal intervals that were time-locked to the saccadic eye movements, but did not find any differences that affected our main conclusions (see Table 2.3). This observation is likely due to low frequency temporal correlations present in the VSDI response (Chen et al., 2008). To remove trials with aberrant VSDI responses, we computed the average response on each trial over a 2.5x2.5 mm^2 region centered on the evoked response and during the temporal averaging window; we subtracted from each trial the mean response across all trials (performed separately for each target contrast condition), and excluded from further analysis trials with residual responses greater than 3 standard deviations from the mean. This simple procedure

eliminated trials in which the animal made excessive movements (typically less than 1% of the trials).

To obtain a single number representing the neural activity on each trial, we first averaged responses at each location over the temporal averaging window. We then pooled responses over space by the application of various pooling algorithms (see below). We normalized all pooled responses by subtracting the mean response during target-absent trials, and dividing the result by the mean response during target-present trials.

We combined experiments across multiple recording sessions and two monkeys. We aligned the VSDI responses across multiple experiments by fitting the stimulus-evoked response to a high contrast (25%) Gabor stimulus (collected during control blocks before each imaging session) with a 2-dimensional Gaussian. We then re-centered the responses of each experiment such that the peak of each experiment's fitted response occurred at a common pixel.

Model and ML estimation

Our model framework of the subject's decision process is outlined in Fig. 2.2. We started with the assumption of three Gaussian, additive noise sources: shared sensory noise n_s; independent downstream decision-related noise n_d; and independent measurement noise n_m. We assume these noise sources to be a zero mean Gaussians with variances σ_s^2, σ_d^2 and σ_m^2, respectively. We have previously shown that our results

are consistent with Gaussian additive noise (Chen et al., 2006) and we performed similar tests to verify these properties in our present data (see Fig. 2.8).

The subject's decision variable is defined as $R_d = X + n_s + n_d$, where $X \in \{0,1\}$ is a binary variable that represents the absence or presence of the visual target. The measured pooled response is defined by $R_m = X + n_s + n_m$. Given these ingredients, the probability of the observed outcomes R_m and the subject's decision D on a single trial is given by:

$$P(R_m, D \mid X) = \frac{1}{\sigma_{tm}} \phi\left(\frac{R_m - X}{\sigma_{tm}}\right) \Phi\left(\frac{T - X + \alpha(X - R_m)}{\gamma}(-1)^D\right) \tag{2.1}$$

where $D \in \{0,1\}$ is a binary variable that represents whether or not the subject reported seeing the target , T is the subject's criterion, $\phi(\cdot)$ and $\Phi(\cdot)$ are the standard normal probability density function (pdf) and cumulative density function (cdf), respectively, $\sigma_{tm}^2 = \sigma_s^2 + \sigma_m^2$ is the total measurement noise variance, $\alpha = \sigma_s^2 / \sigma_{tm}^2$ is the ratio of shared to total measurement noise variance, and $\gamma = \sqrt{\sigma_{td}^2 - \alpha\sigma_s^2}$ is the conditional standard deviation of $R_d \mid R_m, X$. We obtained maximum likelihood fits of the model parameters $\{\sigma_s^2, \sigma_m^2, \sigma_d^2, T\}$ by numerical optimization of the log-likelihood (given by the log of Eq. 2.1, summed over all trials) using MATLAB's `fmincon`.

To obtain an intuition about the dependence of our measured quantities on the relative contribution of various sources of variability, we performed a series of simulated

experiments. In these simulations we fixed the decision criterion T, and the total decision-related variability σ_{td}^2, to values that reproduced the average behavioral accuracy of our monkeys (75%) and the observed distribution of errors (see Table 2.1). The sensory portion of this variability σ_s^2 was varied systematically across simulated experiments from 0 to σ_{td}^2, and in each experiment the subject's downstream variability, σ_d^2, was equal to the remainder, $\sigma_{td}^2 - \sigma_s^2$. In each experiment, the decision variable was compared to a criterion to determine the simulated subject's choices. In addition, we added zero-mean Gaussian noise σ_m to the sensory responses to obtain a simulated measured response. DF was defined as the ratio σ_s^2/σ_{td}^2; MF was defined as the ratio σ_s^2/σ_{tm}^2. We then computed various statistical measures from these responses. Stimulus-choice correspondence index (SCCI) was computed as the difference between the mean measured response during FA trials and that during Miss trials. Choice probability (CP) was the area under the receiver operating characteristic (ROC) curve applied to the distributions of responses belonging to 'choose target-present' and 'choose target-absent' after the mean response was removed from target-present trials. Neural sensitivity (NS) was the area under the ROC curve applied to the distributions of responses belonging to 'target-present' and 'target-absent' trials.

In order to obtain the curves in Fig. 2.4, we used the following. Our quantity of interest, SCCI, has a linear relationship with DF once the total decision-related variability is fixed:

$$SCCI = E[R_m \mid FA] - E[R_m \mid Miss] = \frac{\sigma_s^2}{\sigma_{td}}\left(\psi\left(\frac{-T}{\sigma_{td}}\right) + \psi\left(\frac{T-1}{\sigma_{td}}\right)\right) - 1, \tag{2.2}$$

where $\psi(\cdot) = \phi(\cdot)/\Phi(\cdot)$ is the ratio of standard normal pdf to cdf. To compute choice probability (CP), let f_0 and f_1 denote the pdfs of $P(R_m \mid X, D=0)$ and $P(R_m \mid X, D=1)$, respectively, which are given by (Eq. 2.1) but normalized to sum to 1 by dividing by $\Phi\left((-1)^D (T-X)/\sigma_{td}\right)$. The cdfs F_0 and F_1 are given by a bivariate normal cdf as follows:

$$F_0(R_m) = \int_{-\infty}^{R_m} \int_{-\infty}^{T} N\left(\left[\frac{R_m'}{R_d}\right], \mu, C\right) dR_d dR_m' = bvncdf\left(\left[\frac{R_m'}{R_d}\right], \mu, C\right), \tag{2.3}$$

where $\mu = \begin{bmatrix} X & X \end{bmatrix}^T$ and $C = \begin{bmatrix} \sigma_{td}^2 & \sigma_s^2 \\ \sigma_s^2 & \sigma_{tm}^2 \end{bmatrix}$. Similarly,

$$F_1(R_m) = \int_{-\infty}^{R_m} \int_{T}^{\infty} N\left(\left[\frac{R_m'}{R_d}\right], \mu, C\right) dR_d dR_m' = bvncdf\left(\left[\frac{R_m'}{R_d}\right], \tilde{\mu}, \tilde{C}\right), \tag{2.4}$$

where $\tilde{\mu} = \begin{bmatrix} X - X \end{bmatrix}^T$ and $\tilde{C} = \begin{bmatrix} \sigma_{td}^2 & -\sigma_s^2 \\ -\sigma_s^2 & \sigma_{tm}^2 \end{bmatrix}$. Choice probability is given by

$$CP = \int_{-\infty}^{\infty} F_0(R) f_1(R) dR. \tag{2.5}$$

Neural sensitivity (NS) is given by

$$NS = \Phi\left(\frac{1}{\sqrt{2(\sigma_s^2 + \sigma_m^2)}}\right) \tag{2.6}$$

Pooling algorithms

To examine the dependency of our results on the spatial pooling model, we repeated our analysis for a diverse family of 9 alternative pooling rules. Each rule was defined by a map of weights, and the pooled response on each trial was the dot product of that trial's activity map with the pooling weights. The choice-triggered pooling rule (used as our example pooling rule) had weights proportional to the 2-D Gaussian that best fit the average of all trials culminating in a "target-present" choice, minus the average of those culminating in a "target-absent" choice, after the stimulus-evoked response has been removed. The stimulus-triggered pooling rule had weights proportional to the average 'target-present' response, minus the average 'target-absent' response. The next five pooling rules were defined by 2-dimensional Gaussians with $\sigma = \{0.5, 1, 2, 3, 4\}$ mm respectively. This range of parameters spanned the observed breadth of the fitted mean stimulus evoked response map, which had fit parameters $\sigma_{major} = 1.71$ mm, $\sigma_{minor} = 1.36$ mm. The remaining two pooling rules were defined by difference-of-Gaussian (DOG) weight maps. These DOG's included the weight map that optimally separates target-

present from target-absent trials (Chen et al., 2006), as well as the DOG that optimally separates "choose target-present" from "choose target-absent" trials.

Subsampling analysis

To examine the impact of our assumption that the subject and researcher share equal access to the sensory population (Fig. 2.2), we extended our Monte Carlo simulation to two dimensions. The stimulus-evoked response was a two-dimensional Gaussian with peak amplitude of unity that matched the shape of the stimulus evoked response in the real experiments. As in our real experiments, the stimulus appeared on 50% of trials, and was added to spatially correlated Gaussian noise that occurred on all trials. The spatial noise spectrum was matched to that measured in real experiments. For each of the readout models we considered, the simulated subject and researcher each applied the model to these sensory signals, producing distributions of pooled sensory response amplitudes. We normalized all pairs of distributions such that the target-absent distribution had a mean of zero, and the target-present distribution had a mean of one. We then added independent zero-mean Gaussian noise σ_d to the subject's pooled sensory responses and independent zero-mean Gaussian noise σ_m to the researcher's pooled sensory responses as in our earlier analysis.

To explore the possibility of unequal access to V1 populations, we performed simulated experiments in which the researcher, the subject, or both, are given independent access only to a random sub-population of the simulated cortex (by setting

the pooling weights to zero in the inaccessible pixels). We then observed the relationships between the estimated values of MF and DF under the model that assumed equal access (Fig. 2.2), and the actual values that were used to generate the simulation.

Consider the case when the simulated experimenter is given access to 100% of the available cortical signals, while the simulated monkey samples a random subset, consisting of 70%, 80%, 90%, or 100% of the pixels (Fig. 2.7a-b). Intuitively, as the number of noisy neurons/pixels contributing to the monkey's pooled response decreases, the monkey's signal-to-noise ratio decreases. Because we normalize the pooled responses such that the mean target-absent response is equal to zero and the mean target-present response is equal to unity, sub-sampling causes the monkey's pooled variability to increase. While this additional variability is inherited from the noisy neurons/pixels in our population and thus originates in sensory cortex, our model (which assumes that all noise in sensory cortex is shared; Fig. 2.2) considers *any* choice-related variability that is not measured as downstream noise. Thus when the monkey sub-samples the sensory population, we expect our model to overestimate the amount of downstream noise, or in other words, underestimate DF. Fig. 2.7a shows the relationship between the maximum likelihood estimate of DF and the actual DF value used to generate the simulated experiment. The black line represents the case in which both the simulated experimenter and monkey each sample 100% of the available neurons, and thus our assumption of equal access is met. The grey lines represent cases in which the simulated monkey sub-samples the population. This figure shows that as the monkey sub-samples the

population, the model systematically underestimates the true DF, consistent with our intuition.

In contrast to its effect on DF, sub-sampling by the monkey has no effect on MF. Sub-sampling by the monkey should affect neither the simulated experimenter's pooled sensory signals, nor the total measured variability, and thus the ratio MF should remain unchanged. Fig. 2.7b, which shows the relationship between the maximum likelihood estimate of MF and the actual MF value used to generate the simulated experiment, verifies this intuition. Cases in which the monkey sub-samples the population are not distinguishable from the case in which the monkey samples 100% of the available cortical signals.

Next consider the case when the simulated monkey is given access to 100% of the available cortical signals, while the simulated experimenter samples a random subset, consisting of 70%, 80%, 90%, or 100% of the pixels (Fig. 2.7c-d). We expect these cases to show symmetrical results to those described above. On one hand, sub-sampling by the experimenter has no effect on the model's estimate of DF (Fig. 2.7c), since this sub-sampling affects neither the monkey's pooled signals nor the total decision-related variability. However, as the experimenter samples fewer pixels, the experimenter's SNR decreases, and as above, this loss in SNR manifests as additional noise. While this noise is sensory in origin, our model considers it as measurement noise. Thus in the case when the experimenter sub-samples the population, we expect our model to overestimate measurement noise, or in other words, underestimate MF. Fig. 2.7d illustrates that in these cases, the model systematically underestimates MF.

Finally, we considered cases in which both the simulated experimenter and monkey each sample a subset of the sensory cortical signals (Fig. 2.7e-f). Because sub-sampling by the experimenter has no effect on DF, differences between the estimated and actual DF values in these cases should be related to only the monkey's sub-sampling. Fig. 2.7e shows the relationship between the actual and estimated DF when the experimenter samples just 50% of the available neurons and while the monkey samples 70%, 80%, 90%, or 100% of the pixels. This plot is identical to that of Fig. 2.7a, consistent with our intuition. Similarly, we expect that differences between actual and estimated MF should be driven solely by the degree of sub-sampling by the experimenter. Fig. 2.7f shows the relationship between the actual and estimated MF when the monkey samples just 50% of the available neurons and while the experimenter samples 70%, 80%, 90%, or 100% of the pixels. This plot is identical to that of Fig. 2.7b, also consistent with our intuition.

We repeated this analysis for seven of our nine pooling models (the two pooling models based on the real monkey's choices are undefined in the simulation). Results for the stimulus-triggered readout model are shown in Fig. 2.7, though our choice of readout model did not significantly affect our results.

Eye movements

To test whether small differences in eye movements may have been responsible for some of our results, we examined two eye movement statistics, which summarized the quality of fixation within each trial and across trials. We have performed a similar

analysis previously (Chen et al., 2006). The first statistic was the standard deviation of the eye position over the same time interval used for averaging of VSDI signals, and had a mean of 0.0894 degrees and a standard deviation of 0.0571 degrees. The second statistic was the average distance from the monkey's direction of gaze to the fixation point during this same time interval, and had a mean of 0.0547 degrees and standard deviation of 0.0115 across trials. For each metric, we separated the data into two halves (above median and below median) and re-computed our DF and MF statistics for each half (see Table 2.4). We then computed the bootstrapped sampling distributions of the difference between the two halves. We repeated this procedure for each of our 9 readout models. In no cases were any of the differences significantly different from zero at the 0.05 level. In addition, we examined the population activity maps obtained from each half of the data, for each fixation quality metric. For each half, we obtained bootstrapped sampling distributions of the parameters of the 2-dimensional Gaussian that best fit the evoked response to target-present trials. Neither metric revealed any significant differences in the amplitude, location, or spatial spread of the evoked response. A significant fraction of the variability in measured eye movements is likely due to variability introduced by the eye tracking device.

Other notes

All statistical tests on the behavioral data, physiological data, and Monte Carlo data were performed using bootstrap methods (Efron, 1993).

2.4 Results

We trained two monkeys to perform a simple reaction-time visual detection task (Fig. 2.1). The monkey began each trial by directing gaze to a central fixation point. To obtain a reward, the monkey had to rapidly shift gaze to a small peripheral target during 'target-present' trials (50% of trials), or to maintain fixation on the central fixation point during 'target-absent' trials (the remaining trials). We used a small Gabor patch stimulus (sinusoidal grating in a 2-D Gaussian envelope) to effectively drive V1 cells, and presented the stimulus at one or two contrast levels near each monkey's perceptual detection threshold to maintain task difficulty. Target present trials were classified as 'Hits' if the monkey correctly detected the target and 'Misses' otherwise. Target absent trials we classified as 'False Alarms' (FA) if the monkey reported seeing a target and 'Correct Rejections' (CR) otherwise. Monkeys T and C performed at 76% and 69% accuracy, respectively (see Table 2.1 for details regarding behavioral performance.)

While the monkeys performed the task, we used voltage-sensitive dye imaging (VSDI) to measure population responses from V1, an area likely to play a central role in performance of such tasks. VSDI measures changes in membrane potential from large populations of neurons in layers 1-3 (Chen et al., 2012; Petersen et al., 2003). Previous work showed that this technique can be sufficiently sensitive to outperform monkeys in a similar detection task when combining single-trial VSDI signals optimally (Chen et al., 2006; Chen et al., 2008). Furthermore, because V1 contains a topographic map of visual space, the target activates only a limited region in V1 (Chen et al., 2006; Sit et al., 2009),

and this region can be entirely captured by VSDI. Thus, VSDI may be capable of capturing a large portion of choice-related variability in V1.

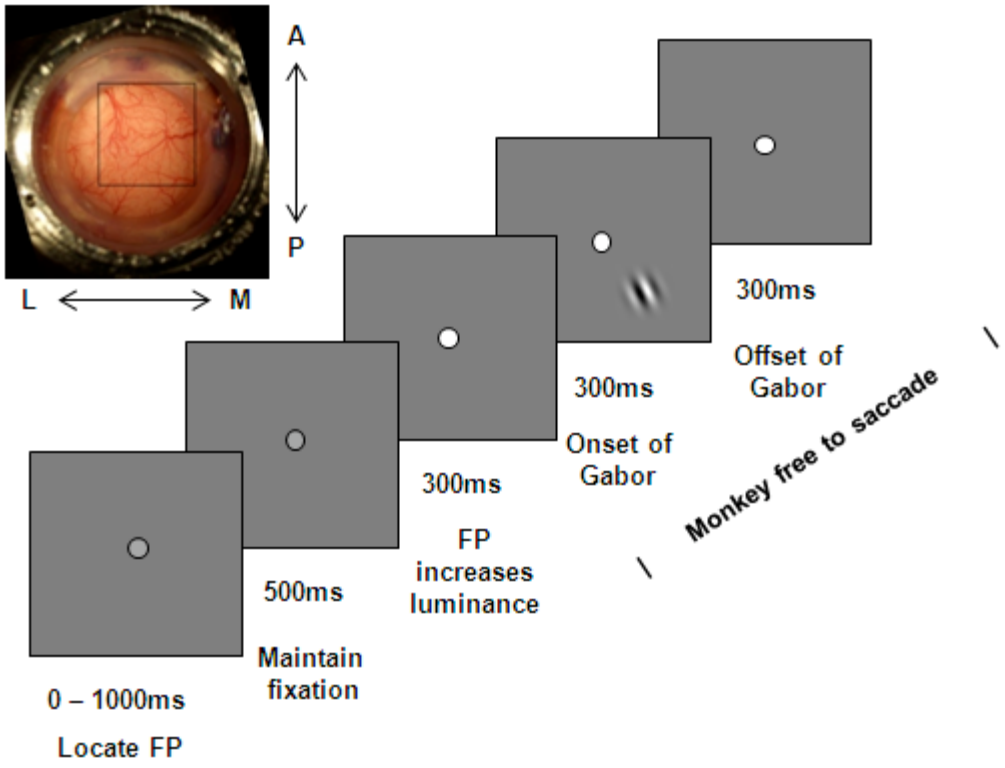

Figure 2.1. Visual detection task and simultaneous VSDI recording. Each trial begins when the subject locates and fixates a central fixation point. After a 500 ms delay during which the subject is required to maintain fixation, the fixation point undergoes a slight increase in luminance to indicate the start of the task portion of the trial. Following a 300 ms delay, a Gabor stimulus appears on 50% of trials. The subject is required to make a saccadic eye movement to the stimulus location when it appears, or to maintain fixation on the central fixation point for an additional 900 ms when it does not appear. The subject receives a drop of juice or water following correct choices, and no reward following incorrect choices. **Inset**, cranial window above dorsal portions of primary visual cortex. Black square indicates VSDI imaging area of 10 x 10 mm^2 in the left hemisphere. Letters indicate approximate cortex orientation (A – anterior; P – posterior; M – medial; L – lateral).

	# Experiments	#Hits	#Miss	#False Alarms	#Correct Rejections	% Correct	Median RT
Example	1	235	89	23	301	83%	346
Monkey T	13	1,189	733	181	1731	76%	352
Monkey C	2	204	83	94	193	69%	282
Combined	15	1,393	816	275	1,924	75%	352

Table 2.1. **Summary of behavioral performance**. 'Example experiment' (from Monkey T) corresponds to data shown in Fig. 2.5a-c; 'Combined' data corresponds to data shown in Fig. 2.5d-f. Physiological results for each of the two monkeys are shown separately in Fig. 2.6.

Theoretical framework

Our goal here is to quantify the trial-to-trial co-variations between VSDI responses and the monkey's choices, and use this co-variation to estimate the fraction of choice-related variability present in V1. A common way to conceptualize the decision process in perceptual tasks is to assume that on each trial the subject computes a decision variable (a scalar) by combining responses from a population of sensory neurons during stimulus presentation. The decision variable is then compared to a criterion to determine the behavioral choice on that trial (Green and Swets, 1966).

Here we followed a similar approach. In each trial we combined the VSDI responses over space and time using several pooling algorithms (discussed below) to obtain a single number that represents the pooled sensory response in that trial. The trial-to-trial variability in this pooled signal is assumed to be correlated with the decision variable. We then developed a simple computational model that allowed us to explore the relationship between pooled sensory responses, downstream variability, and measured variability that is choice-unrelated.

Our model of the subject's decision process begins when a binary signal is presented to the subject. The subject encodes the signal (0 representing target absent, or 1 representing target present), and adds Gaussian sensory variability to this representation, forming a pair of unitless Gaussian distributions with means {0,1} and variance σ_s^2 (Fig. 2.2, 'Sensory Encoding'). During the formation of the decision, additional independent Gaussian decision-related variability with variance σ_d^2 is added to the sensory representation (Fig. 2.2, 'Downstream Variability'). The total decision variability, which controls the subject's accuracy, is the sum of the sensory variability and the downstream variability, $\sigma_{td}^2 = \sigma_s^2 + \sigma_d^2$. The subject reports "target present" if the decision variable exceeded a criterion, and "target absent" otherwise.

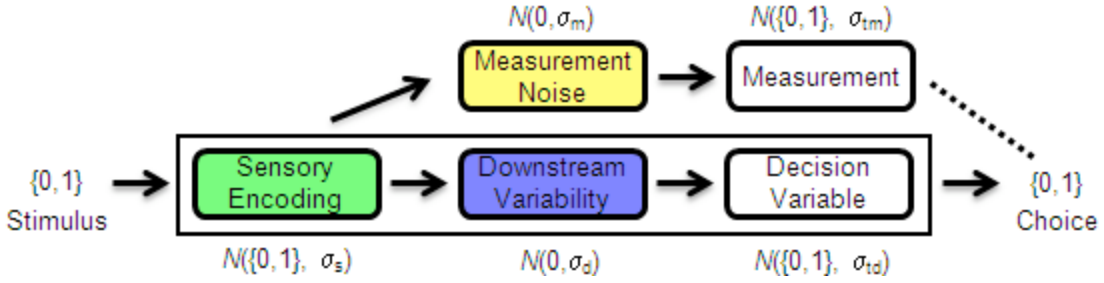

Figure 2.2. Theoretical framework. Model of a subject's formation of a binary decision and a researcher's measurement of neuronal responses. Stimulus-related information is encoded in an early sensory area as a pair of distributions with means {0,1} and variance σ_s^2 (green), to which zero-mean noise with variance σ_d^2 representing downstream variability is added (blue) to form the decision variable. The subject compares the decision variable to a criterion to form a decision on each trial. The upper portion of this panel represents stages in a researcher's measurement, in which zero-mean measurement noise with variance σ_m^2 (yellow) is added to the sensory representation to form the measured signals. The measured signals are then analyzed with respect to the subject's binary choices on a trial-by-trial basis (dashed line).

As experimenters we have access to the sensory neural responses (Fig. 2.2, 'Sensory Encoding'), but we assume that our measurements are contaminated by independent, Gaussian measurement noise with variance σ_m^2 (Fig. 2.2, 'Measurement Noise'). The total measured variability thus includes both the sensory variability and the measurement noise, $\sigma_{tm}^2 = \sigma_s^2 + \sigma_m^2$.

Our main goal is to estimate, given the measured neural responses and observed behavioral choices, the fraction of the total decision-related variability that is present in the sensory area, σ_s^2/σ_{td}^2, which we abbreviate DF ('decision fraction'). While DF quantifies the percentage of the decision-limiting variability present in sensory cortex, it does not by itself reveal the origins of this variability; such variability may arise from stochastic activity of sensory neurons and it may also arise from top-down signals from higher cortical areas that affect the decision. A second quantity of interest is the fraction of measured variability that is sensory, σ_s^2/σ_{tm}^2, which we abbreviate MF ('measurement fraction'). Under the model's assumptions, we can use maximum likelihood to estimate DF and MF from our neural and behavioral data (see Eq. 2.1 in Methods). The initial assumption in our model (Fig. 2.2) is that the experimenter and subject have access to exactly the same sensory neural signals. We later show that in cases in which the experimenter and subject use only partially overlapping neural signals, our model can only *underestimate* the true values of DF and MF.

To obtain an intuition regarding the interplay between the model's parameters and variables of interest, we performed a series of simulated experiments. In these simulations we fixed the decision criterion and the total decision-related variability σ_{td}^2 to

values that reproduced the average behavioral accuracy of our monkeys (75%) and the observed distribution of errors (see Table 2.1). We then systematically varied DF from 0% to 100% (by varying σ_s^2 from 0 to σ_{td}^2).

We next examine how DF influences various measured quantities. Consider first the possibility that most of the subject's choice-related variability resides in our early sensory area, and thus little variability resides downstream (Fig. 2.3a). In the absence of any measurement noise and under the assumption that we capture all of the sensory signals, our measured signals in both target-absent (red) and target-present (green) trials are highly correlated with the decision variable. In the decision variable, by definition, neural responses in FA trials exceed the criterion while responses in Miss trials fall below the criterion, and thus the mean neuronal response associated with FA trials must exceed that of Miss trials. Because the measured responses are highly correlated with the decision variable, the mean *measured* neuronal response associated with FA trials (Fig. 2.3a, dashed red arrow) also exceeds that of Miss trials (dashed green arrow). On the other hand, when the majority of the choice-related variability occurs downstream (Fig. 2.3c), the sign of the difference between the mean FA and Miss responses is reversed. In the absence of significant amounts of sensory variability (i.e., $\sigma_S^2 \ll \sigma_D^2$), the sensory distributions approach deterministic signals; in this case the neuronal activity associated with FA trials is nearly identical to that of all target-absent trials (at a value near zero), and similarly, the activity associated with Miss trials is nearly identical to that of all target-present trials (unity). Thus the difference between the mean neuronal responses associated with the two types of error trials, $\overline{R_{FA}} - \overline{R_M}$, is a useful proxy for the fraction

of choice-related variability present in the sensory area. This difference reflects whether the responses in error trials correspond more closely with the stimulus or with the choice, and thus we introduce the term 'stimulus-choice correspondence index' (SCCI) for its quantity. Importantly, our model and metric generalize to other types of binary decision tasks (see Discussion). SCCI has a linear relationship with DF (Fig. 2.3e; Eq. 2.2); it reaches its maximum value, which depends on the subject's behavioral performance, when DF = 1, and its minimum value of -1 when DF = 0. Under our model's assumptions and given the monkey's behavioral performance, positive values of the SCCI metric (Fig. 2.3a,b) would imply that more than 55% of the choice-related variability is present in our VSDI recordings and thus resides in V1.

Importantly, SCCI is unaffected by the addition of choice-unrelated variability. To illustrate this property, Fig. 2.3d shows the same pair of distributions given in Fig. 2.3a after the addition of a large amount of measurement noise. This additional, zero-mean noise does not bias the mean responses tied to each of the 4 behavioral outcomes, and thus does not affect SCCI. The insensitivity of SCCI to the presence of measurement noise makes this metric advantageous over other metrics of choice-related activity such as choice probability (Britten et al., 1996) (CP). CP measures the discriminability of two distributions of neuronal responses that belong to the same stimulus condition but to two different behavioral choices, such as 'Hits' (solid green line) and 'Misses' (dashed green line). It ranges from 0.5 (no discriminability) to 1 (perfect discriminability). Fig. 2.3a-c shows that CP is also related to DF. However, comparison of Fig. 2.3a and d shows that CP is affected by the presence of measurement noise. This effect is summarized in Fig.

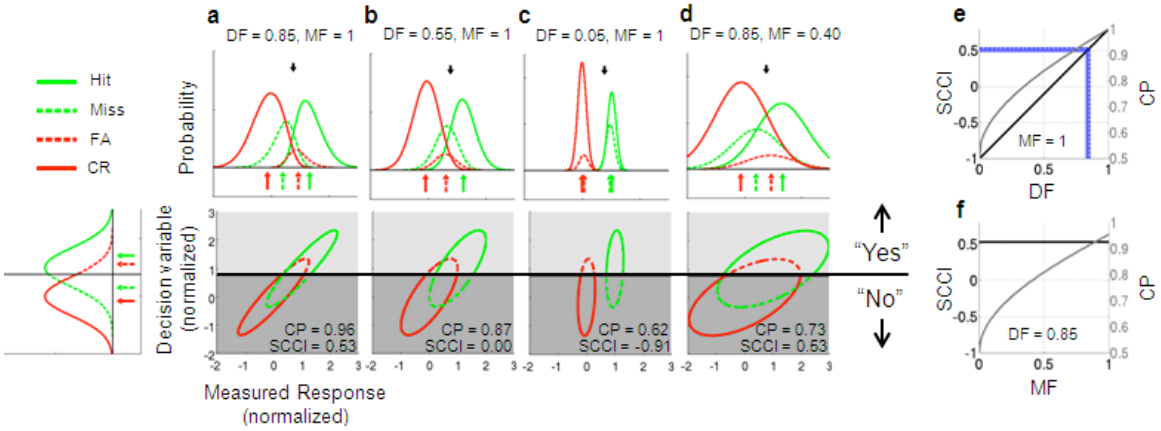

Figure 2.3. **Expected relationship between observable quantities and the underlying properties of a decision**. **a-d (lower)**, Joint distributions of the decision variable (ordinates) and model-predicted neuronal responses (abscissae) under 4 noise scenarios, ranging from 85% of choice-related variability occurring in a measured brain area (**a**) to only 5% of choice-related variability captured by the measurement and the remaining 95% occurring downstream (**c**). In panels **a-d**, marginal distributions are shown for 'Hit' (solid green), 'Miss' (dashed green), 'False Alarm' (dashed red), and 'Correct Rejection' (solid red) trials. The marginal distributions of the ordinate of panel **a** represent the decision variable. Red and green arrows indicate mean neuronal response amplitude for each of the 4 behavioral categories. Black arrows and horizontal black lines indicate the decision criterion. Stimulus-choice correspondence index (SCCI), and choice probability (CP) values (see text for details) are reported for each scenario. In panels **a-c**, no choice-unrelated variability was added to the measured responses (i.e., MF = 1). **d**, Same as panel **a**, after adding a large amount of choice-unrelated variability. **e**, Relationship between SCCI (left ordinate), CP (right ordinate), and DF. Blue lines indicate maximum-likelihood estimated DF solutions (see Methods) and their corresponding SCCI values for the choice-triggered pooling rule (dotted blue line) and each of 8 alternative pooling rules (solid blue lines). **f**, The relationship between SCCI (left ordinate), CP (right ordinate), and MF when DF = 0.85. While SCCI is independent of MF, CP varies systematically with MF.

2.3f (see also Fig. 2.4). Thus while both CP and SCCI are potential indicators of the fraction of choice-related variability captured by the measurement, SCCI has the advantage that it is robust to choice-unrelated variability.

Finally, we examined the behavior of neural sensitivity (Newsome et al., 1989) (NS), which is defined as the discriminability between two distributions of measured

neuronal responses for two stimulus conditions, in our case 'target present' vs. 'target absent'. Intuitively, when most of the choice-related variability resides in sensory cortex (Fig. 2.3a), the pooled sensory variability will be large and therefore NS will be weak. As the percentage of downstream variability increases and behavior becomes limited primarily by downstream noise (Fig. 2.3c), the measured NS (which captures the sensitivity of the measured sensory signals prior to contamination by downstream noise) approaches unity (Fig. 2.4c). Having established a general computational framework for studying the relationship between noisy measures of neural population responses and choice, our next step was to examine our physiological results.

Physiological results

Results from a representative VSDI experiment (Fig. 2.5a-c) reveal robust choice-related modulations at the level of neural populations in V1. Fig. 2.5a shows the spatial spread of activation during stimulus-present and stimulus-absent trials. On average, the stimulus evoked a broad Gaussian-shaped response across the population of neurons in comparison to the stimulus-absent trials, consistent with our previous results (Chen et al., 2006; Chen et al., 2008; Chen and Seidemann, 2012; Sit et al., 2009). The mean stimulus-present and -absent maps were each further partitioned into mean Hit and Miss maps, and mean FA and CR maps, respectively. These maps reveal strong choice-related differences. Responses in Hit trials are strong while responses in Miss trials are extremely weak even though the same visual target was presented in all of these trials.

Similarly, the responses in FA trials are large and widespread even though no visual stimulus was presented on those trials, while no responses can be seen in CR trials.

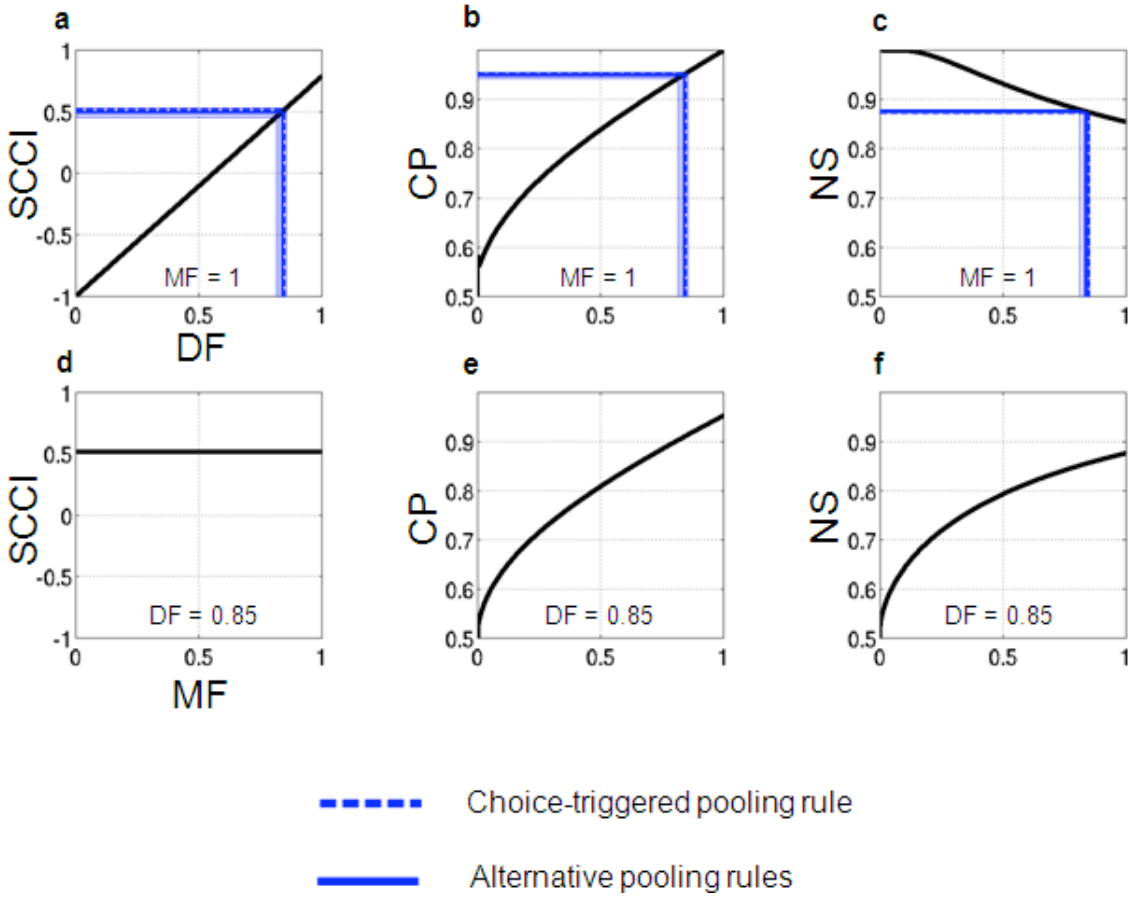

Figure 2.4. **Expected SCCI, choice probability, and neural sensitivity as functions of DF and MF**. **a-c**, SCCI, CP, and NS metrics as functions of DF when MF = 1 (i.e., in the absence of choice-unrelated variability). **d-f**, SCCI, CP, and NS metrics as functions of MF when DF = 0.85 (i.e., the DF inferred from the real data when applying the choice-triggered pooling rule). Dashed blue lines indicate values estimated using the choice-triggered pooling model described in the text; solid blue lines correspond to a family of alternative pooling models.

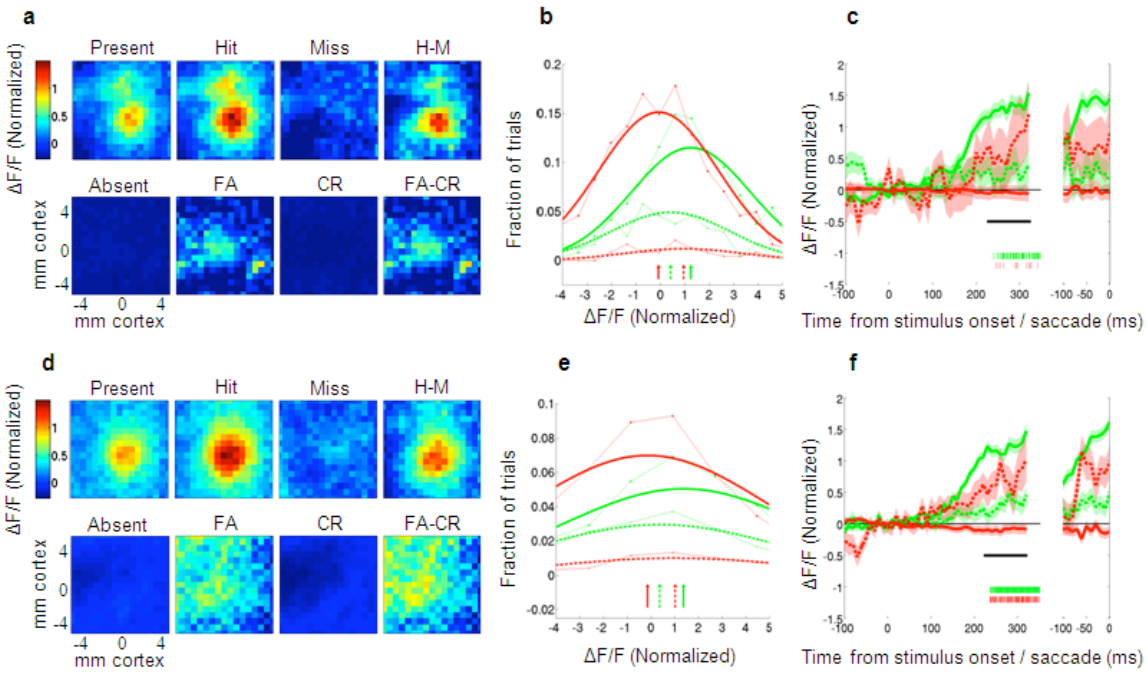

Figure 2.5. VSDI sensory population recordings. **a-c**, Example VSDI experiment in Monkey T. **a**, Average cortical activity maps separated by stimulus condition (rows) and behavioral choice (columns), and averaged over a 100 ms temporal window (see Methods for details). Upper row of panel **a** represents neural activity during target-present trials; lower row shows activity during target-absent trials. Activity maps are shown separately for 'choose target-present' (H and FA) and 'choose target-absent' (M and CR) trials. 'H-M', difference map of activity during Hit and Miss trials. 'FA-CR', difference map of activity during FA and CR trials. Cortical maps represent activity averaged over the time interval indicated by the horizontal black bar in **c**. **b**, Histogram of pooled population responses for each of the 4 behavioral categories: Hit (solid green), Miss (dashed green), False Alarm (dashed red), and Correct Rejection (solid red). Arrows indicate mean population response for each category. Scalar response amplitudes were generated by pooling cortical activity with the choice-triggered decoder (see text for details). **c**, Time evolution of mean neuronal population response for each of the 4 behavioral categories. Shaded areas indicate standard errors. Hash marks at the bottom of the panel indicate saccadic onset times in Hit (green) and FA (red) trials. The left side of panel **c** shows responses aligned to stimulus onset; the right side of panel **c** shows responses aligned to saccadic eye movements. In the right side of panel **c**, traces for trials in which the monkey did not make an eye movement (Miss and CR trials) are shown for intervals re-sampled from those of the Hit and FA trials. DF and MF values obtained by averaging VSDI responses over the saccade-aligned intervals showed results qualitatively similar to those obtained over the stimulus-aligned intervals (see Table 2.3 for quantitative comparison). **d-f**, Aggregate summary of VSDI results collapsed over 13 experiments in Monkey T and 2 experiments in Monkey C. Same organization, space and time windows, and color scheme as in **a-c**.

Examination of the population activity maps reveals two key results. First, choice-related activity, as revealed by the Hit-Miss and FA-CR difference maps, is distributed broadly across the neuronal population rather than being restricted to a small region. Second, comparison of the FA and Miss maps reveals greater activity on FA trials than on Miss trials, suggesting that the population activity in V1 corresponds more closely in this task to the subject's choice than to the stimulus. The strong activity during FA trials extends across a large region of sensory cortex and the activity during Miss trials remains weak across the population, suggesting that our SCCI metric will take on positive values across a wide range of potential spatial pooling algorithms.

The two key findings from the example experiment hold in our combined data set (Fig. 2.5d-f). Because the results from the two monkeys were qualitatively similar (see Fig. 2.6), 13 experiments from Monkey T and 2 experiments from Monkey C were combined to produce our aggregate results. Fig. 2.5d shows robust choice-related activity that is broadly distributed, and FA responses that exceed Miss responses, suggesting that in our task, most choice-related activity may reside in V1.

To estimate the fraction of choice-related variability captured by our VSDI measurements, we combined the signals over cortical space and time into a single value for each trial, and examined the distribution of these scalar responses across trials (see Methods). Neural responses at each location were averaged over a short temporal interval (see Methods). Here, in order to combine the population signals over space, we used a simple choice-triggered pooling rule with weights proportional to the 2-D Gaussian that best fits the average of all trials culminating in a "target-present" choice,

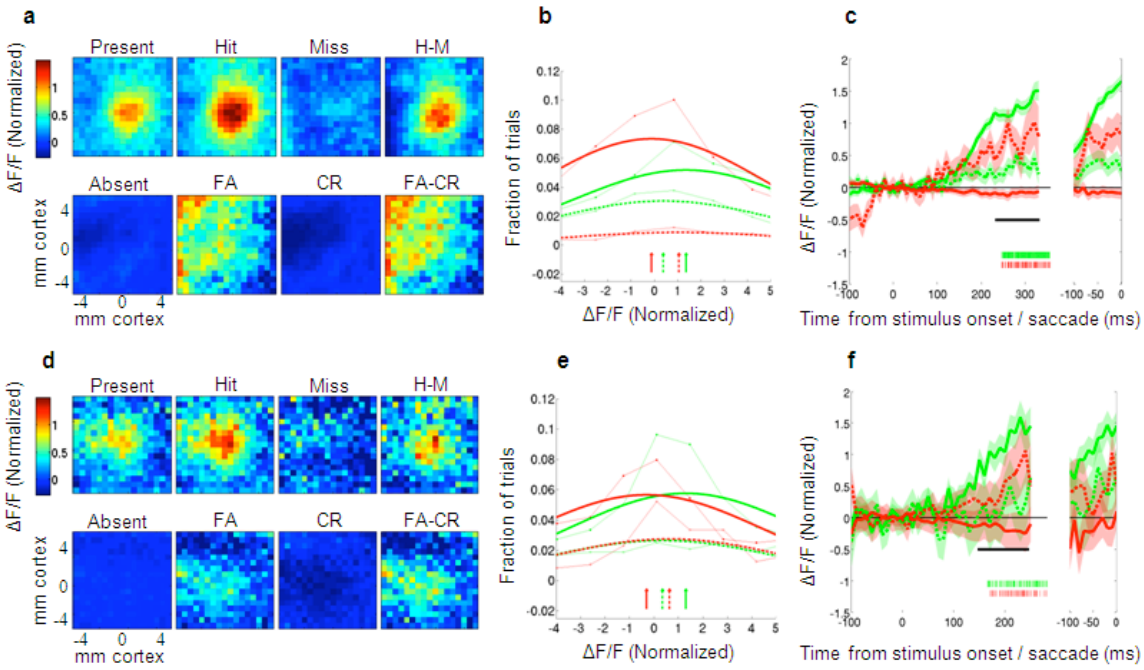

Figure 2.6. VSDI sensory population recordings in the two monkeys. **a-c**, Average of 13 experiments in Monkey T. **d-f**, Average of 2 experiments in Monkey C. Same conventions as in Fig. 2.4.

minus the average of those culminating in a "target-absent" choice, after the stimulus-evoked response has been removed; we consider additional pooling rules later on. The resulting values are plotted in the histogram of Fig. 2.5e. This panel shows that the mean FA response exceeds the mean Miss response (SCCI = 0.53). According to our model, our combined SCCI value of 0.53 corresponds to DF = 0.85 (95% CI: [0.48 1.00]) (Fig. 2.3e, dashed blue line), or in other words, 85% of the choice-related variability is present in V1.

Our model also allows us to estimate the fraction of the total measured variability that is choice-related (MF). Given our result that DF = 0.85, if there is no measurement

noise, the model predicts high CP (0.96) and NS (0.87). Our observed CP (0.55), while significantly above 0.5 ($p<0.01$), is much lower than the predicted value. Similarly, our observed NS (0.56), while significantly above 0.5 ($p<0.01$), is much lower than the predicted value. The observed NS and CP values are therefore consistent with very large amounts of measurements noise (MF = 0.02). In other words, our results show that in the current set of experiments, the vast majority of the measured variability is choice-unrelated (see Discussion for comparison with previous results).

To determine whether our results depend on the particular choice of the spatial pooling model, we repeated our analysis using a diverse family of alternative pooling models. We considered a stimulus-triggered pooling rule with weights proportional to the mean stimulus-evoked response. We also tested pooling rules based on 2-D Gaussians and differences-of-Gaussians (DOGs), such as the optimal decoder derived previously in our lab (Chen et al., 2006) (see Methods). Fig. 2.3e (solid blue lines) shows the SCCI and corresponding DF value obtained for each of the pooling models we considered; DF varied slightly by model, with most models producing a value near 0.84, but no model produced a value less than 0.81. Table 2.2 shows the DF and MF values obtained for each of the 9 pooling rules, shown separately for the example experiment, each monkey, and the combined data. These results suggest that over a broad family of plausible pooling algorithms, our estimate of the fraction of choice-related variability captured by our measurements is at least 81%. In addition, to determine whether our results depended on the temporal interval over which we averaged the neural population activity, we repeated the analysis separately for responses obtained by averaging over

temporal intervals aligned to the stimulus and to the behavioral response. Table 2.3 shows that the results obtained during the saccade-aligned interval supports our main result that the majority of the subject's choice-related activity occurs in V1 in our task.

		1	2	3	4	5	6	7	8	9
Example (N=1)	DF	0.82	0.75	0.88	0.88	0.78	0.74	0.76	0.88	0.92
	MF	0.04	0.03	0.07	0.06	0.04	0.03	0.02	0.07	0.08
Monkey T (N=13)	DF	0.88	0.89	0.86	0.89	0.90	0.88	0.87	0.88	0.91
	MF	0.01	0.02	0.04	0.03	0.02	0.02	0.01	0.04	0.03
Monkey C (N=2)	DF	0.60	0.59	0.51	0.58	0.53	0.58	0.61	0.48	0.53
	MF	0.03	0.03	0.05	0.04	0.03	0.02	0.02	0.05	0.04
Combined (N=15)	DF	0.85	0.84	0.81	0.85	0.86	0.85	0.84	0.84	0.89
	MF	0.02	0.02	0.04	0.03	0.02	0.01	0.01	0.03	0.03

Table 2.2. DF and MF solutions for each of 9 pooling rules. DF and MF values are shown for the example experiment, each of the two monkeys separately, and the combined data, for each of 9 biologically plausible pooling rules (see Methods).

		1	2	3	4	5	6	7	8	9
Aligned to Stimulus	DF	0.85	0.84	0.81	0.85	0.86	0.85	0.84	0.84	0.89
	MF	0.02	0.02	0.04	0.03	0.02	0.01	0.01	0.03	0.03
Aligned to Saccade	DF	0.73	0.68	0.74	0.79	0.73	0.66	0.64	0.79	0.84
	MF	0.01	0.01	0.03	0.03	0.01	0.01	0.01	0.03	0.03

Table 2.3. DF and MF solutions for each of 9 pooling rules, obtained separately for temporal averaging intervals aligned to the stimulus and to the choice. To obtain data for the Miss and Correct Rejection trials during the saccade-aligned interval, averaging intervals were re-sampled from those of the Hit and False Alarm trials (see Methods).

Subsampling analysis

As discussed above, our model (Fig. 2.2) assumes that the subject and researcher share equal access to the V1 population. However in a real experiment, population measures such as VSDI are limited to a finite spatial extent, spatial resolution, and cortical depth. Thus the subject and researcher's pooled sensory responses may overlap only partially. To explore the possible impact of partial overlap, we extended our model by simulating V1 as a 2-dimensional patch of neurons/pixels with signal and noise characteristics that matched those from the real data (see Methods). We then performed simulated experiments in which the researcher, the subject, or both, are given independent access only to a random sub-population of the simulated cortex. Our results (Fig. 2.7) show that in these cases, a portion of the choice-related *sensory* variability may be un-captured by the experimenter, and likewise, a portion of the measured neural variability may be unrelated to choice. Because our model considers *any* choice-related variability that is not measured as downstream noise, the model's estimate of the downstream noise is an upper bound on the actual downstream noise. In other words, because some of what our model considers as downstream noise may actually reside in V1, the DF estimated by our model is a *lower bound* on the true fraction of choice-related variability present in sensory cortex. Similarly, because our model considers *any* measured variability that is choice unrelated as measurement noise, the model's estimate of MF is a *lower bound* on its actual value.

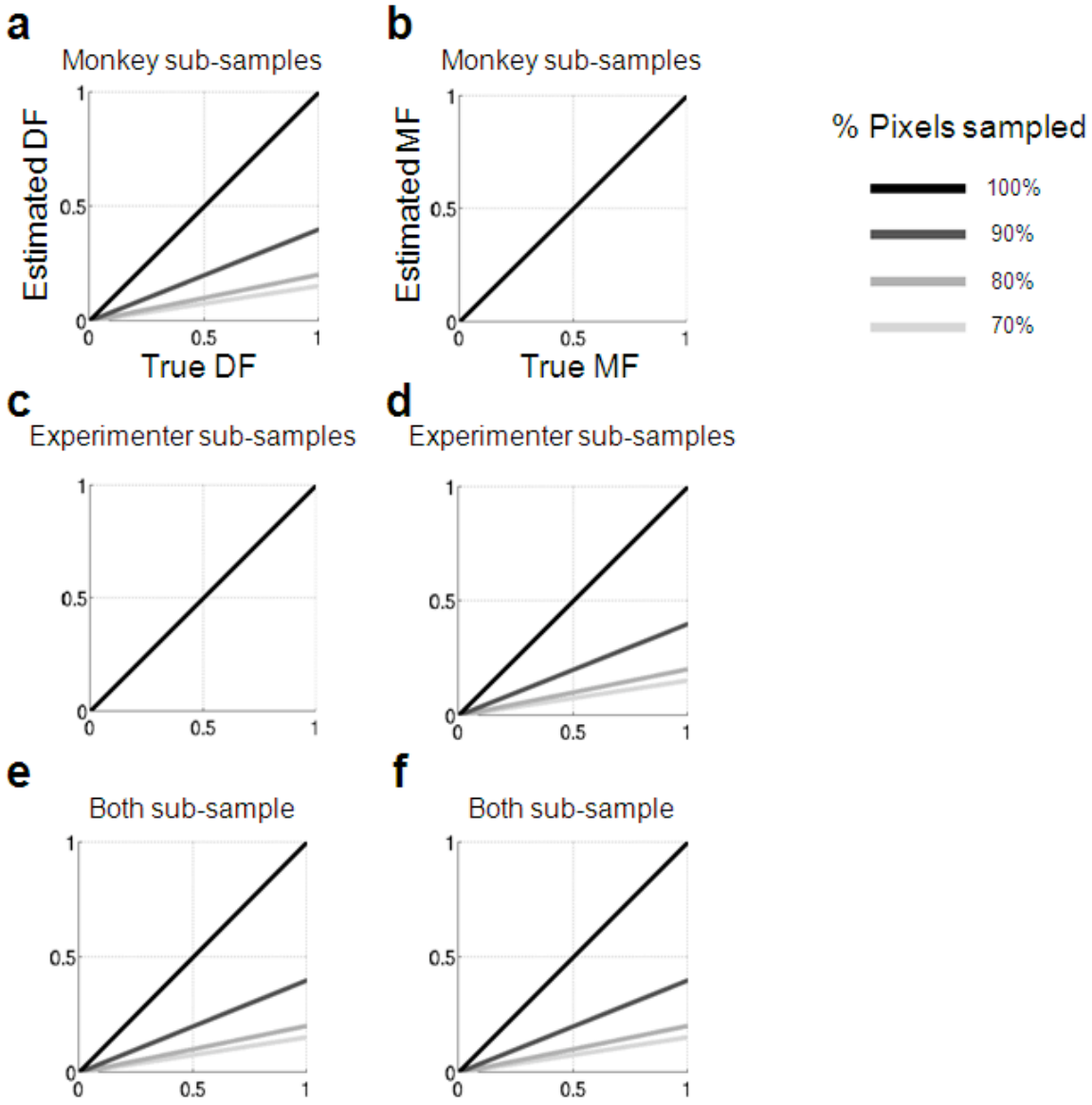

Figure 2.7. **Sub-sampling analysis**. Relationships between DF and MF values inferred using the maximum likelihood method (ordinates) and those used to generate the simulation (abscissae) during conditions in which the simulated monkey sub-samples the cortical population (**a,b**), the simulated experimenter sub-samples (**c,d**), and both the simulated monkey and experimenter sub-sample (**e,f**). Black lines in **a-d** correspond to the case in which our initial assumption of equal access is met (see text for details). Grey lines indicate the percentage of pixels sampled. This figure demonstrates that the DF and MF values inferred with the maximum likelihood method provide lower bounds on their true values.

Eye movements

Small differences in eye movements could have been responsible for some of our results. For example, it is possible that a systematic relationship between direction of gaze and behavioral choice could lead to a spurious correlation between cortical activity and choice. To rule out this possibility, we applied 2 tests of eye movement statistics (Table 2.4; see also Methods), and for each statistic, we re-ran the analysis for the half of trials with the best fixation and compared the results to those from the half with the poorest fixation. None of the differences we observed were significant, suggesting that small variations in eye movements are not responsible for our results.

Fixation Metric \ Response Statistic		Amplitude	X Position	Y Position	Spread
Within-trial fixation	Best half	0.89 (0.09)	-0.27 (0.26)	-0.29 (0.21)	2.03 (0.31)
	Worst half	0.84 (0.09)	0.18 (0.20)	0.07 (0.19)	1.57 (0.32)
Across-trial fixation	Best half	0.84 (0.08)	0.04 (0.17)	0.06 (0.20)	1.68 (0.28)
	Worst half	0.86 (0.08)	-0.01 (0.21)	-0.08 (0.19)	1.60 (0.25)

Table 2.4. **Eye movement controls**. 2-D Gaussian fit parameters of the stimulus-evoked response, obtained separately for the best and worst half of fixation, across two measures of fixation quality (see Methods). None of the differences in amplitude, location, or spread, for either statistic, were significant at the 0.05 level, suggesting that small differences in eye movements are not responsible for our results.

2.5 Discussion

Here we present two main findings. First, in a visual detection task, choice-related activity is distributed across tens of mm^2 of sensory cortex (Figs. 2.5; 2.6). This

finding suggests that subjects combine sensory signals from a broad region of cortical space in order to inform decisions. Second, the sensory population responses we measured correspond more closely to the subject's choices than to the stimulus. This result was captured by a new metric, 'stimulus-choice correspondence index' (SCCI), which is directly related to the fraction of choice-related variability present in sensory cortex and is invariant to choice-unrelated variability. We developed a general computational model for studying the relation between choice-related activity and noisy measures of neural population responses. Using this model, we find that V1 population responses account for the majority of the subjects' choice-related neural variability. This finding suggests that perceptual performance is limited primarily by the quality of the sensory evidence gleaned by the subject from sensory cortex, and only secondarily limited by downstream noise.

Our finding that choice-related information is distributed broadly across sensory cortex is consistent with previous reports of weak single-neuron choice probabilities (Britten et al., 1996; Celebrini and Newsome, 1994; Cook and Maunsell, 2002; de Lafuente and Romo, 2005; Dodd et al., 2001; Nienborg and Cumming, 2006; Nienborg and Cumming, 2009; Palmer et al., 2007; Purushothaman and Bradley, 2005; Uka and DeAngelis, 2004) in the presence of weak inter-neuronal correlations (e.g., Zohary et al., 1994). If these neurons were statistically independent, choice-related activity in a single neuron should be immeasurably small (Shadlen et al., 1996). However, the presence of weak inter-neuronal correlations causes single-neurons to be weakly correlated with the population as a whole (e.g., Chen et al., 2006; Shadlen et al., 1996), making it possible to

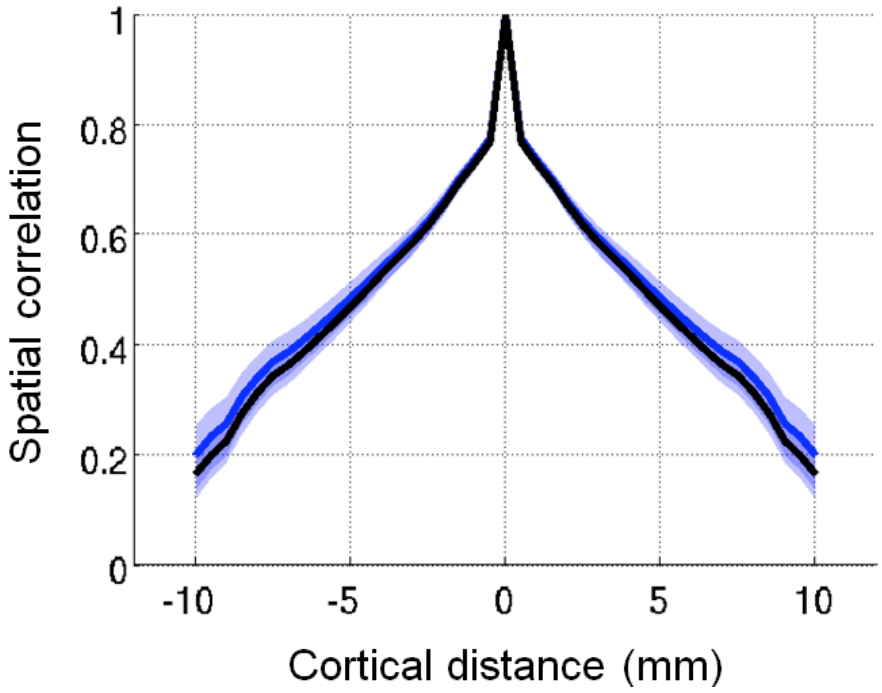

Figure 2.8. **Spatial correlations as a function of cortical distance**. Pixel-to-pixel correlation coefficients computed across all pairs of pixels, plotted as a function of cortical distance. **Blue**, target-present trials; **black**, target-absent trials. Shaded areas indicated 95% confidence intervals (bootstrapped). The spatial correlation profiles during target-present and -absent trials are statistically indistinguishable at all cortical distances tested.

measure significant CP in individual cells. Thus, while subjects are likely to pool broadly from sensory cortex to inform decisions, weak inter-neuronal correlations may have enabled previous studies to find weak correlations between the activity of single-neurons and behavior.

Our result that the sensory population signals correspond more closely to the subject's choices than to the stimulus is similar to findings reported previously in human V1 by fMRI (Ress and Heeger, 2003). Our results go beyond these earlier findings. First, in contrast to the slow and indirect nature of the fMRI signal, VSDI allowed us to

directly measure the spatiotemporal dynamics of these choice-related electrical signals in V1. In addition, by combining our results with a simple computational model, we show that most choice-related variability is present in early sensory cortex.

That variability in behavior can be explained largely by variability in sensory encoding is consistent with the conclusion of a previous study, which compared the fidelity of pursuit eye movements in humans with the limits of motion perception inferred by analysis of neural responses in macaque MT (Osborne et al., 2005). Here we use the direct trial-by-trial relationship between sensory population responses and choice within the same subjects to show that variability in perceptual decisions is dominated by variability in sensory cortex.

The observed co-variation between V1 population activity and behavioral choice may be due to feed-forward (bottom-up) sensory noise. It may also be due to a feedback (top-down) mechanism, whereby signals from higher brain areas influence the neural activity of V1 (e.g., Nienborg and Cumming, 2009). The latter type of signal could be primarily post-decisional, where the decision propagates to and influences V1. It may also contain a pre-decisional component, where top-down signals alter V1 circuits in advance of the trial, influencing the stimulus-evoked response as it arrives. To address these possibilities, we examined the time evolution of the choice-related signals (Figs. 2.5c,f; 2.6c,f). Because stimulus contrast was very low, the target-evoked response is delayed and builds up slowly (Chen et al., 2008). In both target-present (green traces) and target-absent trials (red traces), the mean population response begins to show choice-related differences around the time of the onset of the stimulus-evoked response, and the

differences increase steadily throughout the trial. The near correspondence between the onset and dynamics of the choice-related signals and that of the stimulus-evoked response provides evidence against a *post-decisional* top-down mechanism in which we would expect the choice-related signals to manifest only well after the evoked response. However, we cannot rule out the possibility that the choice-related signals we observe are the result of a pre-decisional attention-like signal. This possibility is nevertheless somewhat unlikely for two reasons. First, in a recent study in which we directly examined the effects of spatial attention in V1 in a similar detection task, we observed attentional effects that occurred shortly *before* stimulus onset and spread over a larger spatial extent than the stimulus evoked response (Chen and Seidemann, 2012), inconsistent with the choice-related responses observed here (Figs. 2.5; 2.6). Second, because the stimulus sequence in our task was random, top-down signals that bias the subject's behavior prior to stimulus onset would only be detrimental to task performance. Since our results were collected in highly trained subjects, the impact of such a biasing signal in our results is likely to be minimal.

Our study speaks to fundamental questions about the relationship between noisy sensory representations and perceptual decisions. Here we show that decision-related neural activity is distributed broadly in early sensory cortex. This finding suggests that subjects pool information over a large population of sensory neurons to inform decisions, rather than relying on a small group of highly informative neurons. Second, we provide evidence that most of the choice-related neural variability is already present in early sensory cortex, suggesting that downstream circuits add little variability that affects

decisions. An important goal for future studies is to determine the extent to which these results hold in other visual perceptual tasks and in other sensory modalities.

Applicability of our model to other binary decision tasks

Our model and metric are not restricted to "yes/no" detection tasks but generalize to other types of binary decision tasks. For example, consider the relationship between our detection task and the ubiquitous motion direction discrimination task (e.g., Newsome et al., 1989). In each case, the subject must make a binary decision about a sensory stimulus while responses are collected from neurons that are sensitive to the stimulus presented. In direction discrimination, the subject is presented with a field of moving dots. A fraction of the dots move coherently in one direction while the remaining dots exhibit random motion. The fraction of dots that move coherently is the 'coherence', where lower coherence trials are more difficult to discriminate. Consider a case in which an experimenter identifies a population of neurons with a preferred direction of motion, and makes repeated measurements of their responses to a near-threshold low-coherence stimulus moving in the preferred direction ('preferred'; e.g., leftward motion) and in the opposite ('null'; e.g., rightward motion) direction; the subject must choose "leftward" or "rightward" in an attempt to correctly indicate the direction of motion presented. The collection of pooled responses to a single coherence and two different directions forms a pair of distributions, analogous to our pair of neural response distributions for target-present and target-absent trials, respectively. The experimenter may then normalize these distributions by subtracting from all responses the mean of the

responses belonging to the 'null' stimulus distribution, then dividing all responses by the mean of the responses belonging to the 'preferred' stimulus distribution. While direction discrimination is a one-interval 2-alternative forced choice task yielding just two possible outcomes (correct and incorrect choices), one may nevertheless identify two distinct distributions of pooled neural responses belonging to incorrect choices. The first distribution is the collection of pooled neural responses to stimuli in the 'null' direction in trials in which the subject chose "preferred" (analogous to our FA trials), and the second distribution is the collection of pooled neural responses to stimuli in the 'preferred' direction in trials in which the subject chose "null" (analogous to our Miss trials). The SCCI in this task may be defined as the difference between the mean of the former distribution and the mean of the latter distribution. As in our experiments, the SCCI quantifies the extent to which responses from this neural population correspond more closely, on average, to the stimulus or to the choice. Under the assumption that these pooled neural responses come from Gaussian, equal variance distributions, the experimenter can use maximum likelihood to estimate the model parameters $\{\sigma_s^2, \sigma_m^2, \sigma_d^2, T\}$ (see Eq. 2.1).

Relationship with previous studies of neural sensitivity

Our findings that the vast majority of measured variability is choice-unrelated and that the observed neural sensitivity is relatively weak are seemingly at odds with results from a previous study which showed that the VSDI responses in V1 are sufficiently sensitive to outperform the monkey in a similar detection task (Chen et al., 2006; Chen et

al., 2008). The most likely explanation for this discrepancy is that the strength of the average VSDI response can vary significantly across animals. The previous studies included for analysis only those experiments in which the responses to the high-contrast stimulus (25%-contrast Gabor) showed high signal-to-noise ratio (d' ≥ 3), whereas the current study considers experiments in which the responses to the 25%-contrast Gabor showed lower SNR (d' ≥ 1). The responses to low contrast stimuli in the current experiment are also much weaker than those in the previous study, while the total measured variability is comparable between the two studies. Because we normalize our responses such that the mean target-absent response is zero and the mean target-present response is unity, this weaker response manifests as additional choice-unrelated noise, which may explain why the MF value we report is so low. Importantly, the estimated DF value we obtain here is independent of this choice-unrelated variability, and can be accurately quantified provided we have sufficient data to estimate the mean neural response from each outcome category. An additional possible source for the discrepancy between the results of the two studies is that the two tasks were not identical. In the Chen et al. studies, monkeys were required to detect Gabor stimuli over a broad range of randomly intermixed contrasts (including contrasts well above psychophysical threshold), while in the current study, the monkeys were required to detect Gabor stimuli at just one or two contrast levels (always near psychophysical threshold). Unfortunately, a direct comparison between the two studies cannot be made because the previous study did not obtain sufficient numbers of trials at low target contrasts.

Chapter 3: Perceptual decisions are limited secondarily by sub-optimal decoding of sensory signals

3.1 Abstract

In Chapter 2, I showed that when monkeys perform a simple visual detection task, choice-related variability is distributed broadly across early sensory cortex, and that the majority of the choice-related variability is already present in the earliest stages of visual cortical processing. While this primary sensory neural variation could account for most of the monkey's task inefficiency, the quantitative contributions of the various stages in the formation of a perceptual decision to the subject's overall task inefficiency are unknown: variability at the level of the decision variable could occur because of sensory variability that is unavoidable, sub-optimal decoding of sensory signals, and additional neural variability introduced downstream from sensory cortex. Here we use a combination of direct measurement of neural population responses in primary visual cortex (V1) by voltage-sensitive dye imaging and a simple computational model to identify a family of possible decoding algorithms likely used by the monkey in our task, and use this result to estimate the relative contributions of these potential sources of inefficiency to the monkey's overall inefficiency. Two key features of our data suggest that the monkey does not employ a linear pooling rule. First, the spatial spread of activation in choice-triggered maps during target-absent trials is approximately twice as broad as during target-present trials. Second, we observed that the spatial spread of saccade endpoints during 'False Alarm' trials is approximately 41% broader than during

'Hit' trials. These observations, together with a recent finding that human detection performance may be limited by intrinsic location uncertainty (Michel and Geisler, 2011), led us to consider pooling algorithms that incorporate spatial uncertainty. Our data is consistent with the use of a decoding algorithm in which the monkey attempts to match a template of the evoked population response over a broad region of sensory cortex. The template is likely to have a space constant less than that of the evoked response, while the search is likely to occur over an area broader than that of the evoked response. In the second half of this study, we tested a family of such 'intrinsic uncertainty decoders' against the optimal rule for combining sensory population signals over cortical space. We found that the sub-optimality resulting from decoding the sensory signals with spatial uncertainty can explain a significant fraction of the overall inefficiency in task performance. Overall, our results suggest that in a simple detection task, perceptual decisions may be limited substantially by intrinsic spatial uncertainty in decoding sensory signals, and to a lesser extent, by downstream variability.

3.2 Introduction

When an organism is faced with a challenging perceptual task, what limits behavioral performance? I have previously shown (Chapter 2) that when monkeys perform a simple visual detection task, both stimulus-related signals and choice-related signals are distributed across a broad population of sensory neurons in primary visual cortex, and that the majority of the choice-related variability is already present in this earliest stage of visual cortical processing. This result suggests that performance may be

limited primarily by variability that occurs in early sensory cortex. However, decision-related variability in early sensory cortex depends both on the fidelity with which the brain encodes stimuli across the sensory cortical population, as well as the brain's efficiency in decoding these population signals. Here we consider the extent to which decision-related variability in primary visual cortex in our task is due to unavoidable sensory variability, and the extent to which it is due to inefficiencies in decoding.

How the subject reads out, or decodes, the distributed sensory population signals in order to form a decision is unknown. To address this question, we used an approach based on signal detection theory. We assumed that on each trial, the subject combines responses from a population of sensory neurons during stimulus presentation to form a single number (the decision variable). The monkey then compares the decision variable to a criterion to determine the behavioral choice on that trial (Green and Swets, 1966). Previous studies have proposed various pooling models to describe how populations of sensory neurons contribute to a perceptual decision (e.g., Shadlen et al., 1996). However, the neural populations used to constrain such models are often, in practice, aggregates of the responses of individual neurons collected one by one.

In contrast to single-neuron electrophysiology, methods for simultaneously measuring the responses of a large population of neurons, such as voltage-sensitive dye imaging (VSDI) (Grinvald and Hildesheim, 2004), can reveal how the spatial distribution of responses of sensory neurons co-varies with behavioral choice on a trial-by-trial basis, potentially providing stronger constraints on models of the population decoding process. For example, by comparing the spatial distribution of sensory activity during trials in

which the subject makes one behavioral choice with that during trials belonging to the alternative behavioral choice, one can potentially identify those neurons that are weighted more heavily in the decision process.

To address the question of how subjects decode signals encoded across a sensory population, we used VSDI to record from a large population of neurons in primary visual cortex (V1) of two monkeys while they performed a difficult visual detection task. We used key features of our data to constrain our search for a likely decoder and identified a family of plausible decoding algorithms. To determine the extent to which performance is limited by inefficiencies in the decoding process, we compared the efficacy of these algorithms with that of the optimal decoding algorithm. This approach allows us to determine whether post-sensory processing is primarily limited by sub-optimal decoding of sensory signals or by additional neural variability occurring downstream from the sensory decoding process.

3.3 Materials and Methods

The monkeys' task, visual stimuli, VSDI recording and signal pre-processing are identical to those described in Chapter 2.

Intrinsic Uncertainty Decoder

Important features of our physiological and behavioral data suggested that subjects are uncertain about the precise location of the visual stimulus in our detection task (see Results for details). To explore this possibility, we developed an intrinsic

uncertainty decoding algorithm, or a hypothesized mechanism by which subjects may attempt to perform the task despite their incomplete knowledge of the stimulus location. We developed a simple model of the decision process (Fig. 3.3) and carried out a series of simulations based on the model. Our model is described in the Results section within a connectionist framework involving three hypothetical cortical layers. Briefly, in this example framework the brain first encodes visual stimuli across a population of primary sensory cortical neurons. Next, this sensory population sends convergent projections onto a second layer of cortex, where the brain attempts to match the population response to a remembered template. Third, the template layer projects to a third layer via unequally weighted, parallel connections, allowing the brain to weight the likelihood that a potential match arose from the presence of a visual stimulus, based on the remembered location of that stimulus. Finally, neurons of this third layer instantiate a winner-take-all-like mechanism via lateral, inhibitory connections, which serve to identify the maximally responding neurons of this cortical layer, whose responses are taken to be the scalar decoded sensory response.

We carried out the simulations by applying a sequence of equivalent mathematical operations. We first simulated the encoding stage in V1 as a 2-dimensional patch of neurons/pixels with signal and noise characteristics consistent with those observed in the real data. To decode these sensory signals, the simulated subject searches for a peak of activation in sensory cortex by convolving the population activity map on each trial with a 2-D Gaussian template (equivalent to Fig. 3.3b, 'Template Matching'). We later extended our model by considering a template with weights proportional to the

difference-of-Gaussians (DOG) that optimally separates target-present trials from target-absent trials in the absence of location uncertainty, and tested this template under varying amounts of location uncertainty. Second, the subject weights potential match locations according to prior knowledge about the target location. We simulated the subject's knowledge of the target location as a 2-D Gaussian (Fig. 3.3b, 'Uncertainty Weighting') centered on the correct cortical location of the stimulus-evoked response. The subject weighted the match locations by multiplying the output of the convolution operation in the first step by the Gaussian spatial uncertainty distribution. Third, the simulated subject selected the pixel with the maximal response, and its value was taken to be the pooled sensory response. We later generalized this stage such that it transforms the population activity into a scalar response via the p-norm operation. The p-norm is defined as

$$\|x\|_p = \left(|x_1|^p + |x_2|^p + \ldots + |x_n|^p \right)^{1/p} \tag{3.1}$$

and is equivalent to the maximum operation when $p = \infty$. We repeated our simulations for $p = \{1,2,3,4,5,10,100, \infty\}$. Finally, we added independent, zero-mean Gaussian noise (Fig. 3.3a, 'Downstream Noise') to the pooled sensory response, producing the decision variable. Trials for which the decision variable exceeded a criterion were classed as "choose target-present" trials; all other trials were "choose target-absent" trials. The amount of downstream noise and the decision criterion were chosen such that the simulated monkey's performance matched the real monkey's percent correct and distribution of behavioral outcomes (see Chapter 2, Table 2.1 for details regarding

behavioral performance). Finally, in order to evaluate the performance of the model, we computed choice-triggered maps by averaging the simulated V1 activity according to the simulated subject's choices; we computed simulated eye movements by multiplying the cortical location of the maximally responding pixel on each trial by a cortical magnification factor based on the retinal location of the target in each monkey.

In order to simulate the sensory encoding stage as a 2-dimensional patch of pixels with signal and noise characteristics consistent with those observed in the real data, we assumed that the total measured variability arose from two sources: neural activity in V1 and measurement noise. Measurement noise in the VSDI recordings consists of camera sensor shot noise and mechanical fluctuations, as well as non-neural biological noise such as residual heartbeat and respiration artifacts. The relative contributions of neural activity and measurement noise to the VSDI signal are unknown. Because the statistics of interest we compute from our simulated data (see below) are based solely on averages, they are unaffected by the presence of zero-mean measurement noise (we performed additional simulations to verify that none of our statistics were affected); therefore we did not include measurement noise in our simulations. However, these statistics depend on the degree to which the simulated neural V1 signals are correlated across space. To address this concern, we performed preliminary simulations under six discrete assumptions about the spatial correlations in neural V1 signals. We started by assuming that the measured correlations arose entirely from neural activity in V1. Based on our empirical results, we also assumed that the variance is identical at each pixel, and that the spatial correlations are isotropic, depending only on cortical distance. In subsequent

simulations, we modeled the neural variability in V1 with a white component and a correlated component, and we varied the ratio of these components such that the simulated neural noise comprised 0%, 5%, 25%, 50%, 75%, or 100% of the total noise correlations observed in the VSDI signals. In these preliminary simulations, when the correlated component of our simulated neural variability was large (> 5%), we were unable to reproduce our result that the average spatial pattern of activity during False Alarm trials exceeds that of Miss trials. Thus, the models presented in the Results section were carried out under the assumption that 5% of the observed correlations originated from neural activity in V1.

Our model contains three free parameters: the average variance of each neuron/pixel in V1, σ_{V1}^2; the breadth of the uncertainty template, $\sigma_{template}$; and the breadth of the uncertainty window, $\sigma_{uncertainty}$. For each pair of ($\sigma_{template}$, $\sigma_{uncertainty}$), σ_{V1}^2 determines the variability of the decoded (scalar) response, which can be expressed as a fraction of the total variability related to choice, DF (see Chapter 2). We aimed to reproduce two key features of our data: greater spread of activation of choice-triggered maps and greater spread in saccade endpoints during target-absent trials than during target-present trials. Additionally, we aimed to reproduce our earlier key finding that FA trials show stronger activity than Miss trials (see Chapter 2).

For each point in parameter space, we computed key statistics from the simulated data. We first computed choice-triggered maps by averaging together the simulated V1 responses belonging to Hit and Miss trials and taking their differences; we similarly averaged together responses belonging to False Alarm and Correct Rejection responses

and taking their difference. We then fitted these target-present and target-absent choice-triggered difference maps to a 2-dimensional Gaussian with a single parameter for the breadth of the activity in each stimulus condition, $\sigma_{H\text{-}M}$ and $\sigma_{FA\text{-}CR}$, respectively, as well as an amplitude parameter and two location parameters. The ratio of these widths, $\sigma_{FA\text{-}CR} / \sigma_{H\text{-}M}$, was the choice-triggered map ratio (CTMR). Next, we computed the saccade ratio (SR) as the ratio of the spread of simulated saccades during False Alarm trials, σ_{FA}, to that of Hit trials, σ_{H}. Additionally, we computed the SCCI statistic (see Chapter 2) in two ways. First, $SCCI_{1D}$ was the difference between the mean scalar decoded response during False Alarm trials and that during Miss trials, identical to the SCCI statistic computed in Chapter 2. Second, $SCCI_{2D}$ was the difference between the fitted 2-D Gaussian amplitude parameter during False Alarm trials and that during Miss trials. We identified the best-fitting model parameters by computing identical statistics in our real data and comparing each statistic to the corresponding statistic of the simulated data, and identified the point in parameter space that minimized the Euclidean distance between the simulated and empirical data.

Comparison between intrinsic uncertainty decoder and optimal decoder

In order to understand the impact of sub-optimal decoding due to intrinsic location uncertainty, we compared the performance of our best fitting intrinsic uncertainty decoder with the performance of the optimal decoder. We first applied the optimal decoder (Chen et al., 2006) to the simulated V1 signals, whose pixel variance and spatial correlation structure was given by the analysis described above. We defined the

variance of the pooled sensory response, when computed with the optimal decoder, as the unavoidable sensory variability. Next, we applied the best-fitting intrinsic uncertainty decoder to the same simulated V1 signals, computed the variance of the pooled sensory response, and defined this value as the effective sensory variability. We then quantified the impact of sub-optimal decoding as the difference between the effective sensory variability and the unavoidable sensory variability. Finally, we computed the downstream variability as the difference between total choice-related variability and the effective sensory variability. Each of these three quantities (unavoidable sensory variability, impact of sub-optimal decoding, and downstream variability) was expressed as a percentage of the total choice-related variability.

Eye Movements

To assess the relationship between saccadic eye movements and choice-related activity, we computed the (x,y) location, in degrees of visual angle relative to the fixation point, of the endpoint of the saccade during Hit and FA trials. The endpoint was defined as the mean eye position during a 50-ms interval beginning at the moment the eye position entered a square window centered on the location of the Gabor target. The location of the visual target was (0.5, -4.25) in Monkey T; and (0.5, -1.5) in Monkey C. The window was ≤ 6° for Monkey T, and ≤ 2° for Monkey C. Each monkey was required to hold fixation in the target window for 100 ms in order to indicate a "choose target-present" response. Before combining saccade endpoint data across the two

subjects, we first removed the mean endpoint vector (across both FA and Hit trials) from each monkey.

In order to determine whether there was a trial-by-trial relationship between the location of saccade endpoints and the locus of cortical activity during individual Hit and FA trials, we re-centered the activity map on each trial based on the saccade endpoint vector. In the present experiments we did not collect detailed retinotopic data; however, because our imaging region-of-interest (ROI) is located over an anterior portion of V1 in the left hemisphere of each monkey, and is aligned such that the top edge of the ROI is parallel to the lunate sulcus, we performed a simple procedure that approximates a correction from visual coordinates to cortical coordinates. Maps corresponding to trials with saccade endpoints below the mean (negative y direction) were shifted to rightward; those from trials with endpoints above the mean (positive y direction) were shifted leftward. Maps corresponding to trials with saccade endpoints to the right of the mean (positive x direction) were shifted downwards; those from trials with endpoints to the left of the mean (negative x direction) were shifted upwards. Each trial's activity map was shifted by an amount equal to the saccade endpoint vector's deviation from the mean, times a cortical magnification factor (CMF). We assumed a CMF of 4 mm / °. We then fit the resulting mean activity maps for each behavioral category with a 2-dimensional Gaussian, and compared the fitted space constants of the re-centered maps with those from the raw activity maps under a bootstrap test.

3.4 Results

We trained two monkeys to perform a simple reaction-time visual detection task (Chapter 2, Fig. 2.1). Each trial began when the monkey directed gaze to a central fixation point. During 'target-present' trials (50% of trials) the monkey was required to rapidly change his direction of gaze to a small visual target in its periphery; during 'target-absent' trials (the remaining trials) the monkey was required to maintain fixation on the central fixation point. The visual target consisted of a small Gabor patch stimulus (sinusoidal grating in a 2-D Gaussian envelope), and importantly, the stimulus was presented at the same location in visual space on all target-present trials. Gabor stimuli are known to drive V1 cells effectively. To make the task difficult, the stimulus was presented at one or two contrast levels near each monkey's perceptual detection threshold. The monkey's response was classed as a 'Hit' (H) if he correctly detected the target, and a 'Miss' (M) if he failed to detect a target when it was presented. The response was classed as a 'False Alarm' (FA) if the monkey incorrectly reported a target and a 'Correct Rejection' (CR) if he correctly indicated that a target was not presented (see Chapter 2, Table 2.1 for details regarding behavioral performance).

We recorded population responses from V1 with voltage-sensitive dye imaging (VSDI) while the monkeys performed the task. V1 contains cells that respond effectively to our visual stimulus, and thus the V1 population is likely to be useful to the monkey in performing the task. Because our visual target is spatially localized and V1 responses are retinotopically organized, task-relevant neuronal population responses are likely to be confined to a small region in V1 (Chen et al., 2006; Sit et al., 2009) that can be entirely

captured by the VSDI technique. Thus, our VSDI recordings are likely to capture most of the neurons that are useful to the monkey in performing the task.

Results from a representative VSDI experiment (Fig. 3.1a) reveal robust, distributed V1 responses to the stimulus. Fig. 3.1a shows the mean spatial spread of activation during stimulus-present and stimulus-absent trials, as well as the mean activity maps associated with each of the four behavioral outcomes, and the choice-related activity maps. These data demonstrate that the visually-evoked response, while distributed over several mm of visual cortex, is nevertheless contained within our imaging region-of-interest; thus our VSDI recordings likely captured most of the cortical signals useful to the monkey. The data in Fig. 3.1a,e is identical to that of Fig. 2.4a,d, and is reproduced here for convenience.

Intrinsic uncertainty decoding algorithm

Our first goal is to identify an algorithm likely used by the monkey in decoding the sensory population. A straightforward approach to this problem is to observe the spatial pattern of activity in choice-triggered averages of the sensory population. This approach is a variant of the standard psychophysical reverse correlation paradigm. In the standard paradigm, the experimenter presents a noisy visual pattern to the subject, who is required to indicate whether a target appeared or did not appear in the display. The experimenter averages together the noisy stimulus maps belonging to one behavioral choice and separately averages together those belonging to the alternative choice (in trials of the same stimulus condition) and produces a choice-triggered map by subtracting the

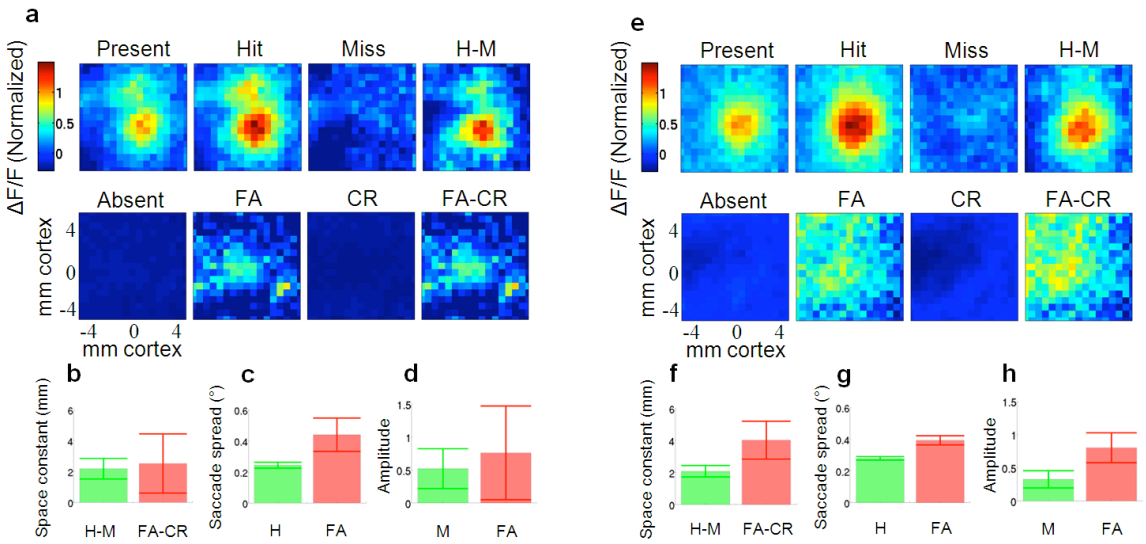

Figure 3.1. VSDI sensory population recordings and eye movements. **a-d**, Example VSDI experiment in Monkey T. **a**, Average cortical activity maps separated by stimulus condition (rows) and behavioral choice (columns), and averaged over a 100 ms temporal window (see Methods for details). Upper row of panel **a** represents neural activity during target-present trials; lower row shows activity during target-absent trials. Activity maps are shown separately for 'choose target-present' (H and FA) and 'choose target-absent' (M and CR) trials. 'H-M', difference map of activity during Hit and Miss trials. 'FA-CR', difference map of activity during FA and CR trials. **b**, Fitted space constants of the choice-triggered maps, in mm of cortex. **c**, Standard deviation of saccade endpoints, in degrees of visual angle. **d**, Fitted amplitude of the Miss and FA maps. In **b-d,f-h**, error bars indicate bootstrapped standard error of the mean. **e-h**, Aggregate summary of VSDI and behavioral results collapsed over 13 experiments in Monkey T and 2 experiments in Monkey C. Same organization as in **a-d**. In **g**, the mean location of each monkey's saccade endpoint data was removed before combining across monkeys (see Methods).

two averages. The resulting map reveals the subject's template, or a map of linear weights by which the subject is assumed to multiply the noisy display on each trial to form the decision variable. In this variant of the paradigm, which may be called neural reverse correlation, we average together trial-to-trial variability in neural population activity rather than that in an external visual display. Fig. 3.2 shows the average choice-related population activity, computed across all trials, after the mean stimulus-evoked

response has been removed from stimulus-present trials, and separately for target-present and target-absent trials. As in the standard paradigm, the resulting choice-triggered map is expected to reveal the decoding template the subject applies to the noisy cortical population on each trial.

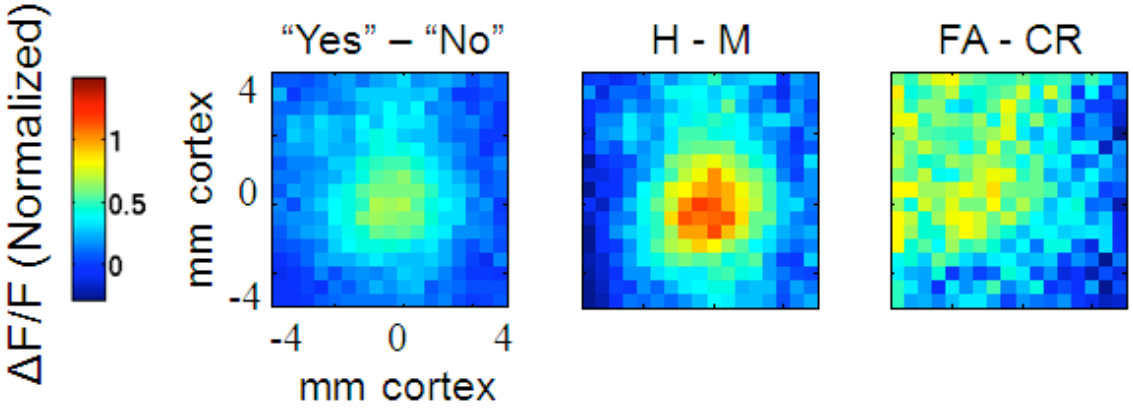

Figure 3.2. Average choice-related population activity maps. **"Yes" – "No"**, mean choice-related population activity computed across all trials, after the mean stimulus-evoked response has been removed from all target-present trials. **H-M**, mean choice-related activity map during target-present trials. **FA-CR**, mean choice-related activity map during target-absent trials.

Importantly, under the assumption that the monkey decodes the sensory population response by the application of a fixed, linear decoding rule as described above, applying the neural reverse correlation procedure to our data should produce identical choice-triggered maps during target-absent trials as during target-present trials. Because the presence of the stimulus does not alter the noise properties of our data (see Chapter 2, Fig. 2.8), and because the neural reverse correlation procedure is applied only

to trials belonging to two alternative choices within the same stimulus condition, the presence or absence of a stimulus should have no effect on the resulting maps. Thus we can test whether the monkey employs such a rule by comparing the choice-triggered map obtained during target-present trials with that obtained during target-absent trials.

Features of our VSDI data suggest that the monkeys' decoding algorithm is inconsistent with a fixed template. Fig. 3.1a-d shows the results of an example experiment in Monkey T. Because the results from the two monkeys were qualitatively similar (see Chapter 2, Fig. 2.6), 13 experiments from Monkey T and 2 experiments from Monkey C were combined to produce our aggregate results (Fig. 3.1e-h). Fig. 3.1a,e ('H-M', 'FA-CR') show the choice-triggered maps obtained during target-present and target-absent trials, respectively. Comparison of these maps reveals that choice-related activity in V1 is distributed more broadly in the absence of a stimulus ($\sigma_{FA\text{-}CR}$ = 4.02 mm) than in the presence of a stimulus ($\sigma_{H\text{-}M}$ = 2.08 mm) (Fig. 3.1f), whose ratio, 1.99 (95% CI: [0.98 3.29]), is significantly greater than unity (p = 0.032, one-tailed bootstrap test). This finding could result from the subject using a distinct linear template during target-absent trials as during target-present trials. However, because the subject has no advance knowledge of whether the target will appear on a given trial, the subject is unable to employ such a strategy.

Instead, these data may be consistent with a decoding algorithm that suffers from location uncertainty. We reasoned that if the subject has imperfect knowledge as to the precise location of the visual target, an effective strategy to decode the sensory population might be to search for a peak of activation over a region of cortex that is likely

to contain the stimulus response. The decoding circuit would look for the best match to a template that resembles the evoked response, and weight the goodness of this match by the likelihood that the response would occur in a given location, based on the subject's memory. Such a strategy would be employed on stimulus-present and stimulus-absent trials alike. We reasoned further that the presence of even a weak stimulus would increase the likelihood that a peak of activation resembling the evoked response would occur at a cortical location that is common to all target-present trials (i.e., the location in cortex that retinotopically corresponds to the actual, fixed, stimulus location). Such a mechanism would lead to choice-triggered maps that are more spatially localized in target-present trials than in target-absent trials, potentially explaining our results.

Analysis of eye movements further supports the hypothesis that the subject is uncertain about the precise location of the target. We require our subjects to make a saccadic eye movement to the target location when a stimulus has been detected. In trials in which the monkey indicates a target-present choice (whether correctly or incorrectly), we extinguished the target immediately upon onset of the eye movement and replaced it with a small point at the target location. Because this visual reminder appeared after saccade initiation, it did not affect the monkey's saccade endpoint, which displayed large trial-to-trial variability. We observe that the location of saccade endpoints is distributed more broadly during incorrect detections (σ_{FA} = 0.39 degrees) than during correct detections (σ_{H} = 0.28 degrees) (Fig. 3.1g), whose ratio is 1.41 (95% CI: [1.19 1.63]), significantly greater than unity ($p \approx 0$, one-tailed bootstrap test). This behavior is also consistent with the general spatial uncertainty decoder framework described above. For

example, a subject who is uncertain about the precise location of the visual target, but who is required to indicate the perceived presence of the target with a saccadic eye movement to its location, could adopt a strategy to make an eye movement to the location he thinks is the most likely. According to the subject, the most likely location in visual space is that which corresponds to the retinotopic location in sensory cortex that shows the strongest activity. Together, the greater spread of activity in the choice-triggered map collected during target-absent trials than during target-present trials, as well as the greater spread of saccade endpoints during target-absent trials than during target-present trials suggests that in our task, subjects may be impacted by some form of spatial uncertainty.

In our effort to discover potential decoding algorithms that are consistent with our physiological and behavioral results, we also aimed to explain a third key feature of our data: that average False Alarm activity exceeds average Miss activity. Recall from Chapter 2 that we introduced a metric, stimulus-choice correspondence index (SCCI), that quantifies the difference between the mean decoded (scalar) response during False Alarm trials and that during Miss trials. In the context of Chapter 2, the value of the SCCI quantity depended on the specific algorithm used to decode the sensory population responses, and we repeated our analysis for a family of 9 alternative, biologically plausible pooling rules. However, in the present analysis we developed a variant of the SCCI metric that is readout-independent. This metric, which we call $SCCI_{2D}$, is the amplitude of the 2-D Gaussian-fitted mean False Alarm population response minus that of the mean Miss population response (see Methods). Fig. 3.1d,h shows the fitted amplitudes of the Miss (green) and False Alarm (red) response. In our combined data,

the False Alarm response amplitude was 0.80, and the Miss response amplitude was 0.33; their difference, $SCCI_{2D}$ = 0.47 (95% CI: [0.00 1.02]), was significantly greater than zero (p = 0.05, two-tailed bootstrap test). This additional formulation of the SCCI metric enabled us to assess the goodness with which potential decoding algorithms could explain this feature of our data.

To determine whether an intrinsic uncertainty decoding algorithm could explain our imaging and behavioral results, we developed a simple model (Fig. 3.3). In our model of the formation of the decision, the brain first encodes the visual stimulus in a sensory population (Fig. 3.3a, 'Sensory Encoding'). The brain then decodes the signals by transforming the distributed sensory signals into a single value, which could occur by convergent and parallel projections to subsequent layers (Fig. 3.3a, 'Decoding'). Finally, we assumed that this single-valued decoded sensory response is corrupted by additional neural variability introduced by a subsequent stage (Fig. 3.3a, 'Downstream Variability'). The resulting single-valued response represents the decision variable, which is compared to a criterion to determine the monkey's binary choice.

We considered a spatial uncertainty decision algorithm by which the brain may transform the distributed sensory responses into a single-valued variable in a series of three layers (Fig. 3.3b), although other neural implementations of our algorithm are possible. We first simulated the encoding stage in V1 as a 2-dimensional patch of neurons/pixels with signal and noise characteristics consistent with those observed in the real data (see Methods). In our model, the decoding circuit could search for a template of an expected evoked response in the sensory layer by sending converging projections to

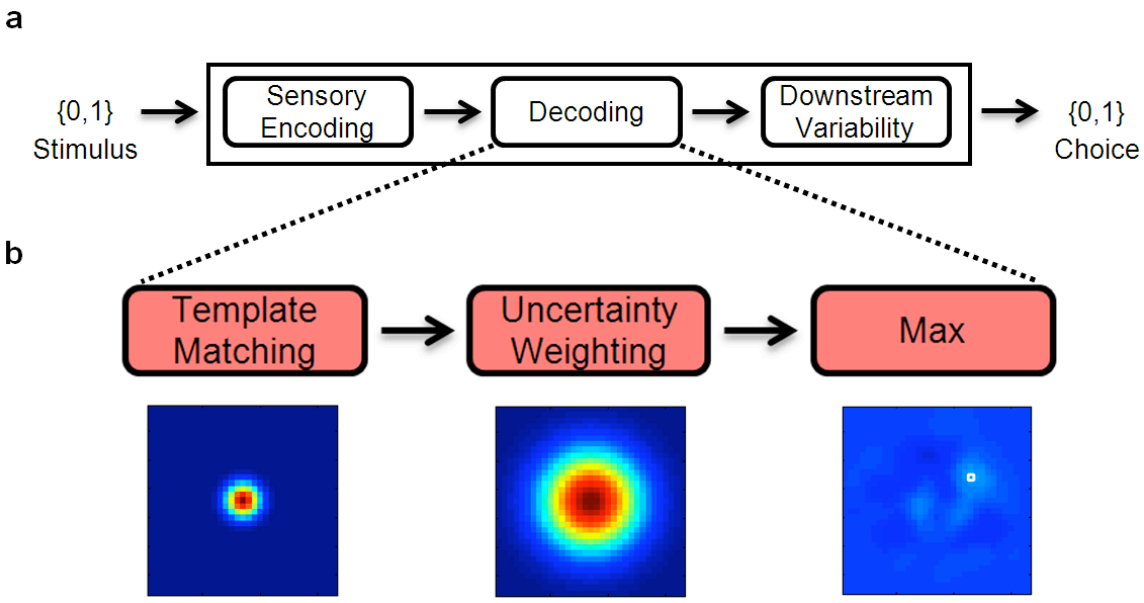

Figure 3.3. Intrinsic uncertainty decoder framework. **a**, General decision framework in which the intrinsic uncertainty decoder is applied. Stimulus-related signals are encoded in a 2-dimensional patch of sensory cortex ('Sensory Encoding'); a decoding algorithm ('Decoding') transforms the 2-dimensional signals into a scalar quantity; independent noise is added to the decoded scalar response ('Downstream Variability'); the result is then compared to a criterion to determine the binary choice. **b**, Successive stages of the intrinsic uncertainty decoding algorithm. On each trial, the decoder first searches sensory cortex for a peak of activity ('Template Matching'); second, the decoder evaluates the likelihood that a potential match occurred due to the presence of a stimulus, given the brain's imperfect knowledge of the stimulus location ('Uncertainty Weighting'); finally, the decoder identifies the maximally responsive pixel ('Max'), whose value is taken to be the decoded scalar response.

the second layer (Fig. 3.3b, 'Template Matching'). Each neuron/pixel in the second layer receives connections from a small neighborhood of sensory neurons and averages their responses together. The inputs from sensory neurons are assigned weights proportional to a 2-D Gaussian centered on the sensory neuron that has the same topographic location of its corresponding neuron in the second layer. Due to convergence, neurons of the

second layer are driven effectively when a collection of nearby sensory neurons are activated together, such as when they respond to a spatially distributed stimulus. In the absence of target location uncertainty, neurons of the second layer could most effectively distinguish between target-absent and target-present trials when the pattern of weights assigned to the converging inputs matches the spatial pattern of sensory activation, assuming the noisy sensory activity is spatially white. When the sensory activity is spatially correlated, the template that most effectively distinguishes between the two stimulus conditions is a Difference-of-Gaussians whose weights are proportional to the average stimulus-evoked response after it has been whitened twice (Chen et al., 2006).

Next, the decision circuit evaluates whether a potential template match identified in the second layer is likely to have arisen from the physical stimulus, based on the subject's imperfect prior knowledge about the location of the stimulus in visual space. Signals from the second layer could be sent via unequally weighted parallel projections to a third layer (Fig. 3.3b, 'Uncertainty Weighting'). In this step, weights are assigned proportional to a 2-dimensional Gaussian centered on the cortical location that corresponds retinotopically to the location in visual space where the target is most likely to appear, based on the subject's memory. Due to unequally weighted parallel connections, potential matches are weighted more heavily when the match occurs near a location the subject believes is the correct target location.

Finally, the decision circuit transforms the distributed responses of the third layer into a single-valued response by selecting the maximally responsive neuron (Fig. 3.3b, 'Max'). In this final stage, inhibitory horizontal connections in the third layer could

instantiate a winner-take-all-like mechanism whereby the activity of the maximally responsive neuron is magnified at the expense of all other neuronal responses. The response of this neuron represents the decoded sensory response. Furthermore, since the decoding circuit preserves topographic information about the cortical responses at each stage, the location in visual space that corresponds retinotopically to the cortical location of this neuron represents the decoded location of the visual target. This neuron's response is corrupted by additional neural variability (Fig. 3.3a, 'Downstream Variability') to form the decision variable. If the decision variable exceeds a criterion, the subject chooses "target-present" and makes a saccadic eye movement to the decoded target location; otherwise the subject chooses "target-absent" by maintaining fixation on the central fixation point.

Our model has three parameters. The degree of convergence from the first layer to the second determines the size of the template being considered, and is quantified as the standard deviation ($\sigma_{template}$, in pixels/cortical distance) of the 2-dimensional Gaussian pattern of weights with which the first layer projects to the second. Similarly, the degree of location uncertainty is determined by the standard deviation, $\sigma_{uncertainty}$, of the 2-dimensional Gaussian pattern of weights with which the second layer projects in parallel to the third. Finally, the variability of the sensory neurons, together with $\sigma_{template}$ and $\sigma_{uncertainty}$, determines the subject's accuracy in performing the task, and is quantified as the variance of the individual neurons/pixels in V1, σ_{V1}^2. We performed a series of simulations to determine whether our model framework could explain our imaging and behavioral results. The simulations were carried out by applying a sequence of

mathematical operations that are equivalent to the example connectionist framework described here (see Methods).

The essential behavior of our model reveals three main results, and can be understood intuitively. First, within our framework, location uncertainty is required to achieve choice-triggered maps that are more broadly distributed during target-absent trials than during target-present trials. Examination of a small number of simulated example trials clarifies how location uncertainty leads to such a result. Fig. 3.4 shows the simulated population activity as it evolves over the three successive stages of the intrinsic uncertainty decoder, for five example trials. Each of the five trials is shown in the absence of a stimulus-evoked response (leftmost three columns) and in the presence of the stimulus-evoked response (rightmost three columns). Consider first the target-absent trials. The simulated V1 activity (Fig. 3.4, left side, 'Encoding') in these example trials is composed of white noise. The uncertainty decoder transforms this activity by its convergent projections to the second layer ('Template Matching'), which results in a blurred version of the same noise pattern. In turn, this second layer projects in parallel to the third with weights proportional to a large (i.e., high uncertainty) 2-D Gaussian. Because the location uncertainty is large in this example, the location of the maximally responding pixel (indicated by a white square) can occur with nearly equal probability at any pixel in the image, and indeed is widely dispersed across the five example trials shown. In contrast, when a simulated, deterministic 2-D Gaussian evoked response is added to the same five noise patterns (rightmost three columns of Fig. 3.4), the increased activity due to the evoked response increases the likelihood that the maximally

responding pixel will occur near the center of the cortical image, despite the large location uncertainty. The tendency for maximally responding pixels to occur near the center of the image during target-present trials, but not target-absent trials, results in a narrowing of the spatial distribution of activity during target-present trials (particularly in 'Hit' trials, in which the value of the maximally responding pixel is large enough to cross the monkey's criterion and elicit a "target-present" response), as compared to that in target-absent trials. The interaction between the stimulus-evoked response and the uncertainty weighting, in turn, results in a narrower spread of cortical activity in choice-triggered maps during target-present trials, as compared to target-absent trials. Additionally, because our simulated saccadic eye movements are determined by the location of the maximally responding pixel in each trial (see Methods), the same reasoning can potentially explain our behavioral result that the spread of the endpoints of the monkey's saccadic eye movements is greater during target-absent trials (i.e., FA trials) than during target-present trials (i.e., Hit trials).

In contrast, in the absence of location uncertainty, choice-related difference maps obtained during target-present trials will be identical to those obtained from target-absent trials. The no-uncertainty case is a special case of our uncertainty decoder in which the uncertainty weighting map is an impulse function, with a weight of unity at the center of the evoked response and weights of zero elsewhere. Because the maximally responding pixel can occur in just one location, this special case of the uncertainty decoder reduces to a linear model whereby sensory signals are transformed into scalar responses through the application of a fixed set of weights, such as those models considered in Chapter 2. For

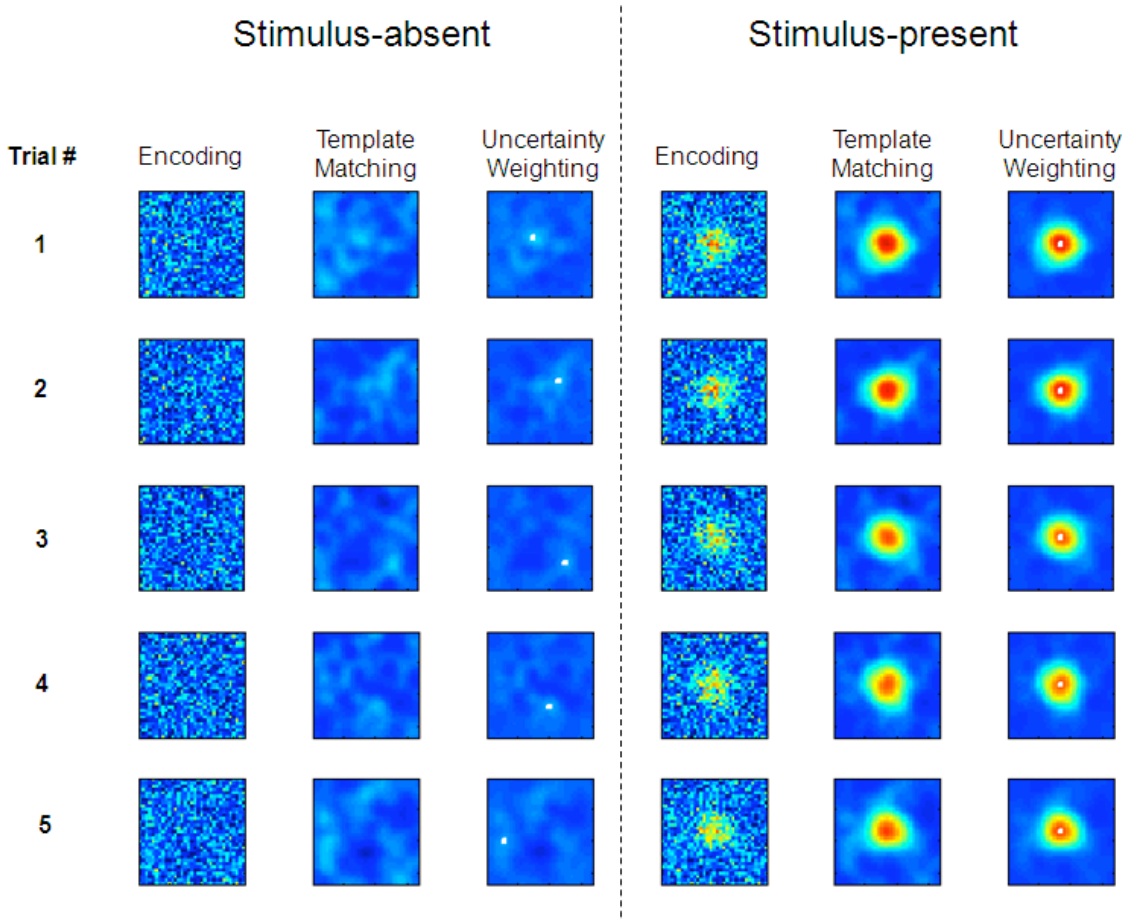

Figure 3.4. Effect of the stimulus on the intrinsic uncertainty decoder. Each row shows the behavior of the intrinsic uncertainty decoder for five example trials without an evoked response (leftmost three columns) and for the same five noise trials with a stimulus-evoked response added (rightmost three columns). In each side of the figure, the first column represents the noise pattern of each trial ('Encoding'); the second column shows the blurred response of the 'Template Matching' stage of the uncertainty decoder; third column shows the 'Uncertainty Weighting' stage of the decoder. See Fig. 3.3 and text for explanation of each stage. White square indicates the location of the maximally responding pixel for each trial.

the same reason, the simulated saccadic eye movement will terminate in the same location in visual space in all trials. Thus, within our framework, location uncertainty is

required in order to obtain stimulus condition-related differences in the spread of the choice-triggered maps as well as the spread in saccade endpoints.

The second main result of our simulation is that the narrowing effect exerted by the stimulus-evoked response on the choice-triggered maps during location uncertainty is parametrically related to the signal-to-noise ratio (SNR) in V1. The narrowing effect described above occurs because the presence of the stimulus-evoked response increases the likelihood that the most highly active pixels will occur near the center of the image. Intuitively, stronger evoked responses will produce a stronger effect. This narrowing effect is strongest when variability in V1 is small (i.e., high SNR), and weakest when variability in V1 is large (i.e., low SNR). This observation suggests that in order to explain our physiological result that the choice-triggered map during target-absent trials is significantly broader than that during target-present trials, our parameter representing the variability in V1, σ_{V1}^2, must be sufficiently small.

The third main result of our intrinsic uncertainty decoder simulation is that our critical finding from Chapter 2 – that average cortical activity during False Alarm trials exceeds average cortical activity during Miss trials only when sensory variability is large – extends to decoding models that suffer from location uncertainty. We learned from the model presented in Chapter 2 that the variability in V1 must be sufficiently large (DF ≥ 0.55, see Chapter 2, Fig. 2.3e, black trace) to explain our finding that average activity during False Alarm trials exceeds that during Miss trials. We performed a similar analysis with our intrinsic uncertainty decoder. For each pair of intrinsic uncertainty decoder parameters ($\sigma_{template}$, $\sigma_{uncertainty}$), we varied the amount of V1 neuron/pixel noise

such that the total fraction of choice-related variability present in V1 (i.e., DF) varied from zero to unity. We then plotted the SCCI statistic as a function of DF for each decoder (see Methods for details on computing the SCCI statistic in the context of the present analysis). In all cases, the SCCI statistic began at -1 when DF = 0, and increased linearly with increasing DF. The slope of the line relating SCCI to DF depended on our assumption about the noise structure in V1 (see Methods). The maximum slope (which occurred under the assumption of white noise) produced a line that is identical to that shown in Fig. 2.3e, black trace; all other cases produced lines with shallower slopes. This result suggests that for all instances of the intrinsic uncertainty decoder considered here, the function shown in Fig. 2.3e yields a lower bound on DF for an observed SCCI. Thus for an intrinsic uncertainty decoder, as in the fixed decoders considered earlier, in order to explain our physiological result that FA activity exceeds Miss activity, σ_{V1}^2 must be sufficiently large.

These observations thus illustrate an important tradeoff in the σ_{V1}^2 parameter. On one hand, V1 variability determines the relationship between the mean False Alarm response and to the mean Miss response, and must be large enough to match our empirical finding that the former exceeds the latter. On the other hand, the amount of V1 variability must be sufficiently small such that the presence of a stimulus has an appreciable effect in narrowing the choice-triggered map and distribution of saccadic eye movements during target-present trials, as described above. Together, these observations suggest that if a pair of intrinsic uncertainty decoding parameters ($\sigma_{template}$, $\sigma_{uncertainty}$) is found that can potentially explain our data, we expect it to do so only over a limited range

of the DF quantity. Thus, any solution to our intrinsic uncertainty model will simultaneously provide lower and upper bounds on the fraction of choice-related variability present in V1.

According to our model, the three critical features of our neural and behavioral data can be reconciled simultaneously only over a narrow region of parameter space. The best-fitting model parameters, which were obtained by minimizing the Euclidean distance between the observed and predicted values of our three key quantities (see Methods), yielded the solution (DF = 0.97, $\sigma_{template}$ = 1.5 mm, $\sigma_{uncertainty}$ = 3.5 mm). The predicted average activity maps of our best-fitting solution, shown in Fig. 3.5a, are qualitatively similar to the average activity maps computed from the real data (Fig. 3.1a,e). Average choice-related activity during target-absent trials ('FA-CR') is more broadly distributed than during target-present trials ('H-M'), and average False Alarm activity exceeds average Miss activity. The quantitative predictions of three key features of our data (Fig. 3.5b-d) resulted in a choice-triggered map ratio ($\sigma_{FA\text{-}CR}$ / $\sigma_{H\text{-}M}$) of 1.18, a saccade ratio (σ_{FA} / σ_{H}) of 1.27, and a difference between the average False Alarm and Miss activity ($SCCI_{2D}$) of 0.27, which fall within the 95% confidence intervals of our real data. Additional solutions, which yielded values within the 95% confidence intervals of our observed quantities, occurred within a neighborhood of this solution: $0.85 \leq DF \leq 0.99$, $0.5 \text{ mm} \leq \sigma_{template} \leq 2 \text{ mm}$, $3 \text{ mm} \leq \sigma_{uncertainty} \leq 5 \text{ mm}$. Our best-fitting solution suggests that subjects decode sensory population signals by searching for a peak of activation that is somewhat smaller ($\sigma_{template}$ = 1.5 mm) than the observed stimulus-evoked response (σ_{evoked} = 2.5 mm), over a region of cortex larger ($\sigma_{uncertainty}$ = 3.5 mm) than the stimulus-

evoked response, and that approximately 97% of the subject's task-limiting neural variability arises from sensory cortex.

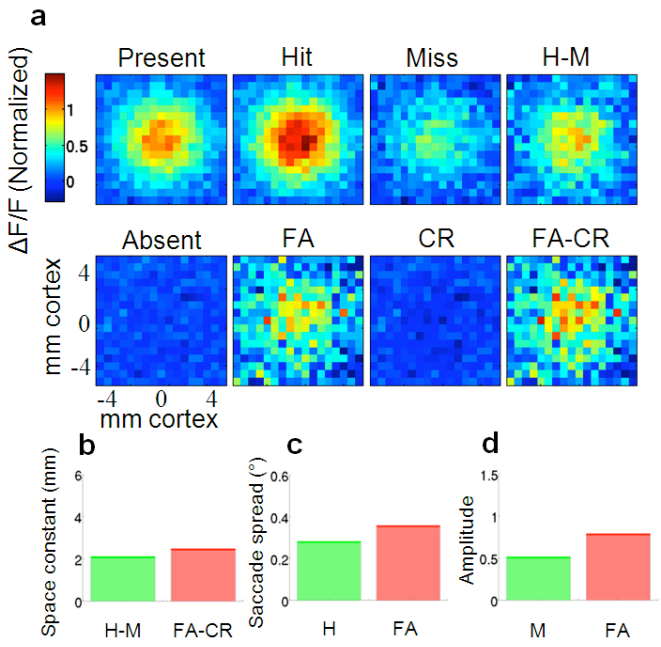

Figure 3.5. Results of an example intrinsic uncertainty decoder applied to simulated data. This model solution occurs at (DF = 0.97, $\sigma_{template}$ = 1.5 mm, $\sigma_{uncertainty}$ = 3.5 mm) (see text for details). Same organization as Fig. 3.1.

Alternative uncertainty decoders

Importantly, while the simplest formulation of the intrinsic uncertainty framework provided solutions that are statistically consistent with the data, it is possible that other uncertainty decoders could provide a better explanation of the data. To address this possibility, we explored two alternative formulations of the uncertainty decoder. First, we considered the possibility that the monkey's search template consisted of weights

proportional to a difference-of-Gaussians (DOG), exploring the hypothesis that the monkey may attempt to apply the optimal decoding strategy (Chen et al., 2006) in the presence of intrinsic uncertainty. In this formulation, the search template was defined as the difference of two Gaussians that optimally separates target-present trials from target-absent trials in the absence of location uncertainty. This template was then tested over a broad range of the $\sigma_{uncertainty}$ parameter. In cases in which the simulated V1 responses contained strong spatial correlations (see Methods), the optimal DOG template, when degraded by uncertainty, was unable to yield positive values for the $SCCI_{2D}$ metric and is therefore inconsistent with our physiological results. In cases in which the simulated V1 responses were composed primarily of white noise, the optimal DOG template was similar to the average evoked-activity map, and therefore performed similarly to the simple uncertainty decoder presented here. Thus we cannot rule out the possibility that the monkey's decoding algorithm contains a DOG template.

Second, we tested formulations in which the severe non-linearity of the maximum operation (Fig. 3.3b, 'Max') was softened by generalizing this stage of the model to the p-norm operation (see Methods) for values of exponent p ranging from 1 to infinity. The p-norm is equivalent to the maximum operation when $p = \infty$, and lesser values of the exponent p represent less severe nonlinearities. We tested this formulation of the model for both Gaussian and difference-of-Gaussian search templates, and found that the important features of our data could be satisfied only for large values of p ($p \geq 10$), suggesting that in order to explain our data, the monkey's decoding algorithm must contain a significant nonlinearity. However, none of the p-norm models we tested with p

$\leq \infty$ provided better explanations of our data than did the model containing the maximum operation.

Impact of sub-optimal decoding

In order to understand the impact of sub-optimal decoding on task performance, we compared the performance of the intrinsic uncertainty decoder with that of the optimal decoder derived previously in our lab (Chen et al., 2006). A sub-optimal decoder produces, by definition, a pooled sensory response that is noisier than that produced by the optimal decoder. The difference between the variance of the pooled sensory response resulting from optimal decoding and that resulting from sub-optimal decoding represents the inefficiency due to sub-optimal decoding. Based on our monkeys' behavioral performance and our assumptions, the total neural variability related to the subjects' decision (i.e., the decision variable) had a variance of 0.4565 (in arbitrary normalized units). Using our solution from the first part of our study, the intrinsic uncertainty decoder yields a pooled sensory variance of 0.4382. In comparison, applying the optimal decoder to the same simulated patch of V1 yields a pooled sensory variance of 0.3332. The difference, 0.1050, accounts for 24% of the total behavioral-related neural variability.

Our model solution, together with the application of the optimal decoder to our simulated sensory responses, allows us to report the relative contributions of unavoidable sensory variability, sub-optimal decoding, and downstream noise to the subject's performance. We defined the unavoidable sensory variability to be the variance of the

pooled sensory response obtained by applying the optimal decoder to the simulated sensory signals. The contribution of sub-optimal decoding to task inefficiency was the difference between the pooled sensory variance obtained with the optimal decoder and that obtained with the intrinsic uncertainty decoder, as outlined above. Finally, we classed the remaining, unaccounted-for variability as downstream noise. The sum of the three variances, $\sigma_{sensory}^2 + \sigma_{sub\text{-}optimality}^2 + \sigma_{downstream}^2 = \sigma_{td}^2$, represents the total decision-related variability. According to our model solution, these sources of variability account for 73%, 24%, and 3% of the total behavioral variability, respectively. Fig. 3.6 depicts these percentages graphically.

Figure 3.6. Partitioning of neural variability that relates to choice. Total area represents 100% of choice-related variability. **green**, 'Unavoidable sensory variability' represents the percentage of the total choice-related variability obtained by decoding the simulated V1 signals optimally. **red**, 'Sensory variability attributed to sub-optimal decoding' is the difference between the variability obtained via the uncertainty decoder shown in Fig. 3.3 and that obtained with the optimal decoder. **blue**, the remaining choice-related variability (3% of total) represents the unaccounted-for variability, and is attributed to downstream noise.

Relationship between saccadic eye movements and cortical activity

To explore the relationship between saccadic eye movements and choice-related activity, we computed the mean location of the endpoints of saccadic eye movements during both types of "choose target-present" trials. In addition to the significantly greater

spread of saccade endpoints during FA than during Hit trials reported above, we found that the mean location of saccade endpoints during FA trials was significantly more foveal than that during Hit trials, by approximately 0.0835 degrees ($p \approx 0$, bootstrap test). We then examined the (x,y) locations of the 2-dimensional Gaussians that best fit each of the choice-related maps. We found that the choice-related activity map during target-absent trials (Fig. 3.1e, 'FA-CR') was shifted by approximately 3.8 mm towards the fovea as compared to that of target-present trials (Fig. 3.1e, 'H-M') ($p \approx 0$, bootstrap test). This result is qualitatively consistent with our model assumption that the monkey makes a saccadic eye movement to the location in visual space that corresponds retinotopically to the location of maximal cortical activity in the final stage of the uncertainty decoder. However, these results appear to be quantitatively inconsistent with one another, given this model assumption. Assuming a cortical magnification factor of 4 mm / °, the observed difference in the mean position of the endpoints of FA saccades and that of Hit saccades (0.0835 degrees) should result from a shift in the mean location of the two choice-related activity maps of just 0.334 mm, in contrast to the 3.8 mm shift we observe in these maps. Thus while the observed shift in saccade endpoints and the observed shift in the locus of choice-related population activity co-occur in the expected *direction*, the relative *magnitudes* of these shifts are inconsistent with our model assumptions.

Because both the mean saccade endpoint and the average locus of cortical activity are shifted towards the fovea during target-absent trials in comparison to target-present trials, we hypothesized that these quantities may be related on a trial-by-trial basis. We tested this hypothesis in two ways. First, we partitioned the data into two halves: those

trials in which the distance from the fixation point to the saccade endpoint was above the median, and those trials that fell below the median. For each half, we fitted 2-D Gaussians to the mean FA activity maps as well as the mean Hit maps, and tested for a difference in location. We did not observe any significant shift in the mean location of either the FA or Hit activity maps in either monkey. Second, we reasoned that if a saccade elicited by the perceived presence of a Gabor target is directed towards the locus of cortical activity in the final stage of the uncertainty decoder, re-centering the population activity maps based on the eye movements on a trial-by-trial basis (see Methods) may reduce the apparent spread of activity. This correction did not yield any significant differences in the space constant of the 2-D Gaussian fits of the maps. The lack of a trial-by-trial relationship between saccade endpoints and cortical activity maps, despite our finding that FA trials are associated with significantly shorter saccades and significantly more foveal cortical activity, could be due to the presence of significant measurement noise and our limited number of trials. However, this result may also provide evidence against our location uncertainty hypothesis, suggesting that a different model could better explain our data.

3.5 Discussion

Here we present two main findings. First, in our visual detection task, performance is likely to be limited by intrinsic uncertainty as to the precise location of the visual target. Using a combination of psychophysical and imaging measures, together with a simple computational model, we identified a family of plausible candidate

decoding algorithms used by the brain to form the decision. Given this uncertainty, in order to decode sensory population signals the brain likely looks for a peak of activation over a region of the sensory cortical population centered on the location of the stimulus-evoked response. The search template ($\sigma_{template} \approx 1.5$ mm) is somewhat narrower than the evoked response ($\sigma_{evoked} \approx 2.5$ mm) and the search area ($\sigma_{uncertainty} \approx 3.5$ mm) is larger than the evoked response. Second, the sub-optimality of this class of decoders, which results from the subject's intrinsic location uncertainty, degrades task performance substantially. We quantified the sub-optimality by comparing our family of intrinsic uncertainty decoders with the optimal decoder. Our results suggest that while performance is likely to be limited primarily by neural variability in sensory cortex (in agreement with the conclusions of Chapter 2), a significant portion of this task-limiting variability occurs due to sub-optimal decoding.

Our findings are consistent with our previous result that the majority of choice-related neural variability is present in the sensory population (Chapter 2). Our simple model framework, when constrained by features of our VSDI recordings, predicts that neural variability in sensory cortex accounts for approximately 97% of the neural variability related to choice, consistent with our previous result that at least 81% of choice-related variability occurs in sensory cortex (Chapter 2). Previously, we tested a diverse class of fixed decoding strategies. Here we demonstrate that a class of intrinsic uncertainty decoders better explains key features of our imaging and behavioral data. In addition, we found that the quantitative relationship between the SCCI quantity and the

fraction of choice-related activity occurring in V1 (Chapter 2) extends to this class of nonlinear decoders.

Our results are consistent with a previous psychophysical study suggesting that human detection and localization performance is limited by intrinsic spatial uncertainty (Michel and Geisler, 2011). Here we extend this finding to non-human primates, and also employ brain imaging to demonstrate a neural signature of such location uncertainty in sensory cortex, thus identifying a potential physiological mechanism underlying this behavioral phenomenon. However, the two studies differ in their quantitative estimate of intrinsic location uncertainty. The human psychophysical study suggests that the amount of intrinsic location uncertainty subjects have can be described with a space constant that is equal to approximately 10% of the target eccentricity. Given their results, the target eccentricities used in our study (4.28 degrees for Monkey T; 1.58 degrees for Monkey C) would be associated with intrinsic uncertainty with space constants of 0.43 and 0.16 degrees, respectively. In contrast, our model solution to the intrinsic uncertainty decoder suggests that the uncertainty region in sensory cortex has a space constant of approximately 3.5 mm, corresponding to approximately 0.875 degrees of visual angle (assuming a CMF of 4 mm/°). Thus our results yielded estimates of intrinsic uncertainty that were 2-6x larger than those of the previous study.

It is possible that alternative formulations of the uncertainty decoder, beyond those considered here, could better explain our imaging and behavioral results. Here we report the results of a simple decoder that assumes 2-D Gaussian shapes for the search template and uncertainty region. These assumptions limit the dimensionality of our

model, while also allowing for a straightforward interpretation of its parameters. However, a more general Bayesian framework, together with a maximum-likelihood estimation procedure, may yield a variant of the uncertainty decoder that can better account for our data. Thus, a formalization of the computational modeling approach we present here is an important goal for future research.

Our findings are consistent with a computational modeling study that suggests behavioral performance is significantly limited by sub-optimal inference (Beck et al., 2012). Whereas the previous study argues that sub-optimal inference is a unique source of noise that is added to neural sensory variability, here we describe sub-optimal decoding as a mechanism that causes downstream brain areas to inherit sensory noise that otherwise would have been removed by applying the optimal decoder. Nevertheless, here we provide physiological and behavioral evidence that sub-optimal decoding of sensory signals indeed largely limits behavioral performance. While sub-optimal decoding leads to a significant reduction in performance, our model also shows that the majority of the task-limiting variability arises from unavoidable sensory variability, suggesting that in our subjects encoding variability dominates decoding inefficiencies in determining behavioral performance.

Finally, our study provides psychophysical and brain imaging evidence apropos to a long-standing debate concerning the lower envelope principle, or the hypothesis that behavioral performance depends on the responses of only the most reliable individual sensory neurons. Our findings suggest, instead, that perceptual decisions are likely based on a large population of sensory neurons, and that in some tasks, intrinsic uncertainty

may prohibit the brain from accurately identifying a small group of the most informative task-relevant neurons.

Chapter 4: General Conclusions

In this dissertation I pursued two fundamental questions that further our understanding of the nature of perceptual decisions. First, what fraction of choice-related variability is present in population activity in primary sensory cortex; and to what degree does this sensory cortical variability limit perceptual decisions? Second, how does the monkey combine information across the sensory population to form the basis of a decision; and to what degree does this decoding process limit perceptual decisions? We used a combination of voltage-sensitive dye imaging in awake, behaving monkeys and simple computational modeling to address these questions in the context of the primate visual system. I report four main findings:

1. Choice-related neural variability is distributed broadly over sensory cortex; in our task significant choice-related variability can be found over an area larger than that activated by the visual stimulus;
2. A large majority of choice-related variability occurs as early as V1 at the level of neural populations;
3. Perceptual decisions are likely based on the combined activity of a large population of sensory neurons, rather than on the activity of a small number of the most sensitive neurons;
4. Perceptual decisions are likely limited by intrinsic uncertainty about the stimulus, and this form of sub-optimality in sensory decoding has a significant impact on task performance.

The quantitative solutions to our models of the decision process, constrained by our physiological and behavioral data, allow us to estimate the relative contributions of various stages in the decision process to behavioral task performance. Our results suggest that performance in our simple task may be limited primarily by the efficiency of the sensory encoding process, secondarily by sub-optimal decoding of the sensory population, and only modestly by the presence of neural variability downstream from the encoding and decoding processes.

In the course of arriving at these general conclusions, we developed a novel statistical framework for quantifying the fraction of choice-related variability present in an experimenter's measurement of neural population activity in the presence of variability that is unrelated to choice, such as measurement noise. Our statistic, 'stimulus-choice correspondence index' (SCCI) can be used by other researchers exploring the relationship between measurements of population activity and choice in a binary decision task.

Finally, we present here for the first time a physiological picture of a spatial pooling algorithm that provides a mechanism for a simple binary decision. Our results suggest that the binary decision procedure in our detection task could be biologically implemented over a series of three cortical layers with convergent and parallel projections. In addition, we describe this decision mechanism by an equivalent sequence of simple mathematical operations.

4.1 Majority of choice-related activity in V1

I presented evidence that during a simple binary perceptual decision, the majority of the subject's decision-related neural activity can be found as early as primary visual cortex. In Chapter 2, we developed a metric, 'stimulus-choice correspondence index' (SCCI), which quantifies the difference between the mean population activity during False Alarm trials and that of Miss trials. We found that SCCI varies linearly with the fraction of choice-related neural variability occurring in our measurement, and used its empirical value to determine that a minimum of 81% of choice-related variability occurs in V1 in our task. In Chapter 3, we identified a simple decision circuit that provides a mechanism for binary decisions under location uncertainty, which, when constrained with our empirical data, also suggests that the vast majority of choice-related information is present in V1, perhaps as much as 97%.

Our finding that the majority of choice-related neural variability occurs in early sensory cortex provides an explanation for the weak choice probabilities often reported in sensory cortex, including the recent discovery of single unit choice probabilities in V1 in a similar task (Palmer et al., 2007). Previous empirical studies, owing to their focus on single neurons in isolation, were unable to determine the reason for weak choice-related signals: the remaining choice-related variability could be distributed across other sensory neurons, or could occur downstream from sensory cortex. In contrast, our population-based approach allowed us to offer a solution to this question in our simple detection task by enabling us to place a quantitative upper bound on the amount of downstream noise. In the work I present here, we suggest that choice probabilities observed in individual

neurons in early sensory cortex are weak not because of the presence of large amounts of downstream noise, but because perceptual decisions are likely based on large populations of sensory neurons rather than on the activity of a single neuron or a small group of neurons. Because neurons within a population are only weakly correlated with one another, the contributions of individual neurons to choice are therefore expected to be modest (e.g., Shadlen et al., 1996).

4.2 Top-down versus bottom-up

In this dissertation I presented physiological evidence that in a simple visual detection task, the majority of the subject's choice-related variability is present in primary visual cortex, and that it is distributed across several square millimeters, an area comprising millions of cells. What is the source of this co-variation?

The presence of choice-related neural variability in sensory cortex could be due to at least three different mechanisms. The simplest explanation is that sensory variability co-varies with choice because it *causes* the choice. This feed-forward (bottom-up) mechanism is consistent with the findings of earlier studies in which artificial stimulation of task-relevant sensory neurons biased the subject's performance, or in which lesions in areas containing these neurons produced performance deficits, which showed that these sensory neurons were necessary to perform the task. A second possibility is that during a task such as ours, which requires the subject to indicate his choice with a saccadic eye movement, a higher brain area involved in the planning of eye movements, such as the frontal eye fields, may send feedback (top-down) signals to sensory cortex. These signals

are likely to be closely related to the subject's decision and thus could drive the activity of sensory cortex in such a way that it too would co-vary with the decision. In this *post-decisional* case, sensory cortical activity would reflect a decision that had already been made. A third possibility is that *pre-decisional* top-down signals from higher brain areas influence sensory cortical activity. For instance, an attention-like signal may modify sensory cortical activity in an attempt to improve encoding efficiency.

In Chapter 2, I argued that a post-decisional top-down signal should be evident in the time course of the sensory signals. Because most stimulus-evoked activity reaching higher brain areas must first pass through primary visual cortex, it is likely that the target-evoked responses we observe in V1 are necessary for the subject to perform the task better than chance allows. If a higher brain area computes the decision and only then sends decision-related information back to V1, this decision-related activity would emerge significantly later than the stimulus-related signals. Instead, we found that the onset and dynamics of the choice-related signals were nearly identical to that of the stimulus-evoked response. This finding could suggest that the choice-related activity we measure is not the result of post-decisional top-down signals. However, we cannot rule out the possibility that the similarity between the onset and dynamics of the choice-related activity and that of the stimulus-evoked activity is the result of a continuous, recurrent feedback signal.

A pre-decisional top-down signal, such as an attention-like signal, is also an unlikely explanation for our results. In principle, an attention-like signal that varies from trial to trial could bias the average sensory cortical activity, leading to a bias in the

subject's choices. To explain our results, such a signal would have to occur with similar temporal dynamics to that of the stimulus-evoked response. However, in a recent study designed to test this possibility in V1 in a similar task and under identical population recording methods, we observed attention-like changes that occurred *earlier* than the onset of the evoked response (Chen and Seidemann, 2012), also inconsistent with the near correspondence of choice-related and stimulus-related signals observed here. Furthermore, top-down signals that bias the subject's behavior, and that arrive in V1 before stimulus onset, would reduce the subject's accuracy in the simple detection task considered here. Such signals would add sensory variability that is unrelated to the stimulus, and would thus impair the subject's ability to distinguish between target-present and target-absent trials. Because our subjects are trained for several months on this task prior to imaging, it is unlikely that they would employ such a detrimental strategy. Finally, a more remote possibility is that a higher brain area sends top-down signals to V1, but keeps a record of these signals and removes or cancels them when forming the decision. While it is unclear why the brain would employ such a strategy, such variability in V1 would nevertheless manifest itself as choice-unrelated variability in the framework presented in Chapter 2. Thus, while it is possible that pre-decisional top-down signals are responsible for the results presented here, these considerations suggest that this explanation is unlikely.

4.3 Population-based decisions

In this dissertation I present new evidence that decisions are formed by combining information broadly from populations of neurons, rather than by relying on the activity of a single neuron or small group of neurons. In Chapter 1, I outlined an ongoing debate regarding the 'lower envelope principle', or the notion that decisions are based – in its most extreme version – on the activity of only the most sensitive neuron. The strongest empirical evidence for the lower envelope principle came from studies in the sensory periphery (e.g., Mountcastle et al., 1972; Talbot et al., 1968) although evidence has also been found in sensory areas of the brain (e.g., Newsome et al., 1989). On the other hand, the lower envelope principle has been criticized as being biologically implausible to implement: how does the brain identify the most informative neuron out of millions of candidates? In Chapter 2, I showed that choice-related activity extends broadly across V1, offering empirical evidence that the brain pools broadly to form decisions. In Chapter 3, we developed a model of the decision circuit under conditions of uncertainty about the stimulus, and our solution to this model also points towards broad pooling.

While the physiological recordings and computational models I present here indeed point towards broad pooling, our results nevertheless offer a richer interpretation than a simple rejection of the lower envelope principle. The model we developed that best accounts for our physiological data, the intrinsic uncertainty decoder, is based on the idea that the subject has uncertainty about the location of the stimulus he must detect. The model solution suggests that the subject searches for a template resembling the evoked response, but conducts the search over an area significantly broader than this

template, owing to this incomplete knowledge. Thus while the choice-triggered maps presented in Chapter 2 reveal choice-related activity that extends across several millimeters of visual cortex, the modeling study of Chapter 3 suggests that, with better information about the location of the stimulus, the subject would likely pool over an area significantly smaller than this region. Based on the quantitative solutions to the model, these regions could differ by as much as a factor of four.

The discrepancy between the breadth of the subject's template and that of the uncertainty region over which the subject searches suggests that a subject may *attempt* to base decisions on a smaller number of the most informative neurons, but, because of intrinsic uncertainty, the subject is unable to precisely identify those neurons. This finding lends support to the notion that while *smaller* groups of neurons could in principle be used to perform the task accurately, in practice finding those neurons may be impossible for a variety of reasons – in this case because of location uncertainty. Nevertheless, the model solution for the breadth of the template (1.5 mm, somewhat narrower than the evoked response) still represents an area comprising hundreds of thousands of neurons. Thus our data suggests that decisions are likely to be based on large populations, but the spatial extent of the neural population showing choice-related activity may be exaggerated by intrinsic uncertainty, incomplete knowledge of the task, or general design limitations of the system.

4.4 Intrinsic uncertainty and sub-optimal decoding

In Chapter 3 I presented evidence that the subject's performance is significantly limited by sub-optimal decoding of sensory signals. We estimated the impact of sub-optimal decoding in two steps. First, we estimated the parameters of the decision model and used these parameters to decode simulated sensory population signals, which allowed us to quantify the variance of the decoded sensory signals. We then applied the optimal decoder with no spatial uncertainty to the same simulated population to determine the variance of the sensory population when decoded under optimal conditions. The difference between these variances represents the quantitative impact of sub-optimal decoding, which we expressed as a fraction of the total variance of the decision variable. Our result suggests that in our task, sub-optimal decoding can explain approximately 24% of the total behavioral variance.

This degree of sub-optimality seems to represent a surprisingly large contribution to behavior. For example, a pair of studies reviewed in Chapter 1 demonstrated that neural variability in a cortical decision area was progressively reduced during an extended period of training in a motion direction discrimination task, while the variability of sensory inputs to this area remained unchanged (Law and Gold, 2008; Law and Gold, 2009). This result suggests that intensive training may involve changes not in how sensory information is encoded in the brain, but in how that information is decoded into signals relevant to a specific task. In light of their findings, one may think of sensory encoding as a fixed process whereby a relatively inflexible early sensory cortex represents low-level features of sensory stimuli as generally as possible for subsequent

use by downstream circuits. In comparison, one may think of sensory decoding as a more flexible process whereby relatively plastic decision circuits must actively and quickly alter the pattern of weights that transforms general low-level information into useful signals that are relevant to a specific task. Under these assumptions, one expects that a highly trained subject demonstrating stable task performance for several months, as in our experiments, should have discovered over time the pattern of weights that most effectively transforms encoded sensory information into signals useful for efficient task performance. In other words, we expect that in highly trained subjects, sensory decoding should be highly efficient.

Here we suggest that the main factor limiting efficient decoding in our task is intrinsic spatial uncertainty about the correct target location. The possibility that subjects have intrinsic uncertainty about stimulus features has been proposed previously (e.g., Pelli, 1985) and tested psychophysically in a detection task (Michel and Geisler, 2011). However, the reason for this limitation is unclear. One consideration is the degree to which the task studied here represents natural behavior. In our task, we require the subject to make repeated judgments about the presence or absence of a stimulus that can occur only in a fixed location in visual space. While it is easy to imagine natural scenarios in which an organism must continuously monitor the potential presence of a stimulus (such as the image of a prey or a predator) in a fixed location in the world (such as behind a patch of leaves or at the top of a nearby tree), the location in question in these examples is fixed in world coordinates, rather than in retinal coordinates. The ability of an organism to precisely remember a location in retinal coordinates may be of limited

importance under natural conditions. Thus the demands of the natural environment may apply little selection pressure on the evolving brain to perform accurately in the specific task our subjects must perform.

4.5 Downstream noise

An additional form of sub-optimality in the decision process occurs downstream from sensory decoding. Researchers often include a final processing stage that adds random variability to the decoded signals. This additional variability is typically modeled as scalar downstream noise, but in practice it may take a number of forms. First, downstream noise may arise from the stochastic firing of a population of neurons responsible for transforming the decision-related signal into motor commands. As in the case of sensory decoding, the ability of the brain to relay the decision to motor circuits likely depends on the pattern of weights that gates the parallel flow of information from one brain structure (e.g., early sensory cortex) to another (e.g., motor cortex or sub-cortical motor structures). As in sensory decoding, optimizing this pattern of weights to the task at hand is expected to reduce the variability introduced by stochastic firing. Thus, limitations in the brain's ability to optimally cancel neural stochasticity through pooling of signals at this later stage may contribute to the total variability of the decision variable, just as it does during sub-optimal decoding of sensory signals.

Second, downstream noise may arise from criterial noise, or variability in the value of the criterion against which the decision variable is evaluated to form the binary decision. Scalar downstream noise reduces both the subject's ability to accurately

perform the task, as well as the researcher's ability to accurately predict choice. This random variability occasionally causes the decision variable to exceed the criterion even though the decoded sensory response fell below the criterion, and vice versa. Variability in the criterion itself produces the same result.

Finally, downstream noise may take the form of variability added by the muscles. For example, small variations in the contraction of striated muscle in response to signals from the decision circuit and upper motor neurons constitute variation in behavior. Such variability is unlikely to play a role in the binary task studied here because the subject's measured behavioral response takes a discrete form: either a saccadic eye movement to a distant location, or no saccadic eye movement. Thus small random variation in the activation of the relevant muscle groups is unlikely to result in a discrepancy between the measured behavioral response and the subject's intended response. Nevertheless, variation in muscle activation may contribute measurably to behavioral variability during tasks requiring a continuous, rather than discrete behavioral response.

4.6 Future directions

The physiological, behavioral, and modeling results presented in this dissertation suggest opportunities for future investigation. In Chapter 2, I presented a novel statistical framework for investigating the relationship between neural population activity and choice. I described how this framework could be extended to studies of the relationship between neural population activity and choice in other binary decision tasks, such as the classic motion direction discrimination ("dots") task. An interesting possibility for future

research is to explore the relationship between single-neuron measures and population measures in the context of this new framework. While outside the scope of this dissertation, which focuses on measuring population activity with VSDI, our framework may allow other researchers to better understand how choice-related variability is distributed across sensory cortex at a finer scale, such as at the level of individual neurons.

In Chapter 3 I reported a class of population decoding algorithms, the intrinsic uncertainty decoders, which can explain key features of our VSDI and behavioral results. I presented an example solution to this class of models, which captures three important features of the data: a broader spread of choice-related activity during target-absent trials than during target-present trials, a broader spread of saccade endpoints during target-absent trials than during target-present trials, and stronger cortical activity during False Alarm trials than during Miss trials. An additional feature of the data that was not captured by this model is a shift in the mean location of the choice-triggered maps: choice-related activity occurs at a more foveal location during target-absent trials than during target-present trials; this result qualitatively agrees with our additional observation that the endpoints of saccadic eye movements occur more foveally during FA trials than during Hit trials. Furthermore, while the model solution I presented in Chapter 3 is statistically consistent with the key features of our data, a fully satisfying model would provide values closer to these quantities' means. Each of these concerns could be addressed by the derivation of a maximum likelihood estimation procedure within a Bayesian framework. A Bayesian estimator will likely enable us to reject certain models

and thereby refine our estimate of the monkey's decoding algorithm. Thus, a formal description of our class of intrinsic uncertainty decoders is an important goal for future research.

4.7 Concluding remarks

In this dissertation, I studied the neural basis of perceptual decisions. I trained monkeys to perform a challenging reaction time visual detection task, and monitored the activity of populations of neurons in primary visual cortex while the monkeys performed the task. By comparing neural population activity during trials culminating in each of four behavioral outcomes, and developing computational models of the relationship between such neural population activity and behavior, I reached several conclusions which further our understanding of perceptual decisions. The results presented here suggest that perceptual decisions are mediated by large populations of sensory neurons; that in highly trained subjects most of the neural variability relating to perceptual decisions resides in early sensory cortex; and that sub-optimality in decoding the sensory population represents a significant contribution to inefficiency in task performance. Important goals for future research include investigating the relationship between population activity and single-neuron activity during binary choice tasks in order to refine estimates of the decision algorithm, and carrying out similar work in other species and brain areas in order to determine the generality of the results presented here.

Bibliography

Alexander G.E., DeLong M.R. (1985a) Microstimulation of the primate neostriatum. I. Physiological properties of striatal microexcitable zones. Journal of neurophysiology 53:1401-16.

Alexander G.E., DeLong M.R. (1985b) Microstimulation of the primate neostriatum. II. Somatotopic organization of striatal microexcitable zones and their relation to neuronal response properties. Journal of neurophysiology 53:1417-30.

Arieli A., Grinvald A., Slovin H. (2002) Dural substitute for long-term imaging of cortical activity in behaving monkeys and its clinical implications. Journal of neuroscience methods 114:119-33.

Arieli A., Sterkin A., Grinvald A., Aertsen A. (1996) Dynamics of ongoing activity: explanation of the large variability in evoked cortical responses. Science 273:1868-71.

Barlow H.B., Levick W.R., Yoon M. (1971) Responses to single quanta of light in retinal ganglion cells of the cat. Vision research Suppl 3:87-101.

Beck J.M., Ma W.J., Pitkow X., Latham P.E., Pouget A. (2012) Not noisy, just wrong: the role of suboptimal inference in behavioral variability. Neuron 74:30-9. DOI: 10.1016/j.neuron.2012.03.016.

Bradley D.C., Maxwell M., Andersen R.A., Banks M.S., Shenoy K.V. (1996) Mechanisms of heading perception in primate visual cortex. Science 273:1544-7.

Britten K.H., Newsome W.T., Shadlen M.N., Celebrini S., Movshon J.A. (1996) A relationship between behavioral choice and the visual responses of neurons in macaque MT. Visual neuroscience 13:87-100.

Britten K.H., Shadlen M.N., Newsome W.T., Movshon J.A. (1992) The analysis of visual motion: a comparison of neuronal and psychophysical performance. The Journal of neuroscience : the official journal of the Society for Neuroscience 12:4745-65.

Britten K.H., van Wezel R.J. (1998) Electrical microstimulation of cortical area MST biases heading perception in monkeys. Nature neuroscience 1:59-63. DOI: 10.1038/259.

Bruce C.J., Goldberg M.E. (1985) Primate frontal eye fields. I. Single neurons discharging before saccades. Journal of neurophysiology 53:603-35.

Bruce C.J., Goldberg M.E., Bushnell M.C., Stanton G.B. (1985) Primate frontal eye fields. II. Physiological and anatomical correlates of electrically evoked eye movements. Journal of neurophysiology 54:714-34.

Celebrini S., Newsome W.T. (1994) Neuronal and psychophysical sensitivity to motion signals in extrastriate area MST of the macaque monkey. The Journal of neuroscience : the official journal of the Society for Neuroscience 14:4109-24.

Celebrini S., Newsome W.T. (1995) Microstimulation of extrastriate area MST influences performance on a direction discrimination task. Journal of neurophysiology 73:437-48.

Chen Y., Geisler W.S., Seidemann E. (2006) Optimal decoding of correlated neural population responses in the primate visual cortex. Nature neuroscience 9:1412-20. DOI: 10.1038/nn1792.

Chen Y., Geisler W.S., Seidemann E. (2008) Optimal temporal decoding of neural population responses in a reaction-time visual detection task. Journal of neurophysiology 99:1366-79. DOI: 10.1152/jn.00698.2007.

Chen Y., Palmer C.R., Seidemann E. (2012) The relationship between voltage-sensitive dye imaging signals and spiking activity of neural populations in primate V1. Journal of neurophysiology.

Chen Y., Seidemann E. (2012) Attentional modulations related to spatial gating but not to allocation of limited resources in primate V1. Neuron 74:557-66. DOI: 10.1016/j.neuron.2012.03.033.

Cinelli A.R., Hamilton K.A., Kauer J.S. (1995a) Salamander olfactory bulb neuronal activity observed by video rate, voltage-sensitive dye imaging. III. Spatial and temporal properties of responses evoked by odorant stimulation. Journal of neurophysiology 73:2053-71.

Cinelli A.R., Kauer J.S. (1995) Salamander olfactory bulb neuronal activity observed by video rate, voltage-sensitive dye imaging. II. Spatial and temporal properties of responses evoked by electric stimulation. Journal of neurophysiology 73:2033-52.

Cinelli A.R., Neff S.R., Kauer J.S. (1995b) Salamander olfactory bulb neuronal activity observed by video rate, voltage-sensitive dye imaging. I. Characterization of the recording system. Journal of neurophysiology 73:2017-32.

Cohen M.R., Newsome W.T. (2004) What electrical microstimulation has revealed about the neural basis of cognition. Current opinion in neurobiology 14:169-77. DOI: 10.1016/j.conb.2004.03.016.

Cohen M.R., Newsome W.T. (2009) Estimates of the contribution of single neurons to perception depend on timescale and noise correlation. The Journal of neuroscience : the official journal of the Society for Neuroscience 29:6635-48. DOI: 10.1523/JNEUROSCI.5179-08.2009.

Cook E.P., Maunsell J.H. (2002) Dynamics of neuronal responses in macaque MT and VIP during motion detection. Nature neuroscience 5:985-94. DOI: 10.1038/nn924.

Croner L.J., Albright T.D. (1999) Segmentation by color influences responses of motion-sensitive neurons in the cortical middle temporal visual area. The Journal of neuroscience : the official journal of the Society for Neuroscience 19:3935-51.

Darian-Smith I., Johnson K.O., Dykes R. (1973) "Cold" fiber population innervating palmar and digital skin of the monkey: responses to cooling pulses. Journal of neurophysiology 36:325-46.

de Lafuente V., Romo R. (2005) Neuronal correlates of subjective sensory experience. Nature neuroscience 8:1698-703. DOI: 10.1038/nn1587.

de Lafuente V., Romo R. (2006) Neural correlate of subjective sensory experience gradually builds up across cortical areas. Proceedings of the National Academy of Sciences of the United States of America 103:14266-71. DOI: 10.1073/pnas.0605826103.

De Valois R.L., Abramov I., Mead W.R. (1967) Single cell analysis of wavelength discrimination at the lateral geniculate nucleus in the macaque. Journal of neurophysiology 30:415-33.

DeAngelis G.C., Cumming B.G., Newsome W.T. (1998) Cortical area MT and the perception of stereoscopic depth. Nature 394:677-80. DOI: 10.1038/29299.

Desimone R., Albright T.D., Gross C.G., Bruce C. (1984) Stimulus-selective properties of inferior temporal neurons in the macaque. The Journal of neuroscience : the official journal of the Society for Neuroscience 4:2051-62.

Ditterich J., Mazurek M.E., Shadlen M.N. (2003) Microstimulation of visual cortex affects the speed of perceptual decisions. Nature neuroscience 6:891-8. DOI: 10.1038/nn1094.

Dodd J.V., Krug K., Cumming B.G., Parker A.J. (2001) Perceptually bistable three-dimensional figures evoke high choice probabilities in cortical area MT. The Journal of neuroscience : the official journal of the Society for Neuroscience 21:4809-21.

Dubner R., Zeki S.M. (1971) Response properties and receptive fields of cells in an anatomically defined region of the superior temporal sulcus in the monkey. Brain research 35:528-32.

Dursteler M.R., Wurtz R.H. (1988) Pursuit and optokinetic deficits following chemical lesions of cortical areas MT and MST. Journal of neurophysiology 60:940-65.

Efron B., & Tibshirani, R. J. (1993) An introduction to the bootstap Chapman and Hall, London.

Eggermont J.J. (1999) Neural correlates of gap detection in three auditory cortical fields in the Cat. Journal of neurophysiology 81:2570-81.

Fujii N., Mushiake H., Tanji J. (1998) Intracortical microstimulation of bilateral frontal eye field. Journal of neurophysiology 79:2240-4.

Gawne T.J., Kjaer T.W., Hertz J.A., Richmond B.J. (1996) Adjacent visual cortical complex cells share about 20% of their stimulus-related information. Cerebral cortex 6:482-9.

Gawne T.J., Richmond B.J. (1993) How independent are the messages carried by adjacent inferior temporal cortical neurons? The Journal of neuroscience : the official journal of the Society for Neuroscience 13:2758-71.

Geisler W.S., Albrecht D.G. (1997) Visual cortex neurons in monkeys and cats: detection, discrimination, and identification. Visual neuroscience 14:897-919.

Gnadt J.W., Andersen R.A. (1988) Memory related motor planning activity in posterior parietal cortex of macaque. Experimental brain research. Experimentelle Hirnforschung. Experimentation cerebrale 70:216-20.

Gold J.I., Shadlen M.N. (2003) The influence of behavioral context on the representation of a perceptual decision in developing oculomotor commands. The Journal of neuroscience : the official journal of the Society for Neuroscience 23:632-51.

Green D.M., Swets J.A. (1966) Signal detection theory and psychophysics Wiley, New York,.

Grinvald A. (2005) Imaging input and output dynamics of neocortical networks in vivo: exciting times ahead. Proceedings of the National Academy of Sciences of the United States of America 102:14125-6. DOI: 10.1073/pnas.0506755102.

Grinvald A., Anglister L., Freeman J.A., Hildesheim R., Manker A. (1984) Real-time optical imaging of naturally evoked electrical activity in intact frog brain. Nature 308:848-50.

Grinvald A., Frostig R.D., Lieke E., Hildesheim R. (1988) Optical imaging of neuronal activity. Physiological reviews 68:1285-366.

Grinvald A., Hildesheim R. (2004) VSDI: a new era in functional imaging of cortical dynamics. Nature reviews. Neuroscience 5:874-85. DOI: 10.1038/nrn1536.

Grinvald A., Lieke E.E., Frostig R.D., Hildesheim R. (1994) Cortical point-spread function and long-range lateral interactions revealed by real-time optical imaging of macaque monkey primary visual cortex. The Journal of neuroscience : the official journal of the Society for Neuroscience 14:2545-68.

Groh J.M., Born R.T., Newsome W.T. (1997) How is a sensory map read Out? Effects of microstimulation in visual area MT on saccades and smooth pursuit eye movements. The Journal of neuroscience : the official journal of the Society for Neuroscience 17:4312-30.

Gross C.G., Rocha-Miranda C.E., Bender D.B. (1972) Visual properties of neurons in inferotemporal cortex of the Macaque. Journal of neurophysiology 35:96-111.

Hecht S., Shlaer S., Pirenne M.H. (1942) Energy, Quanta, and Vision. The Journal of general physiology 25:819-40.

Hernandez A., Zainos A., Romo R. (2002) Temporal evolution of a decision-making process in medial premotor cortex. Neuron 33:959-72.

Hubel D.H., Wiesel T.N. (1962) Receptive fields, binocular interaction and functional architecture in the cat's visual cortex. The Journal of physiology 160:106-54.

Hubel D.H., Wiesel T.N. (1968) Receptive fields and functional architecture of monkey striate cortex. The Journal of physiology 195:215-43.

Huk A.C., Shadlen M.N. (2005) Neural activity in macaque parietal cortex reflects temporal integration of visual motion signals during perceptual decision making. The Journal of neuroscience : the official journal of the Society for Neuroscience 25:10420-36. DOI: 10.1523/JNEUROSCI.4684-04.2005.

Johnson K.O. (1980) Sensory discrimination: neural processes preceding discrimination decision. Journal of neurophysiology 43:1793-815.

Johnson K.O., Darian-Smith I., LaMotte C. (1973) Peripheral neural determinants of temperature discrimination in man: a correlative study of responses to cooling skin. Journal of neurophysiology 36:347-70.

Kenet T., Bibitchkov D., Tsodyks M., Grinvald A., Arieli A. (2003) Spontaneously emerging cortical representations of visual attributes. Nature 425:954-6. DOI: 10.1038/nature02078.

Kiang N.Y., Pfeiffer R.R., Warr W.B., Backus A.S. (1965) Stimulus coding in the cochlear nucleus. Transactions of the American Otological Society 53:35-58.

Law C.T., Gold J.I. (2008) Neural correlates of perceptual learning in a sensory-motor, but not a sensory, cortical area. Nature neuroscience 11:505-13. DOI: 10.1038/nn2070.

Law C.T., Gold J.I. (2009) Reinforcement learning can account for associative and perceptual learning on a visual-decision task. Nature neuroscience 12:655-63. DOI: 10.1038/nn.2304.

Leopold D.A., Logothetis N.K. (2003) Spatial patterns of spontaneous local field activity in the monkey visual cortex. Reviews in the neurosciences 14:195-205.

Liu J., Newsome W.T. (2005) Correlation between speed perception and neural activity in the middle temporal visual area. The Journal of neuroscience : the official journal of the Society for Neuroscience 25:711-22. DOI: 10.1523/JNEUROSCI.4034-04.2005.

Maunsell J.H., Van Essen D.C. (1983) Functional properties of neurons in middle temporal visual area of the macaque monkey. I. Selectivity for stimulus direction, speed, and orientation. Journal of neurophysiology 49:1127-47.

Mazurek M.E., Roitman J.D., Ditterich J., Shadlen M.N. (2003) A role for neural integrators in perceptual decision making. Cerebral cortex 13:1257-69.

Michel M., Geisler W.S. (2011) Intrinsic position uncertainty explains detection and localization performance in peripheral vision. Journal of vision 11:18. DOI: 10.1167/11.1.18.

Mishkin M., Ungerleider L.G. (1982) Contribution of striate inputs to the visuospatial functions of parieto-preoccipital cortex in monkeys. Behavioural brain research 6:57-77.

Mitz A.R., Wise S.P. (1987) The somatotopic organization of the supplementary motor area: intracortical microstimulation mapping. The Journal of neuroscience : the official journal of the Society for Neuroscience 7:1010-21.

Mountcastle V.B. (1957) Modality and topographic properties of single neurons of cat's somatic sensory cortex. Journal of neurophysiology 20:408-34.

Mountcastle V.B., LaMotte R.H., Carli G. (1972) Detection thresholds for stimuli in humans and monkeys: comparison with threshold events in mechanoreceptive afferent nerve fibers innervating the monkey hand. Journal of neurophysiology 35:122-36.

Murasugi C.M., Salzman C.D., Newsome W.T. (1993) Microstimulation in visual area MT: effects of varying pulse amplitude and frequency. The Journal of neuroscience : the official journal of the Society for Neuroscience 13:1719-29.

Newsome W.T., Britten K.H., Movshon J.A. (1989) Neuronal correlates of a perceptual decision. Nature 341:52-4. DOI: 10.1038/341052a0.

Newsome W.T., Pare E.B. (1988) A selective impairment of motion perception following lesions of the middle temporal visual area (MT). The Journal of neuroscience : the official journal of the Society for Neuroscience 8:2201-11.

Newsome W.T., Wurtz R.H., Dursteler M.R., Mikami A. (1985) Deficits in visual motion processing following ibotenic acid lesions of the middle temporal visual area of the

macaque monkey. The Journal of neuroscience : the official journal of the Society for Neuroscience 5:825-40.

Nienborg H., Cumming B. (2010) Correlations between the activity of sensory neurons and behavior: how much do they tell us about a neuron's causality? Current opinion in neurobiology 20:376-81. DOI: 10.1016/j.conb.2010.05.002.

Nienborg H., Cumming B.G. (2006) Macaque V2 neurons, but not V1 neurons, show choice-related activity. The Journal of neuroscience : the official journal of the Society for Neuroscience 26:9567-78. DOI: 10.1523/JNEUROSCI.2256-06.2006.

Nienborg H., Cumming B.G. (2007) Psychophysically measured task strategy for disparity discrimination is reflected in V2 neurons. Nature neuroscience 10:1608-14. DOI: 10.1038/nn1991.

Nienborg H., Cumming B.G. (2009) Decision-related activity in sensory neurons reflects more than a neuron's causal effect. Nature 459:89-92. DOI: 10.1038/nature07821.

Noda H., Fujikado T. (1987a) Involvement of Purkinje cells in evoking saccadic eye movements by microstimulation of the posterior cerebellar vermis of monkeys. Journal of neurophysiology 57:1247-61.

Noda H., Fujikado T. (1987b) Topography of the oculomotor area of the cerebellar vermis in macaques as determined by microstimulation. Journal of neurophysiology 58:359-78.

Osborne L.C., Bialek W., Lisberger S.G. (2004) Time course of information about motion direction in visual area MT of macaque monkeys. The Journal of neuroscience : the official journal of the Society for Neuroscience 24:3210-22. DOI: 10.1523/JNEUROSCI.5305-03.2004.

Osborne L.C., Lisberger S.G., Bialek W. (2005) A sensory source for motor variation. Nature 437:412-6. DOI: 10.1038/nature03961.

Palmer C., Cheng S.Y., Seidemann E. (2007) Linking neuronal and behavioral performance in a reaction-time visual detection task. The Journal of neuroscience : the official journal of the Society for Neuroscience 27:8122-37. DOI: 10.1523/JNEUROSCI.1940-07.2007.

Palmer C.R., Chen Y., Seidemann E. (2011) Uniform spatial spread of population activity in primate parafoveal V1. Journal of neurophysiology. DOI: 10.1152/jn.00117.2011.

Parker A., Hawken M. (1985) Capabilities of monkey cortical cells in spatial-resolution tasks. Journal of the Optical Society of America. A, Optics and image science 2:1101-14.

Parker A.J., Newsome W.T. (1998) Sense and the single neuron: probing the physiology of perception. Annual review of neuroscience 21:227-77. DOI: 10.1146/annurev.neuro.21.1.227.

Pelli D.G. (1985) Uncertainty explains many aspects of visual contrast detection and discrimination. Journal of the Optical Society of America. A, Optics and image science 2:1508-32.

Petersen C.C., Grinvald A., Sakmann B. (2003) Spatiotemporal dynamics of sensory responses in layer 2/3 of rat barrel cortex measured in vivo by voltage-sensitive dye imaging combined with whole-cell voltage recordings and neuron reconstructions. The Journal of neuroscience : the official journal of the Society for Neuroscience 23:1298-309.

Petersen C.C., Sakmann B. (2001) Functionally independent columns of rat somatosensory barrel cortex revealed with voltage-sensitive dye imaging. The Journal of neuroscience : the official journal of the Society for Neuroscience 21:8435-46.

Platt M.L., Glimcher P.W. (1997) Responses of intraparietal neurons to saccadic targets and visual distractors. Journal of neurophysiology 78:1574-89.

Prince S.J., Pointon A.D., Cumming B.G., Parker A.J. (2000) The precision of single neuron responses in cortical area V1 during stereoscopic depth judgments. The Journal of neuroscience : the official journal of the Society for Neuroscience 20:3387-400.

Purushothaman G., Bradley D.C. (2005) Neural population code for fine perceptual decisions in area MT. Nature neuroscience 8:99-106. DOI: 10.1038/nn1373.

Ress D., Backus B.T., Heeger D.J. (2000) Activity in primary visual cortex predicts performance in a visual detection task. Nature neuroscience 3:940-5. DOI: 10.1038/78856.

Ress D., Heeger D.J. (2003) Neuronal correlates of perception in early visual cortex. Nature neuroscience 6:414-20. DOI: 10.1038/nn1024.

Roitman J.D., Shadlen M.N. (2002) Response of neurons in the lateral intraparietal area during a combined visual discrimination reaction time task. The Journal of neuroscience : the official journal of the Society for Neuroscience 22:9475-89.

Romo R., Hernandez A., Zainos A. (2004) Neuronal correlates of a perceptual decision in ventral premotor cortex. Neuron 41:165-73.

Romo R., Hernandez A., Zainos A., Brody C.D., Lemus L. (2000) Sensing without touching: psychophysical performance based on cortical microstimulation. Neuron 26:273-8.

Romo R., Hernandez A., Zainos A., Lemus L., Brody C.D. (2002) Neuronal correlates of decision-making in secondary somatosensory cortex. Nature neuroscience 5:1217-25. DOI: 10.1038/nn950.

Romo R., Hernandez A., Zainos A., Salinas E. (1998) Somatosensory discrimination based on cortical microstimulation. Nature 392:387-90. DOI: 10.1038/32891.

Romo R., Hernandez A., Zainos A., Salinas E. (2003) Correlated neuronal discharges that increase coding efficiency during perceptual discrimination. Neuron 38:649-57.

Saito H., Yukie M., Tanaka K., Hikosaka K., Fukada Y., Iwai E. (1986) Integration of direction signals of image motion in the superior temporal sulcus of the macaque monkey. The Journal of neuroscience : the official journal of the Society for Neuroscience 6:145-57.

Salzman C.D., Britten K.H., Newsome W.T. (1990) Cortical microstimulation influences perceptual judgements of motion direction. Nature 346:174-7. DOI: 10.1038/346174a0.

Salzman C.D., Murasugi C.M., Britten K.H., Newsome W.T. (1992) Microstimulation in visual area MT: effects on direction discrimination performance. The Journal of neuroscience : the official journal of the Society for Neuroscience 12:2331-55.

Salzman C.D., Newsome W.T. (1994) Neural mechanisms for forming a perceptual decision. Science 264:231-7.

Seidemann E., Arieli A., Grinvald A., Slovin H. (2002) Dynamics of depolarization and hyperpolarization in the frontal cortex and saccade goal. Science 295:862-5. DOI: 10.1126/science.1066641.

Seidemann E., Zohary E., Newsome W.T. (1998) Temporal gating of neural signals during performance of a visual discrimination task. Nature 394:72-5. DOI: 10.1038/27906.

Shadlen M.N., Britten K.H., Newsome W.T., Movshon J.A. (1996) A computational analysis of the relationship between neuronal and behavioral responses to visual motion. The Journal of neuroscience : the official journal of the Society for Neuroscience 16:1486-510.

Shadlen M.N., Newsome W.T. (2001) Neural basis of a perceptual decision in the parietal cortex (area LIP) of the rhesus monkey. Journal of neurophysiology 86:1916-36.

Shoham D., Glaser D.E., Arieli A., Kenet T., Wijnbergen C., Toledo Y., Hildesheim R., Grinvald A. (1999) Imaging cortical dynamics at high spatial and temporal resolution with novel blue voltage-sensitive dyes. Neuron 24:791-802.

Siebert W.M. (1965) Some implications of the stochastic behavior of primary auditory neurons. Kybernetik 2:206-15.

Sit Y.F., Chen Y., Geisler W.S., Miikkulainen R., Seidemann E. (2009) Complex dynamics of V1 population responses explained by a simple gain-control model. Neuron 64:943-56. DOI: 10.1016/j.neuron.2009.08.041.

Skottun B.C., Bradley A., Sclar G., Ohzawa I., Freeman R.D. (1987) The effects of contrast on visual orientation and spatial frequency discrimination: a comparison of single cells and behavior. Journal of neurophysiology 57:773-86.

Slovin H., Arieli A., Hildesheim R., Grinvald A. (2002) Long-term voltage-sensitive dye imaging reveals cortical dynamics in behaving monkeys. Journal of neurophysiology 88:3421-38. DOI: 10.1152/jn.00194.2002.

Talbot W.H., Darian-Smith I., Kornhuber H.H., Mountcastle V.B. (1968) The sense of flutter-vibration: comparison of the human capacity with response patterns of mechanoreceptive afferents from the monkey hand. Journal of neurophysiology 31:301-34.

Tanaka K., Fukada Y., Saito H.A. (1989) Underlying mechanisms of the response specificity of expansion/contraction and rotation cells in the dorsal part of the medial superior temporal area of the macaque monkey. Journal of neurophysiology 62:642-56.

Tehovnik E.J., Slocum W.M., Schiller P.H. (2004) Microstimulation of V1 delays the execution of visually guided saccades. The European journal of neuroscience 20:264-72. DOI: 10.1111/j.1460-9568.2004.03480.x.

Tolhurst D.J., Movshon J.A., Dean A.F. (1983) The statistical reliability of signals in single neurons in cat and monkey visual cortex. Vision research 23:775-85.

Ts'o D.Y., Gilbert C.D., Wiesel T.N. (1986) Relationships between horizontal interactions and functional architecture in cat striate cortex as revealed by cross-correlation analysis. The Journal of neuroscience : the official journal of the Society for Neuroscience 6:1160-70.

Tsao D.Y., Freiwald W.A., Tootell R.B., Livingstone M.S. (2006) A cortical region consisting entirely of face-selective cells. Science 311:670-4. DOI: 10.1126/science.1119983.

Tsodyks M., Kenet T., Grinvald A., Arieli A. (1999) Linking spontaneous activity of single cortical neurons and the underlying functional architecture. Science 286:1943-6.

Uka T., DeAngelis G.C. (2003) Contribution of middle temporal area to coarse depth discrimination: comparison of neuronal and psychophysical sensitivity. The Journal of neuroscience : the official journal of the Society for Neuroscience 23:3515-30.

Uka T., DeAngelis G.C. (2004) Contribution of area MT to stereoscopic depth perception: choice-related response modulations reflect task strategy. Neuron 42:297-310.

Uka T., Tanabe S., Watanabe M., Fujita I. (2005) Neural correlates of fine depth discrimination in monkey inferior temporal cortex. The Journal of neuroscience : the official journal of the Society for Neuroscience 25:10796-802. DOI: 10.1523/JNEUROSCI.1637-05.2005.

van Kan P.L., Scobey R.P., Gabor A.J. (1985) Response covariance in cat visual cortex. Experimental brain research. Experimentelle Hirnforschung. Experimentation cerebrale 60:559-63.

Yamasaki D.S., Wurtz R.H. (1991) Recovery of function after lesions in the superior temporal sulcus in the monkey. Journal of neurophysiology 66:651-73.

Zohary E., Celebrini S., Britten K.H., Newsome W.T. (1994) Neuronal plasticity that underlies improvement in perceptual performance. Science 263:1289-92.

Vita

Charles Andrew Michelson was born in Cleveland, Ohio on November 17, 1977. He attended Tulane University in New Orleans, Louisiana where he earned a Bachelor of Science in Physics in 2001 and a Master of Science in Neuroscience in 2003. Chuck held internships at Brookhaven and Argonne National Laboratories where he developed software for the RHIC and LHC accelerators, and was employed at the Center for Gene Therapy developing software for analysis of online RNA databases. He studied natural language processing with EEG at the Attention and Emotion Laboratory at Tulane before entering the Institute for Neuroscience at The University of Texas at Austin in 2003.

Permanent Address: 3316 Guadalupe #219, Austin, TX 78705

This dissertation was typed by the author.